GLASILO SLOVENSKIH TEKSTILCEV • SLOVENE JOURNAL FOR TEXTILE AND CLOTHING TECHNOLOGY, DESIGN AND MARKETING

tekstilec

4/2019 • vol. 62 • 229–298
ISSN 0351-3386 (tiskano/printed)
ISSN 2350 - 3696 (elektronsko/online)
UDK 677 + 687 (05)

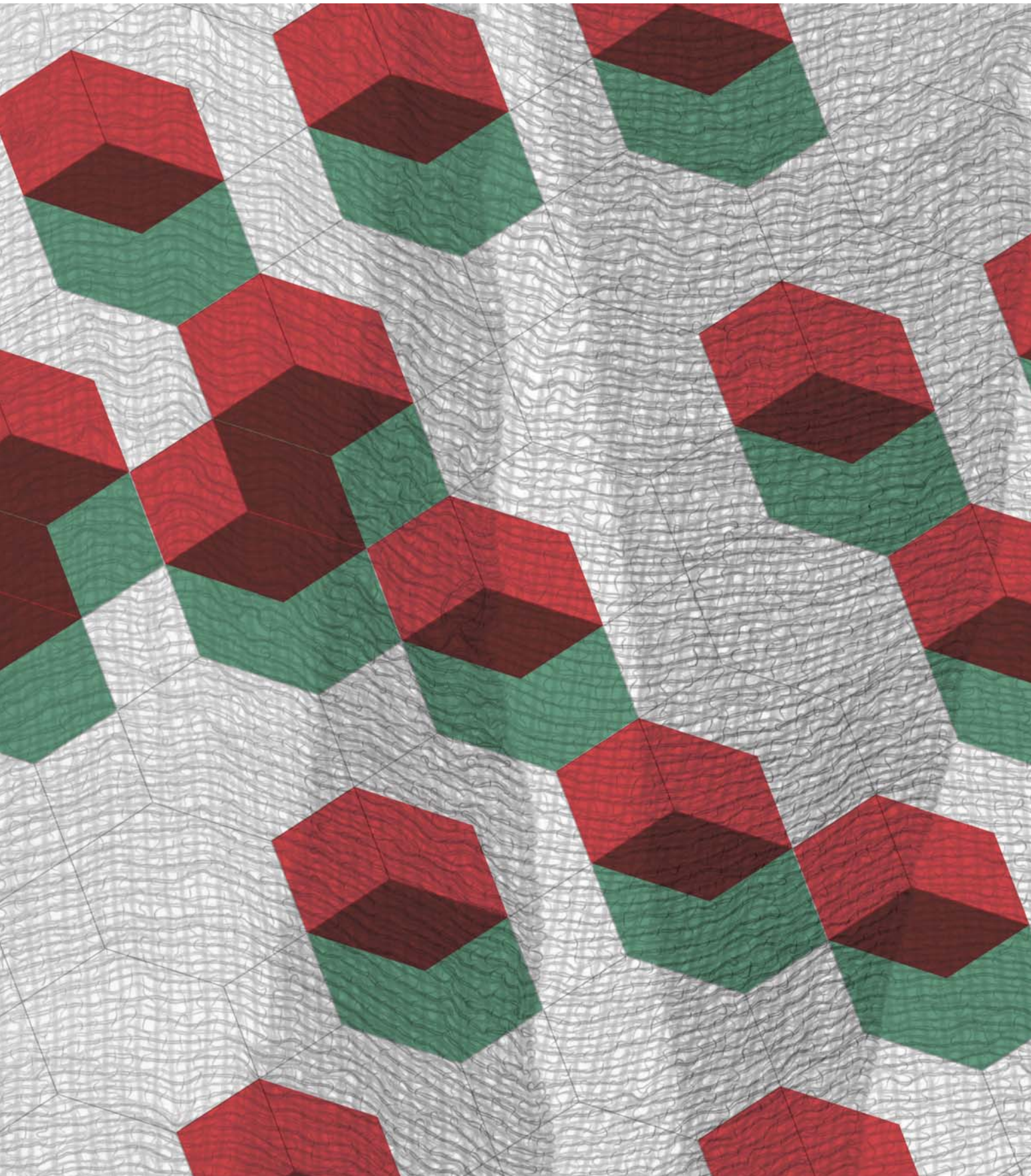

http://www.tekstilec.si

tekstilec (ISSN: 0351-3386 tiskano, 2350-3696 elektronsko) je znanstvena revija, ki podaja temeljne in aplikativne znanstvene informacije v fizikalni, kemijski in tehnološki znanosti, vezani na tekstilno in oblačilno tehnologijo, oblikovanje in trženje tekstilij in oblačil. V prilogah so v slovenskem jeziku objavljeni strokovni članki in prispevki o novostih v tekstilni tehnologiji iz Slovenije in sveta, prispevki s področja oblikovanja tekstilij in oblačil, informacije o raziskovalnih projektih ipd.

tekstilec *(ISSN: 0351-3386 printed, 2350-3696 online) the scientific journal gives fundamental and applied scientific information in the physical, chemical and engineering sciences related to the textile and clothing industry, design and marketing. In the appendices written in Slovene language, are published technical and short articles about the textile-technology novelties from Slovenia and the world, articles on textile and clothing design, information about research projects etc.*

Dosegljivo na svetovnem spletu/*Available Online at*
www.tekstilec.si

Tekstilec je indeksiran v naslednjih bazah/*Tekstilec is indexed in*
Emerging Sources Citation Index – ESCI/Clarivate Analytics
SCOPUS/Elsevier (2018: Q3, SJR 0.16, Cite Score 0.45)
Ei Compendex
DOAJ
WTI Frankfurt/TEMA® Technology and Management/TOGA® Textile Database
World Textiles/EBSCO Information Services
Textile Technology Complete/EBSCO Information Services
Textile Technology Index/EBSCO Information Services
Chemical Abstracts/ACS
ULRICHWEB – global serials directory
LIBRARY OF THE TECHNICAL UNIVERSITY OF LODZ
dLIB
SICRIS: 1A3 (Z, A', A1/2)

tekstilec

Ustanovitelja / *Founded by*
• Zveza inženirjev in tehnikov tekstilcev Slovenije /
Association of Slovene Textile Engineers and Technicians
• Gospodarska zbornica Slovenije – Združenje za tekstilno,
oblačilno in usnjarsko predelovalno industrijo /
Chamber of Commerce and Industry of Slovenia – Textiles, Clothing and Leather Processing Association

Revijo sofinancirajo / *Journal is Financially Supported*
• Univerza v Ljubljani, Naravoslovnotehniška fakulteta / *University of Ljubljana, Faculty of Natural Sciences and Engineering*
• Univerza v Mariboru, Fakulteta za strojništvo /
University of Maribor, Faculty for Mechanical Engineering
• Industrijski razvojni center slovenske predilne industrije /
Slovene Spinning Industry Development Centre – IRSPIN
• Javna agencija za raziskovalno dejavnost Republike Slovenije /
Slovenian Research Agency

Izdajatelj / *Publisher*
Univerza v Ljubljani, Naravoslovnotehniška fakulteta /
University of Ljubljana, Faculty of Natural Sciences and Engineering

Naslov uredništva/*Editorial Office Address*
Uredništvo Tekstilec, Snežniška 5, SI–1000 Ljubljana
Tel./*Tel.*: + 386 1 200 32 00, +386 1 200 32 24
Faks/*Fax*: + 386 1 200 32 70
E–pošta/*E–mail*: tekstilec@ntf.uni–lj.si
Spletni naslov/*Internet page*: http://www.tekstilec.si

Lektor za slovenščino / *Slovenian Language Editor* Milojka Mansoor
Lektor za angleščino / *English Language Editor* Barbara Luštek Preskar, Tina Kočevar Donkov, Glen David Champaigne

Oblikovanje platnice / *Design of the Cover* Tanja Nuša Kočevar
Oblikovanje / *Design* Vilma Zupan
Oblikovanje spletnih strani / *Website Design* Jure Ahtik

Tisk / *Printed by* PRIMITUS, d. o. o.

Revija Tekstilec izhaja štirikrat letno / *Journal Tekstilec appears quarterly*
Revija je pri Ministrstvu za kulturo vpisana v razvid medijev pod številko 583.
Letna naročnina za člane Društev inženirjev in tehnikov tekstilcev je vključena v članarino.
Letna naročnina za posameznike 38 € za študente 22 €
za mala podjetja 90 € za velika podjetja 180 €
za tujino 110 €
Cena posamezne številke 10 €

Na podlagi Zakona o davku na dodano vrednost sodi revija Tekstilec med proizvode, od katerih se obračunava DDV po stopnji 9,5 %.

Transakcijski račun 01100–6030708186
Bank Account No. SI56 01100–6030708186
Nova Ljubljanska banka d.d.,
Trg Republike 2, SI–1000 Ljubljana,
Slovenija, SWIFT Code: LJBA SI 2X.

tekstilec VOLUME 62 • TEKSTILEC 4 • 2019 ISSN 0351-3386 (tiskano/printed)
UDK 677 + 687 (05)

SCIENTIFIC ARTICLES/ Znanstveni članki

Ajda Car, Sabina Bračko
University of Ljubljana, Faculty of Natural Sciences and Engineering, Aškerčeva 12, 1000 Ljubljana, Slovenia

Influence of Basic Colour Parameters on Colour Memory

Vpliv osnovnih parametrov barve na barvni spomin opazovalca

Original Scientific Article/ *Izvirni znanstveni članek*
Received/*Prispelo* 05-2019 • Accepted/*Sprejeto* 09-2019

Abstract

We frequently need to compare two or more colours, and we can rely only on the colour impression from our memory. Colours are not stored in our memories in their actual state and they can gradually be erased. This paper addresses the subject of short-term colour memory. The approach is based on an experiment where subjects observed a given colour for a certain period of time. The purpose of the research was to determine the relation between the reference colour, time delay and the accuracy in recalling of the colour from the subject's memory. The colours studied in the research were presented with no association to bodies, shapes or textures. The main variables in the observing conditions were the basic colour parameters which define the colour, i.e. hue, saturation and brightness. The analysis of the final results showed that colour is not stored in our memories correctly and that it loses its basic parameters after 10 s. As the time delay increases, the accuracy of the colour impression in our memory diminishes. Colour is stored in our memory as clearer and more saturated. Bright colours are remembered as even brighter, while dark colours are stored as darker. The sensation of hue is generally stored very precisely, while the deviation in hue depends on the observed colour.
Keywords: colour memory, simultaneous colour comparison, colour perception, hue, saturation, brightness

Izvleček

V vsakdanjem življenju se pogosto znajdemo v situaciji, ko želimo primerjati dve ali več barv, ki jih ne opazujemo hkrati eno ob drugi, temveč si moramo pomagati z barvnim vtisom iz spomina. Pri tem si ljudje barvo zapomnijo z napako ali sčasoma postopno pozabijo videno barvo. Raziskava se navezuje na področje kratkoročnega barvnega spomina. Raziskovalni pristop je temeljil na poskusu opazovanja, v katerem so udeleženci določen čas opazovali dodeljeno barvo. Namen raziskave je bil ugotoviti, kakšna je povezava med opazovano referenčno barvo, časovnim zamikom in ponovnim priklicem barve iz spomina. Barva je bila v raziskavi obravnavana neodvisno od asociacij z različnimi telesi, oblikami ali teksturami. Glavne spremenljivke pri nespremenjenih opazovalnih pogojih so bili tako osnovni parametri, ki določajo barvo, tj. barvni ton, nasičenost in svetlost. Analiza pridobljenih rezultatov je pokazala, da si ljudje barvo zapomnijo z napako ali jo v spominu pomešajo že po desetih sekundah. Natančnost barvnega vtisa v spominu se z večjim časovnim zamikom postopno manjša. Barve se v spominu ohranijo kot bolj nasičene in bolj čiste. Svetle barve si zapomnimo svetlejše, temne si zapomnimo temnejše. Pomnjenje barvnega tona je razmeroma dobro, spominski preskok pa je odvisen od opazovane barve.
Ključne besede: barvni spomin, sočasna primerjava barv, zaznavanje barv, barvni ton, nasičenost, svetlost

1 Introduction

The memorial restoration of a certain event or sensation (e.g. colour) is far from being perfect. Contrary to a common belief, our memory is not infallible. As confirmed by several investigations, our colour memory is rather poor and the sensation of a colour is not always remembered accurately [1–3].

Corresponding author/*Korespondenčna avtorica:*
Assoc Prof dr. Sabina Bračko
E-mail: sabina.bracko@ntf.uni-lj.si
ORCID: 0000-0002-3140-7263

This can present a serious obstacle when selecting or buying an item which is meant to be of a defined colour or to be matching a certain hue, for example, when buying a textile or apparel.

The ability to discriminate and remember different colours depends on several conditions, e.g. the age and gender of the observer, the viewing conditions and the colour itself. Although the research in this area has been intensified in the last years, the results are not easily compared as different authors apply various approaches to study the colour memory [4]. According to Pérez-Carpinell [3], the colour memory is a successive colour matching which occurs when some time has elapsed between the observation of a colour and its restoration from the memory. In our daily life, the situations where a remembered colour has to be reproduced or a present colour has to be judged in comparison with the remembered one are much more common than a simultaneous comparison of two colour samples. For example, we often need to evaluate the quality of food in a store regarding its colour or we want to buy a garment to match the one we have at home [5–7].

On the basis of our everyday experience, we gradually build a library of colours and hues in our long-time memory, where the colours from our daily life are incorporated. The colours can be easily described by using suitable words. However, when such a "memory colour" of a known object is compared to the colour observed some time ago, a change in colour appearance may occur [1, 8]. A comparison from our long-time memory happens automatically and it has been observed with natural and artificial objects [9]. Consequently, the testing of colour memory strongly depends on the selection of reference colours and surrounding conditions [10].

Bodrogi and Tarczali [4] investigated in what way the colour memory is affected when a coloured sample is observed within the image context. Memory (i.e. *prototypical)* colours of known objects such as sky, plants and skin were observed either as a simple colour patch or as a part of a photo-realistic image. The results showed that an association can be triggered by the image context, and during the time delay, the observed colour was compared to the memorized colour of a known object, stored in the long-term memory. The shifts in detection occurred in the direction of the memory colour of the observed object.

The restoration of such memory colours, i.e. prototypical colours of known objects, works in a similar way and is influenced by the association with a known object even if it is observed in the absence of the image context. Obviously, colour is a subjective sensation which occurs in the brain as a consequence of three factors, i.e. light source, coloured object and observer [10]. Colours which are perceived in our daily life are always connected to a certain object and are also stored in our memory in this way. It is therefore not unexpected that a colour shift into the direction of a memory colour was detected also in the experiment where uniform coloured rectangles were observed [11].

One of the researches concerning memory colours showed that memory shifts are also affected by the nature of the observed object [12]. Apparently, the shifts proved to be much smaller or even negligible when the colour of food was involved. A reasonable explanation could be given by the fact that the colour of food is an extremely important information from the view point of a consumer as it reflects its quality, ripeness and edibility, whereas the colour of the sky is generally not crucial for survival. A similar effect was observed by Seliger [1] as the colour of a yellow banana was remembered much more precisely than the blue sky, green grass or the red traffic light.

The changes in memory can be provoked merely by a hint, for example if context is added to the observed colour. Such denotation influences the perception of colour and consequently the colour memory, which leads to a colour shift towards the colour which is stored in our memory in connection with the given context [12]. Tarczali *et al* [2] compared the precision of remembered memory colours in two cases: in the first one, the colour was given merely by its name and in the second one, a black and white photography was enclosed, showing a scene in connection with the given colour. Based on the study results, the accordance between the observed reference colour and the long-term memory colour was far better when the photography was enclosed.

According to the examined literature, the investigations of colour memory in which the colours are represented independently and without any context are very rare [7, 10, 13]. The research focuses mainly on the observers (age, gender) and does not answer the question, how well the colour is remembered or what kind of shift occurs in our colour memory. Colour is a subjective perception which depends on several physical, physiological and psychological factors. The colour memory also depends on the former

experiences of an individual and its understanding represents a complex problem. The purpose of our research was therefore to establish the relationship between the observed reference colour and the ability of the observer to recall this colour from the memory when the reference colour is presented independently, without any connotation to shapes, textures or environment. In the experiment, the reference colours, which were defined merely by their basic characteristics, i.e. hue, saturation and lightness, were observed for a certain period of time under controlled and constant conditions. After a short pause (10 s, 60 s, 300 s), the observers were asked to restore the reference colour from their memory on the basis of selected colour samples. The colour differences were calculated in order to establish the deviations in hue, saturation and lightness, and the dependence of total colour difference on time, with the aim to evaluate the influence of basic colour properties on our ability to remember colours and to predict the colour changes which occur with time.

2 Experimental

2.1 Selection of reference colours and samples

To study colour memory, ten reference colours were systematically selected using the HSB and afterwards converted to the CIELAB colour space, regarding the following conditions: 1. reference colours should not be associated with well-known coloured objects, 2. reference colours should be positioned as widely as possible to cover the visible spectrum. The aim of the research was to study the colour memory separately from any associations; therefore, the selection of independent reference colours was crucial. The CIELAB coordinates of ten reference colours are presented in Table 1.

For each of the ten reference colours, six accompanying samples were carefully selected. To define each of them, only one basic colour parameter was changed in such a manner that the possibility of selecting all directions in the colour space is given (cf. Figure 1). The colour difference between the reference colour and an individual sample was approximately 5 CIELAB units, as suggested in previous research [3].

Table 1: CIE $L^*a^*b^*$ coordinates of reference colours I–X

Reference colour	L^*	a^*	b^*
I	39	27	12
II	79	–26	68
III	76	–35	–11
IV	24	1	6
V	14	30	–25
VI	20	–1	–17
VII	84	–15	15
VIII	68	–40	21
IX	46	11	–23
X	26	46	–9

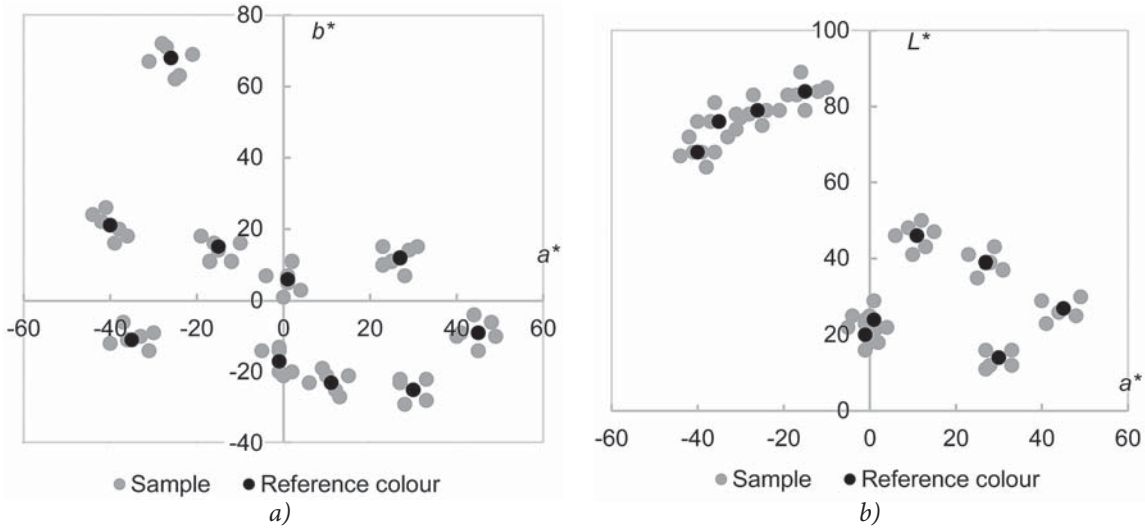

a) *b)*

Figure 1a and 1b : Reference colours I-X and corresponding colour samples in CIEa^*b^* and CIEa^*L^* plane of CIELAB colour space

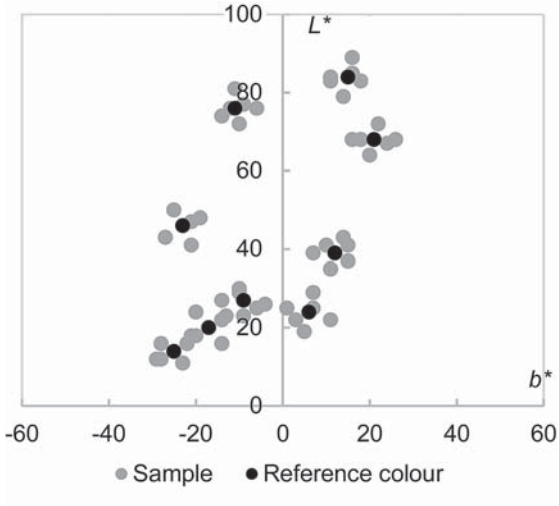

*Figure 1c: Reference colours I-X and corresponding colour samples in CIEb*L* plane of CIELAB colour space*

2.2 Observers

The research was based on 18 graduated or undergraduated student volunteers (convenience sampling method), 9 male and 9 female, aged 20–30 years. At this age, the colour vision is at its peak, which also affects the colour memory [7, 13]. Prior to the testing, the participants were subjected to the Ishihara and Farnsworth-Munsell hue tests to prove their normal colour vision and the ability to distinguish colours. As several investigations proved that there are no major differences between the observers with different experiences, our group of observers was not divided according to their previous education or field of work [4, 10, 14].

2.3 Testing conditions

The experiment was conducted at constant and controlled conditions. The reference colours and corresponding samples, all 6 cm × 6 cm in size, were shown on a neutral grey background ($L^* = 75$, $a^* = -3$, $b^* = -2$), on a 27-inch monitor with the resolution 1920 dpi × 1080 dpi, which was previously calibrated and set to D65 standard illumination ($T_C = 6500$ K). The colour temperature was controlled before and after each set of testing to ensure a constant display of colours throughout the testing procedure. The monitor was the only source of light in an isolated dim room. The observers were positioned at the distance of 70 cm from the monitor. The height was adjusted to ensure the viewing angle of 90°.

2.4 Testing procedure

Prior to the testing, the observers were asked to take time to adjust to the conditions of illumination (5 min) and afterwards, to the neutral grey background of the monitor (3 min). In the first part, the colour memory after a certain period of time (10 s, 60 s, 300 s) was tested. The procedure started with the observation of the reference colour for 10 s, after which the observer focused on the grey background. After 10 s (60 s, 300 s), seven colour samples appeared on the monitor, showing the previously displayed reference colour together with six similar, randomly positioned colour samples, lined in two rows. The observer was asked to find the previously displayed reference colour. The time for the decision was not limited since no significant impact of time limitation was noted by the examined literature [2, 7, 13]. Afterwards, the procedure was repeated for different time delays, whereas the seven colour samples were displayed to the observer at each time delay positioned in diverse order.

In the second part of the experiment, a simultaneous comparison of colour samples was performed to establish whether the deviations in colour sensations were a consequence of the limited short-time memory or of the observer's disability to distinguish colours. The observers were asked to select the matching colour among the seven colour samples, prior used in the first part of the experiment, positioned around the central reference colour. The time for the decision was not limited. The position of the reference colour (example: colour III) and appropriate samples is presented in the supplement of the web version of this paper. The testing procedure was repeated for each of the ten reference colours. The reference colours and appropriate samples were marked only with numbers, no names were mentioned in connection with colours in order to avoid any associations which could influence the results of colour memory testing [12, 15].

3 Results and discussion

The analysis of a simultaneous comparison (i.e. time delay $t = 0$ s) and colour memory testing ($t = 10$ s, 60 s, 300 s) was based on the average CIE $L^*a^*b^*$ values of selected samples at a given time for each reference colour. The CIELAB equation was used to calculate the total colour difference, ΔE^*_{ab}, as well as its components,

i.e. difference in hue, ΔH^*_{ab}, difference in lightness, ΔL^*, and difference in chroma, ΔC^*_{ab}.

3.1 Simultaneous comparison of colour samples

The results of a simultaneous comparison, i.e. $t = 0$, showed that 96% of total replies were correct (cf. Figure 2), meaning that the observers found the correct reference colour among the seven samples displayed simultaneously. Due to the remaining 4% of incorrect replies, the colour difference $\Delta E^*_{ab} = 0.48$ was calculated (cf. Table 2). The calculated average colour difference at a simultaneous comparison of colours is in accordance with the results obtained in previous research. Pèrez-Carpinell *et al* reported the average $\Delta E^*_{ab} = 0.58$ [7] in a group of observers of the same age as in our experiment, while the difference was slightly higher ($\Delta E^*_{ab} = 1.00$) in a group of various age [3].

Table 2: Average change in basic colour parameters, ΔH^*_{ab}, ΔC^*_{ab}, ΔL^*, and total colour difference, ΔE^*_{ab}, for all samples after different time delays (0 s, 10 s, 60 s, 300 s)

Colour change	Time delay [s]			
	0	10	60	300
$\lvert\Delta H^*_{ab}\rvert$	0.12	0.66	0.65	0.82
$\lvert\Delta C^*_{ab}\rvert$	0.46	1.14	1.44	1.71
$\lvert\Delta L^*\rvert$	0.00	0.74	0.80	1.00
ΔE^*_{ab}	0.48	1.80	1.92	2.29

Table 2 shows a comparison of the three basic parameters, i.e. hue, lightness and chroma, and their change with time. First of all, we were interested in establishing the magnitude of deviation from the reference colour, not its direction; hence, the changes are represented as absolute values. According to the results, there were no deviations in lightness ($\lvert\Delta L^*\rvert = 0.00$) and only small differences in hue were established ($\lvert\Delta H^*_{ab}\rvert = 0.12$). On the other hand, the average difference in chroma was $\lvert\Delta C^*_{ab}\rvert = 0.46$ units, meaning that the difference in chroma represents the major part of the total colour difference. We can conclude that when comparing two colours simultaneously, an error in saturation is most likely to occur.

For the majority of reference colours, the colour difference at a simultaneous comparison was zero (cf. Table 3), meaning that the selected sample was identical to the observed reference colour. However, some discrepancies were found at reference colours II ($\Delta E^*_{ab} = 1.41$), V ($\Delta E^*_{ab} = 1.41$), VIII ($\Delta E^*_{ab} = 1.00$) and X ($\Delta E^*_{ab} = 1.00$). All of these samples exhibited the largest difference in chroma ($\Delta C^*_{ab} = -1.29$, $\Delta C^*_{ab} = 1.41$, $\Delta C^*_{ab} = 0.89$ and $\Delta C^*_{ab} = -0.98$, respectively). The deviations occurred in both directions, positive and negative; therefore, a colour to be matched was perceived as more or less saturated than the original one. One of the previous researches reported that at a simultaneous comparison of colours, deviations occur randomly [7]. In our research, samples II, V and X with higher chroma also exhibited limited matching at a simultaneous comparison. We can conclude that comparing and distinguishing colours with higher saturation is connected with difficulties. Such limitations of the human eye are also evident from the size and shape of the MacAdam's ellipses [16, 17].

3.2 Total colour difference depending on time delay

The human capability to remember colours is relatively scarce and the reconstruction of a colour sensation becomes even more inaccurate with time [1, 7, 18]. The results of our investigation confirm such findings.

Figure 2 represents the decrease in colour matching with time, which is especially evident during the starting period. The most substantial change occurs during the first time interval as the share of perfect matches decreases from 96% at a simultaneous comparison to 49% after 10 s, decreasing to 28% after 60 s and to 17%

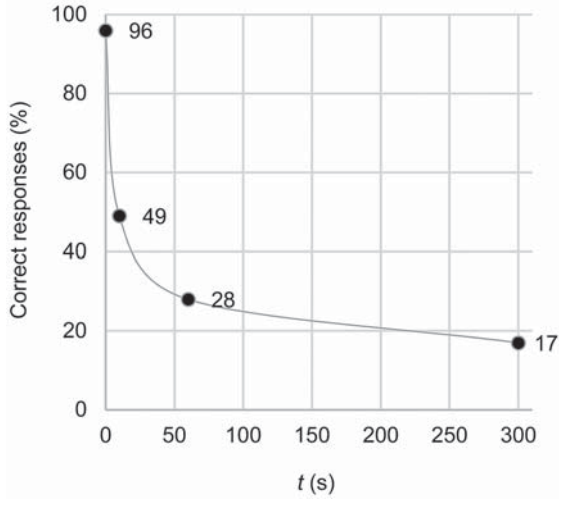

Figure 2: Percentage of correct responses in dependence on time

Table 3: Change in basic colour parameters, ΔH^*_{ab}, ΔC^*_{ab}, ΔL^* and total colour difference, ΔE^*_{ab}, after different time delays (0 s, 10 s, 60 s, 300 s) for samples I–X

Reference colour	Colour difference	Time delay [s]			
		0	10	60	300
I	ΔH^*_{ab}	0.00	0.50	0.21	0.99
	ΔC^*_{ab}	0.00	1.32	2.23	2.65
	ΔL^*	0.00	0.00	0.00	0.00
	ΔE^*_{ab}	0.00	1.41	2.24	2.83
II	ΔH^*_{ab}	–0.57	–1.63	–1.63	–1.63
	ΔC^*_{ab}	–1.29	1.53	1.53	1.53
	ΔL^*	0.00	1.00	1.00	2.00
	ΔE^*_{ab}	1.41	2.45	2.45	3.00
III	ΔH^*_{ab}	0.00	0.00	–0.29	–0.61
	ΔC^*_{ab}	0,00	0.00	0.95	1.91
	ΔL^*	0.00	1.00	1.00	1.00
	ΔE^*_{ab}	0.00	1.00	1.41	2.24
IV	ΔH^*_{ab}	0.00	0.00	0.00	0.00
	ΔC^*_{ab}	0.00	0.00	0.00	0.00
	ΔL^*	0.00	–1.00	–1.00	0.00
	ΔE^*_{ab}	0.00	–1.00	–1.00	0.00
V	ΔH^*_{ab}	0.00	–0.88	–0.87	–0.87
	ΔC^*_{ab}	1.41	2.06	2.06	2.06
	ΔL^*	0.00	0.00	–1.00	–1.00
	ΔE^*_{ab}	1.41	2.24	2.45	2.45
VI	ΔH^*_{ab}	0.00	0.11	0.11	1.03
	ΔC^*_{ab}	0.00	1.00	1.00	0.97
	ΔL^*	0.00	–1.00	–1.00	–2.00
	ΔE^*_{ab}	0.00	1.41	1.41	2.45
VII	ΔH^*_{ab}	0.00	0.50	0.65	0.65
	ΔC^*_{ab}	0.00	0.72	2.14	2.14
	ΔL^*	0.00	2.00	2.00	2.00
	ΔE^*_{ab}	0.00	2.24	3.00	3.00
VIII	ΔH^*_{ab}	0.46	0.21	0.91	0.21
	ΔC^*_{ab}	0.89	2.23	1.78	2.23
	ΔL^*	0.00	0.00	0.00	0.00
	ΔE^*_{ab}	1.00	2.24	2.00	2.24
IX	ΔH^*_{ab}	0.00	–0.44	0.44	–0.86
	ΔC^*_{ab}	0.00	0.90	0.90	1.81
	ΔL^*	0.00	0.00	0.00	–1.00
	ΔE^*_{ab}	0.00	1.00	1.00	2.24
X	ΔH^*_{ab}	0.20	2.31	1.34	1.34
	ΔC^*_{ab}	–0.98	1.63	1.79	1.79
	ΔL^*	0.00	–1.00	–1.00	–1.00
	ΔE^*_{ab}	1.00	3.00	2.45	2.45

after 300 s. A similar trend was discovered by Seliger [1]. He reported an evident decrease between the time interval 1 s and 5 s, while no major changes were observed with increasing time, between 5 s, 10 s and 15 s. According to the results of our study, the percentage of correct answers decreased more slowly after a longer period of time, which indicates only a gradual change in the colour impression in the memory. After 60 s, 28% of answers were correct and after 300 s, 17%. Considering the curve of decrease (cf. Figure 2) and the results of previous investigations, an even smaller decrease is expected with increasing time; therefore, it is very likely that the colour memory remains at an approximately the same level. Perez-Carpinell *et al* [3] tested the colour memory after 15 s, 15 min and 24 h, and they found that the colour memory after 15 s is distinctively better than after a longer period of time. However, there were no major differences in the results obtained after 15 min or 24 h. Hamwi and Landis [19] tested the colour memory after a longer period of time, i.e. 15 min, 24 h and 64 h, and the results showed no major differences.

Similar conclusions regarding the colour memory can be obtained on the basis of calculated colour differences (cf. Tables 2 and 3). With no exception, a simultaneous comparison of colours was more accurate than the comparison after a different period of time. After 10 s, the average colour difference was ΔE^*_{ab} = 1.80, after 60 s ΔE^*_{ab} = 1.92 and after 300 s ΔE^*_{ab} = 2.29 (cf. Table 2). Similar results were obtained by de Fez *et al* [20] who found that a simultaneous comparison was more accurate than a successive one for 31 out of 34 colour samples.

According to previous investigations, the colour memory is not equally precise for all colours. The results of our investigation (cf. Table 3) show that samples IV (ΔE^*_{ab} = 0.67), IX (ΔE^*_{ab} = 1.41) and III (ΔE^*_{ab} = 1.55) were remembered most accurately as the colour differences were considerably small. On the other hand, the biggest colour differences were found for samples VII (ΔE^*_{ab} = 2.75), X (ΔE^*_{ab} = 2.63) and II (ΔE^*_{ab} = 2.63). Such results imply that a larger colour difference at a simultaneous comparison is connected with the reduced colour memory and that the colours which are hard to differentiate fade more quickly in our memory. These results, however, cannot be generalized. According to Jin and Sheyell [21], the colours of medium and long wavelength region are remembered more easily and with higher precision. Fez *et al*, on the other hand, claim that the colours along the blue-yellow axis are the easiest and those along the green-red axis the most difficult to remember [20].

3.3 Change in basic colour parameters depending on time delay

Each colour is defined by its three basic parameters, i.e. hue, lightness and saturation. Several authors discovered that at restoring colour from our memory, the three parameters are not remembered equally accurately [3, 21]. The aim of our study was therefore to examine the changes in hue, ΔH^*_{ab}, lightness, ΔL^*, chroma, ΔC^*_{ab}, and the total colour difference in dependence on time for the selected reference colours (cf. Table 2). Regardless the time interval (10 s, 60 s, 300 s), the difference in chroma represented on average the major part of the total colour difference ($|\Delta C^*_{ab}|$ = 1.14, $|\Delta C^*_{ab}|$ = 1.44 or $|\Delta C^*_{ab}|$ = 1.71, for increasing time delay), the saturation of colour being remembered the least accurately. A very small contribution to the total colour difference represents the calculated difference in hue, which varies between 0.66 units (after 10 s) and 0.88 units (after 300 s), reflecting that, in general, we are able to memorise a certain hue very well. Only slightly bigger differences in lightness were detected ($|\Delta L^*|$ = 0.74, $|\Delta L^*|$ = 0.80 and $|\Delta L^*|$ = 1.00, respectively).

Analysis of change in chroma

The colours which are recalled after a certain time delay are remembered with a considerable difference in saturation. The calculated values ΔC^*_{ab} were positive for all samples (cf. Table 3), indicating that we remember a colour as more saturated than it originally is. Similar observations were reported by other authors [4, 12, 20]. In some cases, on the other hand, the authors reported that colours with high chroma were remembered as more saturated and vice versa; however, this only occurred in the cases where the colour was connected to a certain object [18, 22].

According to the results (cf. Table 4), remembering the correct colour can be difficult especially for the colours with higher chroma whereas the samples with lower chroma are the least problematic. We can conclude that remembering colours with lower or moderate saturation is relatively easy compared to highly saturated colours which are in general also difficult to distinguish by the human eye. Our samples did not show any correlation between the difference in chroma and their hue.

Table 4: Average change in basic colour parameters, ΔH^*_{ab}, ΔC^*_{ab}, ΔL^* and total colour difference, ΔE^*_{ab}, after different time delays (10 s, 60 s, 300 s) for samples I–X

Colour change	Reference colour									
	I	II	III	IV	V	VI	VII	VIII	IX	X
$\lvert\Delta H^*_{ab}\rvert$	0.57	1.63	0.30	0.00	0.87	0.42	0.60	0.44	0.58	1.66
$\lvert\Delta C^*_{ab}\rvert$	2.07	1.53	0.95	0.00	2.06	0.99	1.67	2.08	1.20	1.74
$\lvert\Delta L^*\rvert$	0.00	1.33	1.00	0.67	0.67	1.33	2.00	0.00	0.33	1.00
ΔE^*_{ab}	2.16	2.63	1.55	0.67	2.38	1.76	2.75	2.16	1.41	2.63

Analysis of change in lightness

The results showed that our memory for lightness is relatively accurate and comparable to our memory for hue. This is in accordance with previous investigations [12]. We also established that a similar deviation in lightness can be found for colours with similar original lightness.

When recalling colour after a certain period of time, a deviation in lightness can occur. According to the results in Figure 3b, the difference in lightness, ΔL^*, can be either positive or negative. The colours with higher lightness were positioned above its original position; thus, the colours with higher lightness are remembered as even lighter. In contrast, the colours with moderate or lower lightness were positioned lower; hence, dark colours are remembered as even darker.

In some cases, when colours were connected with a certain object, the authors reported only the changes in the direction of lower lightness [4, 18]. The majority of researches which include independent colours confirm that colours with higher lightness are remembered as slightly lighter and those with lower lightness as considerably darker. Colours with medium lightness are remembered relatively accurately or slightly darker [3, 12].

A comparison of the average change in lightness $\lvert\Delta L^*\rvert$ with the original lightness of a colour (cf. Table 4) shows that the biggest changes were observed at the samples with higher lightness, i.e. samples II ($L^* = 79$) and VII ($L^* = 84$), and at a darker sample VI ($L^* = 20$). On the other hand, the samples with medium lightness, i.e. samples I ($L^* = 39$), VIII ($L^* = 68$) and IX ($L^* = 46$) were remembered very accurately, exhibiting very small values ΔL^* with time. The differences in colour memory between the colours of different lightness are not as evident as at colours of different chroma; nevertheless, the results show that very dark and very light colours are more difficult to remember.

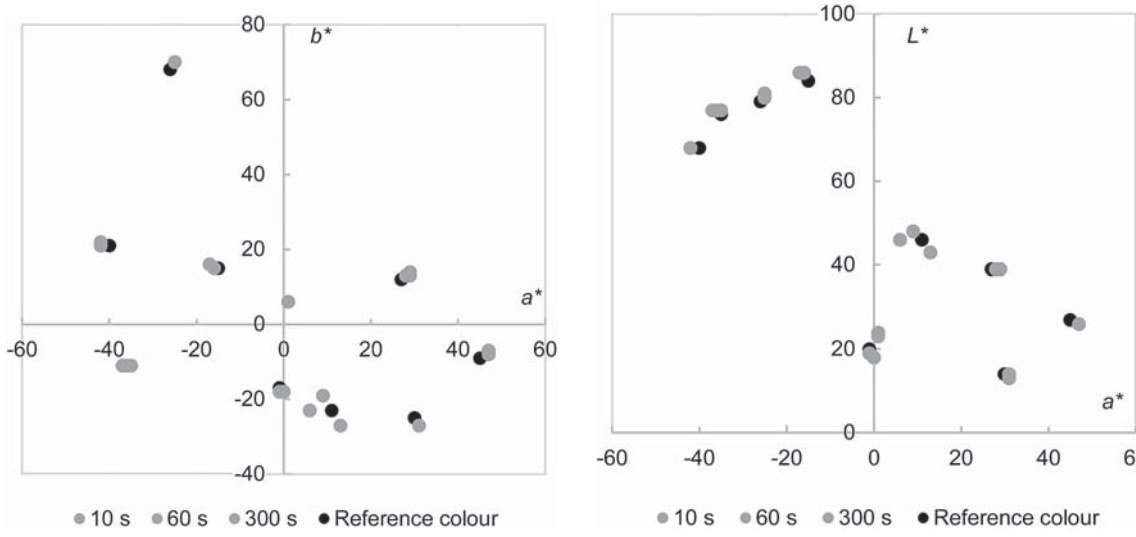

a) *b)*

Figure 3: Reference colours I–X and colour samples, selected after different time delays (10 s, 60 s, 300 s), in CIEa^*b^* plane (a) and in CIEa^*L^* plane (b) of CIELAB colour space

Analysis of change in hue

According to our results, the hue of a colour is the characteristic which is remembered the most accurately. The biggest differences in hue were observed at highly saturated samples, but no correlation was found between the difference in hue and the difference in chroma. Only small, barely noticeable differences in hue were reported with time also by other authors [3, 4, 12, 21]. As explained by Pérez-Carpinell *et al* [18], we quickly forget or neglect less important information and properties. The hue, however, is a basic characteristic which enables distinguishing the colours; therefore, the probability for it to be kept in our memory is increased.

Figure 3 shows the reference samples and the memorized colours after a certain time delay in the CIEa^*b^* plane. Generally, a slight shift towards an adjacent axis can be noticed. Sample X (scarlet) shifted towards the positive a^* axis, meaning that the scarlet colour is remembered as more reddish. Samples III (light blue), VII (light green) and VIII (green) moved to the negative a^* axis; thus, they are remembered as greener. Samples V (dark violet) and VI (dark blue) moved to the negative b^* axis, meaning that they are set in our memory as bluer. Similar shifts towards the axis which is closer and appropriate basic colours of the CIELAB colour space were reported by other authors [4]. An exception was noticed at sample IX (light purple), which did not show any systematic deviations, but rather random shifts. Our assumption is that this sample resembled to a colour of lavender (plant), which was also remarked by most subjects. According to the examined literature, if a reference colour resembles strongly to any known object, shape or texture, the colour sensation can be compared to our long-term memory which can potentially lead to a deviation of colour memory [1, 8].

4 Conclusion

Several investigations show that our colour memory is not reliable and that it depends on the observed colour. This can present a serious obstacle when selecting or buying an item which is meant to be of a defined colour or to be matching a certain hue, for example, when buying a garment. Namely, our perception of colour depends on several physical, physiological and psychological factors and our colour memory depends also on the former experience of individual. The purpose of our research was to focus on the properties of colour to discover which colours are remembered more accurately and how the basic parameters of colour influence our ability to preserve the colour sensation. The research was focused on colours, which were presented independently, without any connotation to shapes, textures or environment.

The results confirmed that our colour memory is rather poor. With no exception, for all samples tested, a simultaneous comparison of colours was more accurate than the recalling of a colour after a certain period of time. As soon as after 10 s, our impression of a colour is changed and the deviations increase with time. According to the results, the perceived colour difference includes the change in all three basic parameters of a colour.

The hue of a colour is the property which is remembered the best. We can conclude that the properties which are considered as less important are neglected or forgotten sooner. Hue, on the other hand, is a basic property which enables distinguishing and naming colours, and is therefore more likely to be preserved in our memory. The deviation in hue with time depends on the colour. According to our study, it is very likely that a colour shift will occur towards the closest axis of the CIEa^*b^* plane.

The ability to remember the lightness of a colour is relatively good and comparable to that of remembering its hue. The biggest errors were observed for the colours with extremely low or high lightness; lighter colours were remembered as even lighter and dark colours as darker. Our colour memory functions most accurately for the samples with medium lightness; these are usually remembered as only slightly darker or even identical to the original.

The saturation of a colour is a property which is the most difficult to be preserved in the memory. Regardless the colour, it is remembered as more saturated than it originally was. The increase in saturation is less obvious for the colours with higher chroma. According to the results, colours with lower saturation are remembered more accurately. On the other hand, the colours with higher saturation, which are also more problematic to be distinguished, are recalled from our memory with a significant deviation.

References

1. SELIGER, Howard. H. Measurement of memory of color. *Color Research and Application,* 2002, **27**(4), 233–242, doi: 10.1002/col.10067.
2. TARCZALI, Tünde, PARK, Du-Sik, BODROGI, Peter, KIM, Chang Yeong. Long-term memory colors of Korean and Hungarian observers. *Color Research and Application,* 2006, **31**(3), 176– 183, doi: 10.1002/col.20192.
3. PÉREZ-CARPINELL, Joaquín, BALDOVÍ, Rosa, DE FEZ, M. Dolores, CASTRO, José. Color memory matching: time effect and other factors. *Color Research and Application,* 1998, **23**(4), 234–247, doi: 10.1002/(SICI)1520-6378-(199808)23:4<234::AID-COL8>3.0.CO;2-P.
4. BODROGI, Peter, TARCZALI, Tünde. Colour memory for various sky, skin and plant colours: effect of the image context. *Color Research and Application,* 2001, **26**(4), 278–289, doi: 10.1002/col.1034.
5. HUNT, Robert William Gainer, POINTER, Michael R. *Measuring colour. Second edition*. West Sussex : Ellis Horwood Limited, 1991, pp. 24–37.
6. UCHIKAWA, Keiji, SHINODA, Hiroyuki. Influence of basic color categories on color memory discrimination. *Color Research and Application,* 1996, **21**(6), 430–439.
7. PÉREZ-CARPINELL, Joaquín, CAMPS, Vicente J., TROTTINI, Mario, PÉREZ-BAYLACH, Carmen M. Color memory in elderly adults. *Color Research and Application,* 2006, **31**(6), 458–467, doi: 10.1002/col.20258.
8. RATNER, Carl, McCARTHY, John. Ecologically relevant stimuli and color memory. *The Journal of General Psychology,* 1990, **117**(4), 369–377.
9. LEWIS, David E., PEARSON, Joel, KHUU, Siev K. The color "Fruit": object memories defined by color. *PLoS One,* 2013, **8**(5), 1–8, doi: 10. 1371/journal.pone.0064960.
10. BYNUM, Carlisle, EPPS, Helen H., KAYA, Naz. Color memory of university students: Influence of color experience and color characteristic. *College Student Journal,* 2006, **40**(4), 824–831.
11. JELER, Slava, GOLOB, Vera. Znanost o barvi in njena uporaba v tekstilni proizvodnji. *Tekstil,* 1989, **38**(4), 199–206.
12. SIPLE, Patricia, SPRINGER, Robert M. Memory and preference for the colors of objects. *Perception and Psychophysics,* 1983, **34**(4), 363–370, doi: 10.3758/BF03203049.
13. PÉREZ-CARPINELL, Joaquín , CAMPS, Vicente J., TROTTINI, Mario. Color memory in children. *Color Research and Application,* 2008, **33**(5), 372–380, doi: 10.1002/col.20433.
14. EPPS, Helen H., KAYA, Naz. Color matching from memory. *Color and paints, Interim meeting of the International color association,* 2004, pp. 18–21.
15. LOFTUS, Elizabeth F. Shifting human color memory. *Memory and Cognition,* 1977, **5**(6), 696–699, doi: 10.3758/BF03197418.
16. WOOD, Mike. MacAdam ellipses. *Mike Wood consulting,* 2010, pp. 15–18 [cited 27. 11. 2018]. Available on World Wide Web: <http://www.mikewoodconsulting.com/articles/Protocol Fall 2010 - MacAdam ellipses.pdf.
17. BERNS, Roy S. *Billmeyer and Slatzman´s principles of color technology. 3rd edition*. New York : John Wiley and Sons, 2000, pp. 109–110.
18. PÉREZ-CARPINELL, Joaquín, DE FEZ, M. Dolores, BALDOVÍ, Rosa, SORIANO J. C. Familiar objects and memory color. *Color Research and Application,* 1998, **23**(6), 416–427, doi: 10.1002/(SICI)1520-6378(199812)23:6<416::AID-COL10>3.0.CO;2-N.
19. HAMWI, Violet, LANDIS, Carney. Memory for color. *The Journal of Psychology,* 1955, **39**(1), 183–194, doi: 10.1080/00223980.1955.9916168.
20. DE FEZ, M. Dolores, CAPILLA, Pascual, LUQUE, M. José, PÉREZ-CARPINELL, Joaquín, DEL POZO, Juan Carlos. Asymmetric colour matching: memory matching vs. simultaneous. *Color Research and Application,* 2001, **26**(6), 458–468, doi: 10.1002/col.1066.
21. JIN, Elaine W., SHEVELL, Steven K. Color memory and color constancy. *Optical Society of America,* 1996, **13**(10), 1981–1991, doi: 10.1364/JOSAA.13.001981.
22. OPPER, Jamie K. *Color memory for objects with prototypical color mismatch.* Fort Collins : Colorado State University, 2013, pp. 16–25.

Habiba Halepoto[1, 2], Tao Gong[1, 2], Kashif Kaleem[2]
[1] Donghua University, Engineering Research Center of Digitized Textile and Fashion Technology, Shanghai 201620, China
[2] Donghua University, College of Information Science and Technology, Shanghai 201620, China

Real-Time Quality Assessment of Neppy Mélange Yarn Manufacturing Using Macropixel Analysis

Ocenjevanje kakovosti proizvodnje nopkaste melanžne preje v realnem času z analizo makrotočk

Original Scientific Article/*Izvirni znanstveni članek*
Received/*Prispelo* 6-2019 • Accepted/*Sprejeto* 8-2019

Abstract

The aim of this paper is to provide a simple MATLAB-based model to determine the real-time homogeneity of neppy mélange yarn fabrics. Currently, the mélange yarn industry relies solely on visual assessment and experience. This algorithm, however, proposes a solution for the mélange yarn industry. The designed algorithm presented in this paper, which is based on kernel density function and macropixel analysis, was implemented for the real-time nep detection of neppy mélange yarns and calculated an inhomogeneity of neps of around 91%. This strategy would be useful for the mélange yarn industry and can also be used in other types of fashion yarns.
Keywords: computer vision, neppy yarn, macropixel analysis, real-time

Izvleček

V članku je predstavljen preprost model, zasnovan v programu MATLAB, za določitev homogenosti pletiv iz melanžne preje v realnem času. Danes se v industriji pri izdelavi melanžne preje opirajo le na vizualne ocene in izkušnje, zato je predlagani algoritem rešitev za industrijsko proizvodnjo melanžne preje. Zasnovani algoritem temelji na oceni gostote jedra in analizi makrotočk za sprotno zaznavanje nopkov v melanžni preji. Izračunana nehomogenost efektne preje je bila približno 91-odstotna. Ta strategija je uporabna v proizvodnji melanžne preje in tudi drugih tipov modnih prej.
Ključne besede: računalniški vid, nopkasta preja, analiza makrotočk, realni čas

1 Introduction

Blending different fibres yields different types of fancy yarns [1]. There is still strong market potential for fancy yarns, which remain more eye-catching than conventional yarns [2]. Mélange yarns is one type of fancy yarn [3]. Mélange yarns come in a wide variety of looks and colours [4]. This class of yarns is produced by either mixing different coloured fibres in a blow room, or by mixing or blending in draw frames [5]. One of the major classes of these mélange yarn is neppy mélange yarn, in which a certain number of neps are introduced to achieve unique aesthetics.

Textile image processing has gained a great deal of attention recently. To date, several researchers have focused on various aspects of textile image processing, including defect detection in woven fabrics [6–7], fabric weave pattern recognition and yarn colour recognition [8–9]. To the best of our knowledge, however, none of the researchers have focused on textile image processing for the mélange yarn industry.

Quality assurance and textile testing constitute one of the central departments of any yarn spinning

Corresponding author/*Korespondenčni avtor:*
Tao Gong
E-mail: taogong@dhu.edu.cn
ORCID: 0000-0003-0248-9404

operation. Some quality tests, including yarn count, evenness, tenacity, elongation at break, shade matching, variation and the visual appearance of finished goods, are performed before shipment in order to avoid the cancelation of orders. A couple of decades ago, shade matching and variation were one of the main reasons for the cancelation of orders. Thus, in past decades, too much research was performed on shade matching and minimising variation. As a result, various technologies have been developed to avoid the rejections of orders.

Despite a great deal of research regarding other quality parameters, less attention has been given to assessing the visual appearance of finished goods. Even today, neppy yarn texture recognition relies on human skills and experience, and is thus performed manually by visual inspection. The method of visual inspection is, of course, inadequate, laborious and time-consuming, and leads to problems of subjective human factors, monotony and fatigue, physical and mental overload, and low efficiency. In order to fully understand the aesthetics of mélange yarn, however, full image feature extraction or image segmentation is necessary to understand the different spatial/lattice positions and range/colour domain of a single element in an image (simply matching the shade of yarn is insufficient). This might be understood easily by two related features, i.e. tone and texture, in terms of greyscale in which each pixel in an image has its own intensity value [10]. In this paper, tone is defined as the variation in the grey level of an image, while texture is defined as the dimensional distribution of tone as a cluster of pixel intensities that repeats itself in a specific region of an image [11]. To date, the mélange yarn industry has relied solely on spectrophotometry which, despite being very expensive, fails to determine the homogeneity or inhomogeneity of the yarn texture generated by neps in mélange yarn.

Two images would have a similar greyscale tone histogram if both images have similar elements, but a different dimensional distribution due to the same number of pixels and pixel resolution from the same elements. Thus, the tone level characterisation in itself is insufficient to fully understand an image, as it might only be good for analysing colour distribution. Consequently, texture must also be considered to match the requirement of similar aesthetics and appearance, which vary from fully disorganised to highly systematic in terms of dimensional distribution. This dimensional distribution might be analysed in terms of regularity in a histogram (statistically), in parallel lines (structurally) with empiric prototypical (model-based) and post-wavelet transformation (transform-based) [12]. Haralick et al proposed a grey-level co-occurrence matrix by generating a matrix through clustering and correlating those clusters with their neighbouring clusters [10]. In the grey-level co-occurrence matrix, the scale of scrutiny is a critical step for ensuring all important information is present [13].

In this paper, we have proposed a simple MATLAB-based algorithm to determine the homogeneity of neppy mélange yarn, which might be useful for the textile mélange yarn industry for determining the textural effect, together with shade matching and other quality parameters.

2 Experimental

2.1 Materials

Xinjiang medium-grade cotton from the Wuxi No. 1 cotton-spinning mill for routine production was used for this study. Basic fibre and yarn properties are presented in Table 1.

Table 1: Basic properties of fibre and yarn

Property	Value
Fibre staple length	28.7 mm
Fibre fineness[a)]	4.38 μg/inch
Yarn count	295.25 dtex[b)]
Nep content	3%

[a)] Micronaire value, [b)] 20 Ne

2.2 Methods

We made a real-time video of the manufacturing of neppy mélange yarn fabric using a digital camera (Canon EOS 6D S, 20.2 megapixels with pixel dimensions of 5472 × 3648 and pixel size of 6.54 μm). Simulations of all images and the analysis of the continuous-level moving block algorithm were performed using MATLAB v2017b (Mathworks, MA, USA). The aim of this paper was to define real-time monitoring for final neppy yarn. Initially, we monitored and studied a real-time analysis of neppy mélange fabric during the manufacturing process (see, Figure 1). For the first time, we have proposed a

strategy for the real-time monitoring of neps and the homogeneity thereof in neppy yarn fabrics by installing a digital camera adjacent to the production line. In this study, the rotation speed of the sock sampling machine was set at 80 rpm during the production of single-jersey fabric from cotton yarn of 295.25 dtex (20 Ne).

Figure 1: Test image of neppy mélange yarn fabric

2.2.1 Kernel density function

Kernel density function is one of the most popular non-parametric density functions. The multivariate kernel density function, with the points x_i, I = 1, 2, 3 … n, characterises the population and unknown density functions *f(x)* [14–15] and which is mathematically expressed as equation 1:

$$\hat{f}(x) = \frac{1}{nh^d} \sum_{i=1}^{n} K\left(\frac{x - x_i}{h}\right) \quad (1),$$

where K is the kernel (a non-negative function) and h is the bandwidth smoothing parameter, which is greater than 0.

2.2.2 Macropixel analysis

Macropixel analysis scrutinises the self-information contained in an image at different sublevels (macropixels) to generate a homogeneity curve using the collective standard deviation of all sublevels [16]. Macropixel analysis works through the collaborative scanning of discrete level tiling and the continuous-level moving block, which uses non-coinciding tiles and all possible sublevels of an image, respectively. Moreover, it should be assumed that the elements that form an image are indivisible and that images are binary, i.e. they only contain object values of either 0 or 1.

Consider the images shown in Figure 2: if, these images have dimensions $I \times J$ which are divided into sublevels $S_{I'J'}$ and each square is indivisible with the dimensions $I' \times J'$, the total number of possible sublevels of an image can be calculated using equation 2, while the shift of sub-windows is illustrated in Figure 2.

$$TOTAL_{sI'J'} = [I - (I' - 1)] \times [J - (J' - 1)] \quad (2)$$

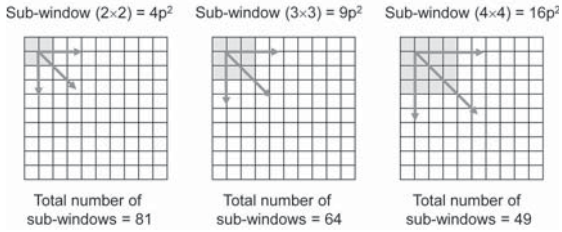

Figure 2: Three examples of sub-windows, i.e. 2, 3 and 4 squared pixels

The standard deviation (*SD*)for each sublevel can be determined using equation 3.

$$SD_{S_{I'J'}} = \sqrt{\frac{\sum_{i'=1}^{I'} \sum_{j'=1}^{J''} (TOTAL_{S_{I'J'}} - \bar{s})}{PIX_{S_{I'J'}} - 1}} \quad (3)$$

Consequently, the mean standard deviation (*Sw*) for each sublevel can be determined using equation 4. Their corresponding values are plotted in Figure 3.

$$Sw_{I'J'} = \frac{\sum \mathrm{STD}_{S_{I'J'}}}{TOTAL_{S_{I'J'}}} \quad (4)$$

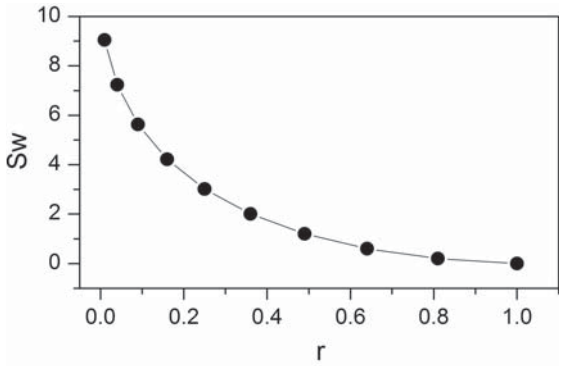

Figure 3: Corresponding value of the mean standard deviation of all the sub-windows

Because the image size plays a vital role, the calculated standard values should be comparable between images. This comparison might be done using the relative size of macropixels (r) in the image, which can be determined using equation 5:

$$r = \frac{I' \times J'}{I \times J} \quad (5).$$

3 Results and discussion

3.1 Nep detection

We first obtained results from the application of an algorithm. This algorithm was applied to segmented images of the dataset of neppy mélange yarn fabric. Segmentation was performed according to the pixels of images. The performance of the proposed method was tested. The kernel density estimation plots of neppy yarn fabric are illustrated in Figure 4. This kernel function helped to determine the neps in real-time during the manufacturing of neppy mélange yarn fabric.

A total of 388 frames were analysed for the neppy yarns, and their corresponding coloured images transformed into binary images, as shown in Figure 5. This binary conversion of images would result in the better analysis of homogeneity in order to avoid the surficial and textural effects of the neppy mélange fabric.

3.2 Homogeneity analysis

Analysing the homogeneity of neppy mélange yarn fabric is very beneficial for this segment of the textile industry in terms of discussing the homogeneity parameter, together with other parameters to meet the relevant standards and avoid the cancelation of orders. Actual homogeneity, and modelled homogenous and inhomogeneous neppy mélange yarn fabric are illustrated in Figure 6a. The matching sample was less homogenous and

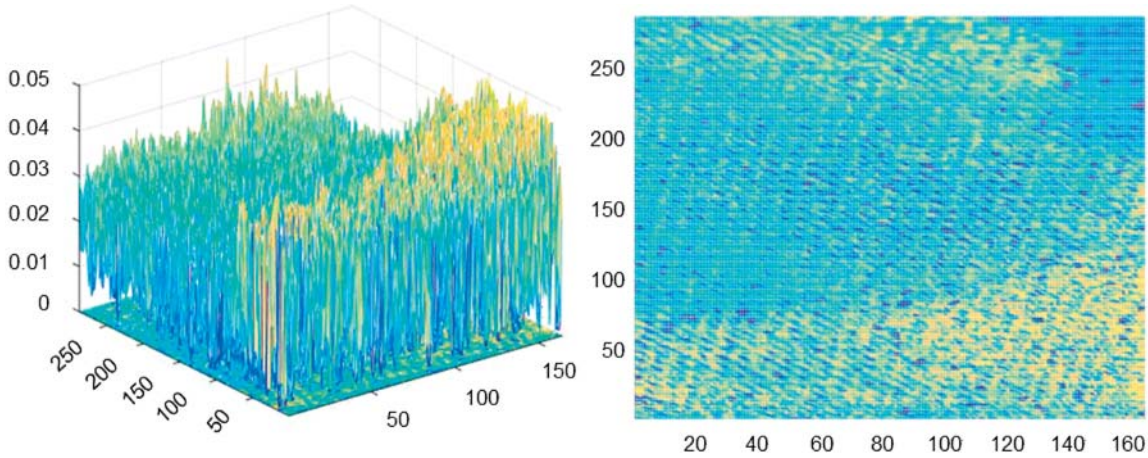

a) *b)*

Figure 4: Kernel density estimation plots of neppy mélange yarn fabric: a) 3D view, b) top view

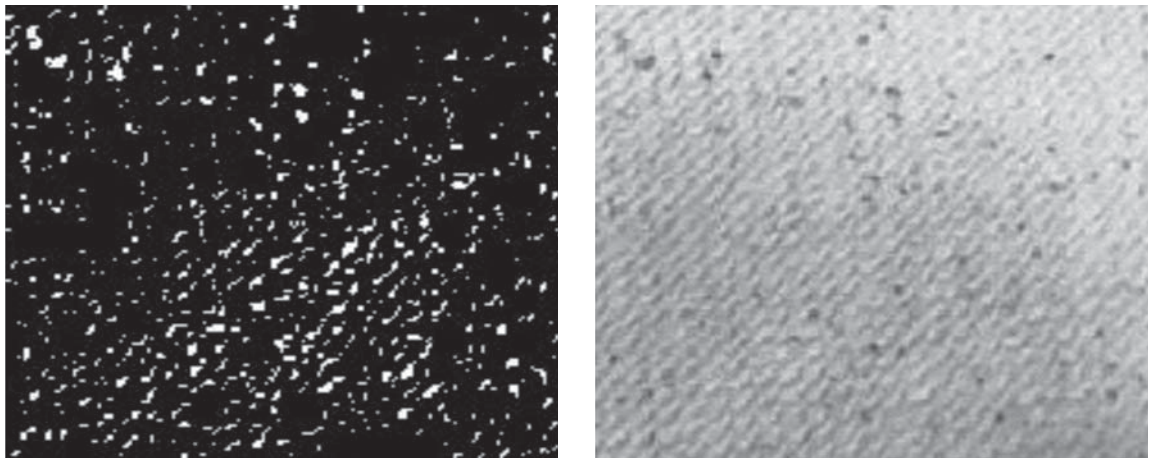

a) *b)*

Figure 5: Nep detection of neppy mélange yarn fabric (a); and neps detection using 388 frames (b) – original frame from 388 frames

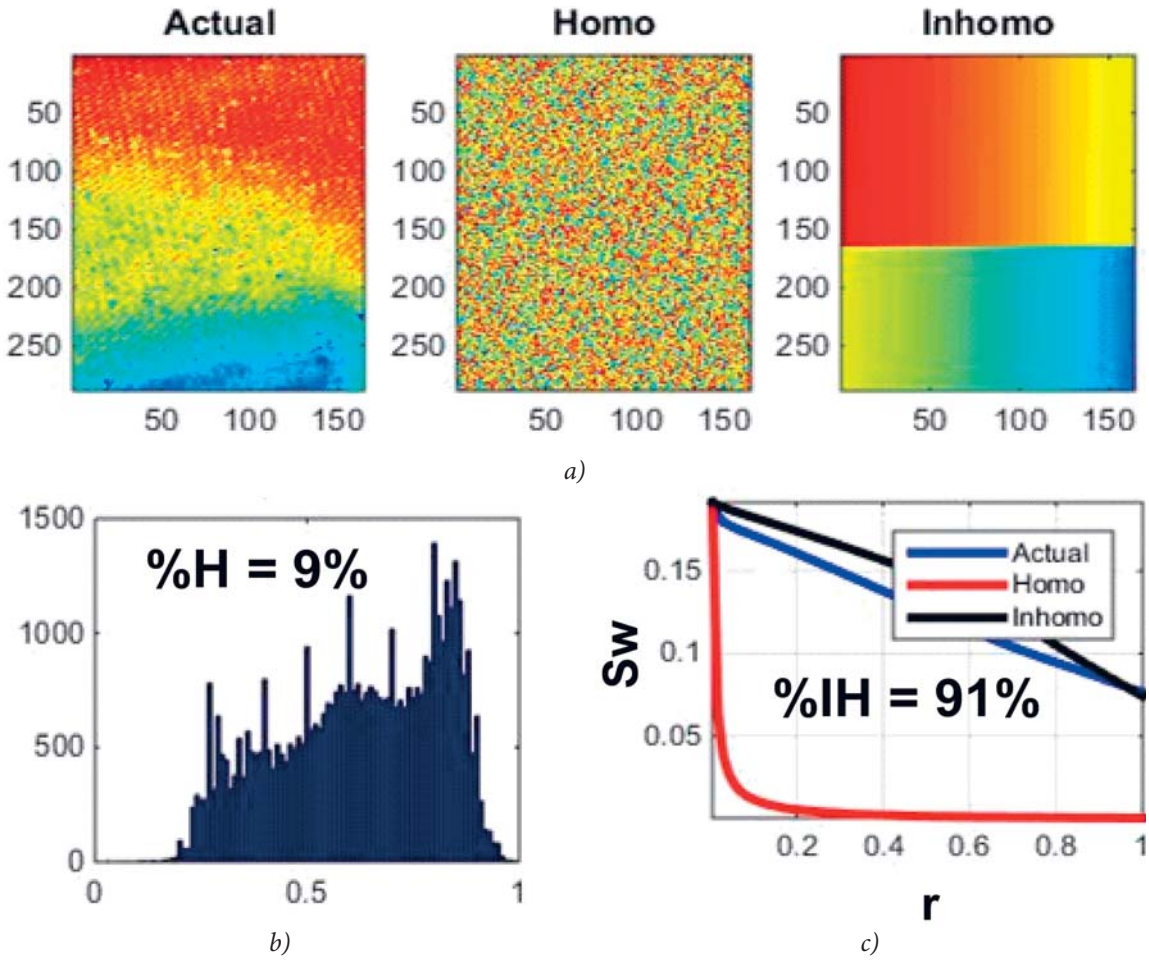

Figure 6: Homogeneity analysis of neppy mélange yarn fabric (a), actual homogeneity and modelled homogenous and inhomogeneous neppy mélange yarn fabric; (b) histogram of actual neppy mélange yarn fabric; and (c) homogeneity curve showing a homogeneity of 9%

was thus more similar to the inhomogeneous sample. It is also useful to see the distribution of homogeneity, which is shown in the histogram of actual neppy mélange yarn fabric (see Figure 6b). In addition, a homogeneity curve showing a homogeneity of neps over the fabric of 9% is presented in Figure 6c.

Because homogeneity was only 9%, the curve of neppy fabric is close to the inhomogeneous curve. The inhomogeneity of the image can be calculated using equation 6. This means that the fabric was more inhomogeneous, i.e. 91%. This inhomogeneity is desired for aesthetic functionality and for attracting the observer's attention to the design of neppy mélange yarn.

$$IH = 100 - H\% \ (\%) \qquad (6)$$

4 Conclusion

In this study, a simple MATLAB-based model was proposed for determining the real-time homogeneity of neppy mélange yarn fabrics. This might serve as a helpful tool for quality assessment in the textile mélange yarn industry with the aim of replacing the current inconsistent visual assessment based solely on experience. The neps from neppy mélange yarn fabric production were identified using kernel density algorithm. We determined that the inhomogeneity determined using the MATLAB code was as high as 91%, which is, of course, impossible to determine using only the bare eye. It is therefore very helpful for the textile industry and can also be used in other different types of fashion yarns. This research may be expanded in several ways, i.e. by

studying the effect of homogeneity on mechanical properties using an image processing technique. The surficial effect of a fabric, which requires a 3D model and thus pixel analysis in three dimensions, can also be analysed. Moreover, multi-coloured neps might also be analysed directly without converting them to greyscale.

References

1. BEHERA, B. K., HARI, P. K., BANSAL, S., SINGH, R. Effect of different blending methods and blending stages on properties of mélange yarn. *Indian Journal of Fibre and Textile Research*, 1997, **22**, 84–88.
2. GONG, R. H., WRIGHT, R. M. Structures and formation of fancy yarns. In *Fancy yarns: their manufacture and application*. Boca Raton, FL: CRC Press, Cambridge : Woodhead Publishing, 2002, pp. 33–59, doi: 10.1533/9781855737525.33.
3. MOGHASSEM, Abdolrasool. Damaging of dyed cotton fibers with direct dye in spinning processes and its effect on the properties of cotton mélange yarn. *International Journal of Engineering – Transactions B: Applications*, 2007, **20**(2), 203–210.
4. KAN, Chi-Wai, WONG, Wai-Yin. Color properties of cellulase-treated cotton denim fabric manufactured by torque-free ring spun yarn. *Textile Research Journal*, 2011, **81**(9), 875–882, doi: 10.1177/0040517510391699.
5. GHAREHAGHAJI, Ali Akbar, TAVANAIE, H., KARIM, S. Study on the interactions between mélange yarn properties and fiber damage. *Arabian Journal of Geosciences*, 2011, **4**(7–8), 1117–1130.
6. ZHANG, Kaibing, YAN, Yadi, LI, Pengfei, JING, Junfeng, LIU, Xiuping, WANG, Zhen. Fabric defect detection using salience metric for color dissimilarity and positional aggregation. *IEEE Access*, 2018, **6**(1), 49170–49181, doi: 10.1109/access.2018.2868059.
7. LI, Yundong, ZHAO, Weigang, PAN, Jiahao. Deformable patterned fabric defect detection with fisher criterion-based deep learning. *IEEE Transactions on Automation Science & Engineering*, 2017, **14**(2), 1256–1264, doi: 10.1109/TASE.2016.2520955.
8. KHAN, Babar, WANG, Zhijie, HAN, Fang, IQBAL, Ather, MASOOD, Rana Javed. Fabric weave pattern and yarn color recognition and classification using a deep ELM network. *Algorithms,* 2017, **10**(4), 117–129, doi: 10.3390/a10040117.
9. KHAN, Babar, FANG, Han, WANG, Zhijie, MASOOD, Rana J. Bio-inspired approach to invariant recognition and classification of fabric weave patterns and yarn color. *Assembly Automation*, 2016, **36**(2), 152–158, doi: 10.1108/AA-11-2015-100.
10. HARALICK, Robert Martin, SHANMUGAM, K., DINSTEIN, Its'Hak. Textural features for image classification. *IEEE Transactions on Systems, Man, and Cybernetics*, 1973, **SMC-3**(6), 610–621, doi: 10.1109/TSMC.1973.4309314.
11. BHARATI, Manish H., MACGREGOR, John F. Texture analysis of images using principal component analysis. In *SPIE/Photonics Conference on Process Imaging for Automatic Control : proceedings*. Boston : The International Society for Optical Engineering, 2001, pp. 27–37, doi: 10.1117/12.417179.
12. BHARATI, Manish H., LIU, Jay, MACGREGOR, John F. Image texture analysis: methods and comparisons. *Chemometrics & Intelligent Laboratory Systems*, 2004, **72**(1), 57–71, doi: 10.1016/j.chemolab.2004.02.005.
13. MISSIAEN, J. M., THOMAS, G. Homogeneity characterization of binary grain mixtures using a variance analysis of two-dimensional numerical fractions. *Journal of Physics Condensed Matter*, 1995, **7**(15), 2937–2948, doi: 10.1088/0953-8984/7/15/002.
14. FUKUNAGA, Keinosuke, HOSTETLER, Larry D. The estimation of the gradient of a density function, with applications in pattern recognition. *IEEE Transactions on Information Theory*, 1975, **21**(1), 32–40, doi: 10.1109/TIT.1975.1055330.
15. COMANICIU, Dorin I. *Nonparametric robust methods for computer vision : thesis*. New Brunswick : Rutgers The State University of New Jersey, 2000.
16. HAMAD, Mazen L., ELLISON, Christopher D., KHAN, Mansoor, LYON, Robbe C. Drug product characterization by macropixel analysis of chemical images. *Journal of Pharmaceutical Sciences*, 2007, **96**(12), 3390–3401, doi: 10.1002/jps.20971.

Rimma Uysal, Jack B. Stubbs
University of Central Florida, Institute for Simulation and Training, Prototype Development and 3D Print Lab, Orlando, FL 32826, USA.

A New Method of Printing Multi-Material Textiles by Fused Deposition Modelling (FDM)

Nova metoda tiskanja tekstilij iz več materialov s pomočjo tehnologije ciljnega nalaganja

Original Scientific Article/*Izvirni znanstveni članek*
Received/*Prispelo* 9-2019 • Accepted/*Sprejeto* 9-2019

Abstract

3D printing is considered to be the key technology for future production processes. It has recently found its way into the field of the textile industry and promises to revolutionise the textile supply chain. It is of particular interest for the production of customised items and other structures which cannot be produced with common techniques. Large apparel companies have already integrated 3D printing into their manufacturing processes to print parts like soles and accessories. However, 3D printed garments that are ready to wear can still not be found. Due to the lack of suitable printing materials, research in 3D printed textiles is still in its initial stage. This research contributes to the development of 3D printed textiles by using Fused Deposition Modelling (FDM). In this study, a new method for printing textile-like surfaces was developed which combines different materials into an interrelated flexible structure. Several textile-like surfaces were designed on this basis and finally applied to a wearable garment. Furthermore, the advantages of 3D printing for the textile supply chain were demonstrated.
Keywords: 3D printing, 3D printed textiles, textile-like structures, multi-material printing, FDM printing, novel structures

Izvleček

3D tiskanje velja za ključno tehnologijo proizvodnih procesov v prihodnosti. Tudi na področju tekstilne industrije si je že utrla pot, kjer se napovedujejo revolucionarne spremembe tekstilne dobavne verige. Zlasti je zanimiv za izdelavo izdelkov po meri in drugih struktur, ki jih ni mogoče izdelati z običajnimi tehnologijami. Velika oblačilna podjetja so v svoje proizvodne procese že vključila 3D tiskanje, da bi natisnili dele, kot so podplati in dodatki. Vendar 3D natisnjenih oblačil, ki so primerna za nošenje, še ni na voljo. Zaradi pomanjkanja primernih tiskarskih materialov so raziskave 3D tiskanih tekstilij še v začetni fazi. Ta raziskava prispeva k razvoju 3D tiskanega tekstila z uporabo tehnologije ciljnega nalaganja. V tej raziskavi je bila razvita nova metoda tiskanja tekstilijam podobnih površin, ki združuje različne materiale v medsebojno prožno strukturo. Na tej podlagi je bilo oblikovanih več, tekstilijam podobnih, površin, ki so bile končno nanešene na nosljivo oblačilo. Prikazane so tudi prednosti 3D tiska za tekstilno dobavno verigo.
Ključne besede: 3D tisk, 3D tiskani tekstil, tekstilijam podobne strukture, tisk z več materiali, ciljno nalaganje, nove strukture

1 Introduction

The 3D printing technology is increasingly used in the textile industry. Additive manufacturing is a generic term for all manufacturing processes in which material is applied layer by layer to produce three-dimensional objects. 3D printing offers the decisive advantage of customised products, which

Corresponding author/*Korespondenčna avtorica:*
Rimma Uysal
E-mail: Rimma.uysal@gmail.com
ORCID: 0000-0002-2879-8056

are accessible to everyone due to the low cost. In addition, 3D printing can reduce complexity in the supply chain and reduce time to market by accelerating prototyping [1]. The creative minds of the textile industry have quickly realised that the potential of 3D printing lies in the development of new structures that cannot be achieved with common processes. Large apparel companies have already integrated 3D printing into their manufacturing processes. Increasingly more fashion items, e.g. 3D printed soles [2] and accessories [3], can be now purchased in stores.

While these products are ready for the market, the development of 3D printed textiles is still in its initial stage. Despite the increased interest in 3D printing in the textile industry, it is surprising that so little research has been conducted to 3D printed textiles. In this field, the researchers are faced with special challenges. The lack of suitable materials and techniques complicates the development of 3D printed textiles. Thus, the development of 3D printed textiles seems to be very difficult, resulting in the same wearing comfort and durability as conventional garments. Past studies have shown that 3D printing is not yet suitable for the reproduction of textile surfaces and that the potential lies in creating novel textile-like structures [4]. Some studies have tried to combine the old and new technology. 3D printing on textile surfaces has been investigated allowing creating new multicomponent textiles and new optical properties [5, 6]. Here, the adhesion between both materials still remains challenging and has led to further studies to enhance the bonding properties between two different materials [7] due to fabric pre-treatment [8, 9]. Furthermore, a study where fibrous materials were embedded in the printing process served as an input for this research [10].

This study was focused on creating textile-like surfaces by using the FDM technology and led to the development of a new printing method. The new printing method combines different materials into one structure, similar to that of a conventional textile. Another focus of this study was on creating flexible and wearable textile-like surfaces.

2 Materials and methods

To create textile-like surfaces, a new printing method was developed and applied. This method influences the printing behaviour of a 3D printer. Since usually, the settings in the slicer software determine the printing behaviour, detailed sketches were made in this study for each layer of the print model to intend or at least to influence the printing behaviour. The sketches were made in Adobe Illustrator by taking specific units of measurement into account and then processed into 3D models by using the animation software Blender. Afterwards, the 3D models were scaled and placed in a print position in the CAD software Autodesk Netfabb. Simplify3D was used to slice the STL files. Here, several print settings were made to optimise the print results. The 3D models were printed in the Prototype Development and 3D Print Lab (PD3D) at the University of Central Florida in Orlando. In this study, two FDM printers were used. Models made of two different materials were printed with the 3D printer X400 (German RepRap GmbH, Feldkirchen, Germany). Models made of more than two different materials were printed with the 3D printer CR-10 (Creality3d, Shenzhen, China) in combination with Palette 2 Pro (Mosaic Manufacturing Ltd, Toronto, Canada). For printing, the filaments PLA (Hatchbox 3d, Pomona, CA, USA) and LAY-FOMM 40 (CC-Products, Cologne, Germany) were used. In the last step, the printed models were post-treated. In the continuation, a step-by-step example of the printing method, using various programs, materials and tools is presented.

2.1 Structure of 3D printed textile-like surfaces

The printing method is illustrated in the following steps by means of a 10 cm × 10 cm textile-like surface. This model was printed from two different materials and consists of 11 layers. Layers 2, 4, 6, 8, 9, 10 and 11 represent the elastic basic structure of the model, the last four layers being intended for contact with the skin surface. This basic structure consists of several parallel strands with varying orientation in different layers. The basic structure was printed from the material LAY-FOMM 40. Layers 1, 3, 5 and 7 result in the visible surface of the model and consist of many repeating patterns, here polygons, printed from PLA. All layers are coordinated with each other and together form a system of structures (cf. Figure 1A). If a polygon surface is printed on another polygon surface during the printing process, the two join through the thermoplastic process and enclose the strands in-between (cf. Figure 1B). The strands connect the polygons and result in a coherent structure (cf. Figure 1C) in which both materials cannot be separated from each other.

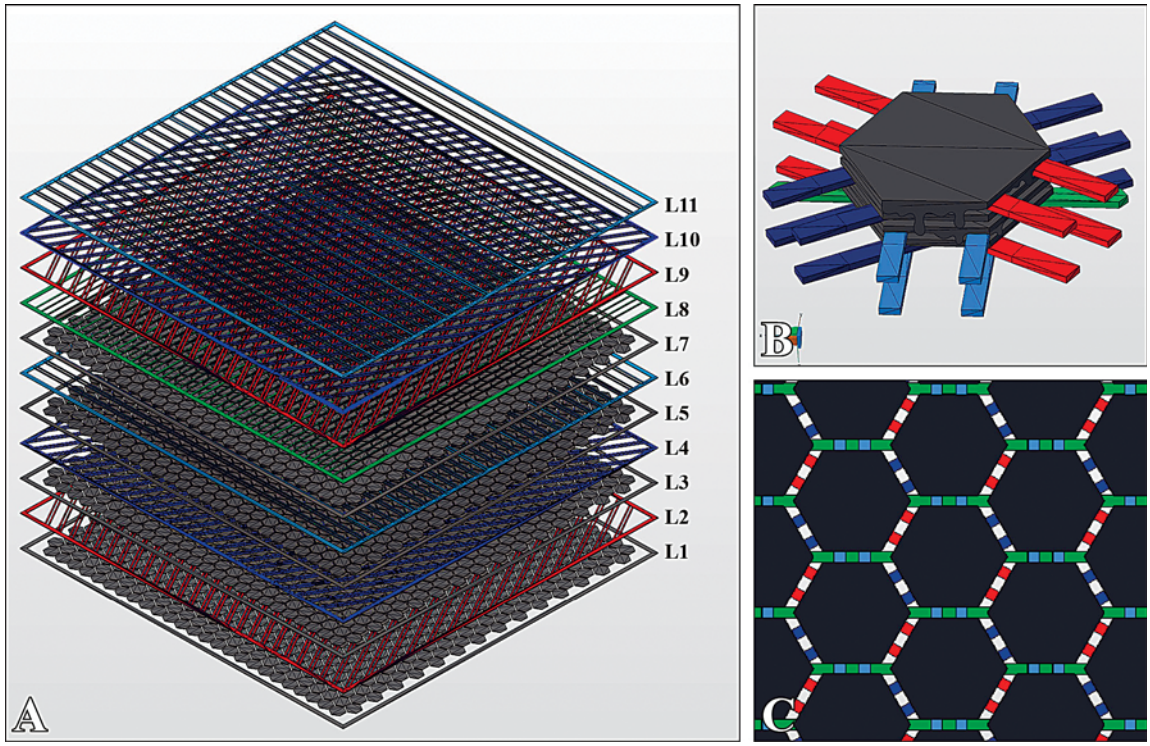

Figure 1: Illustration of textile-like surface in Netfabb: A) structure of layers, B) connected polygons through thermoplastic process, C) coherent structure

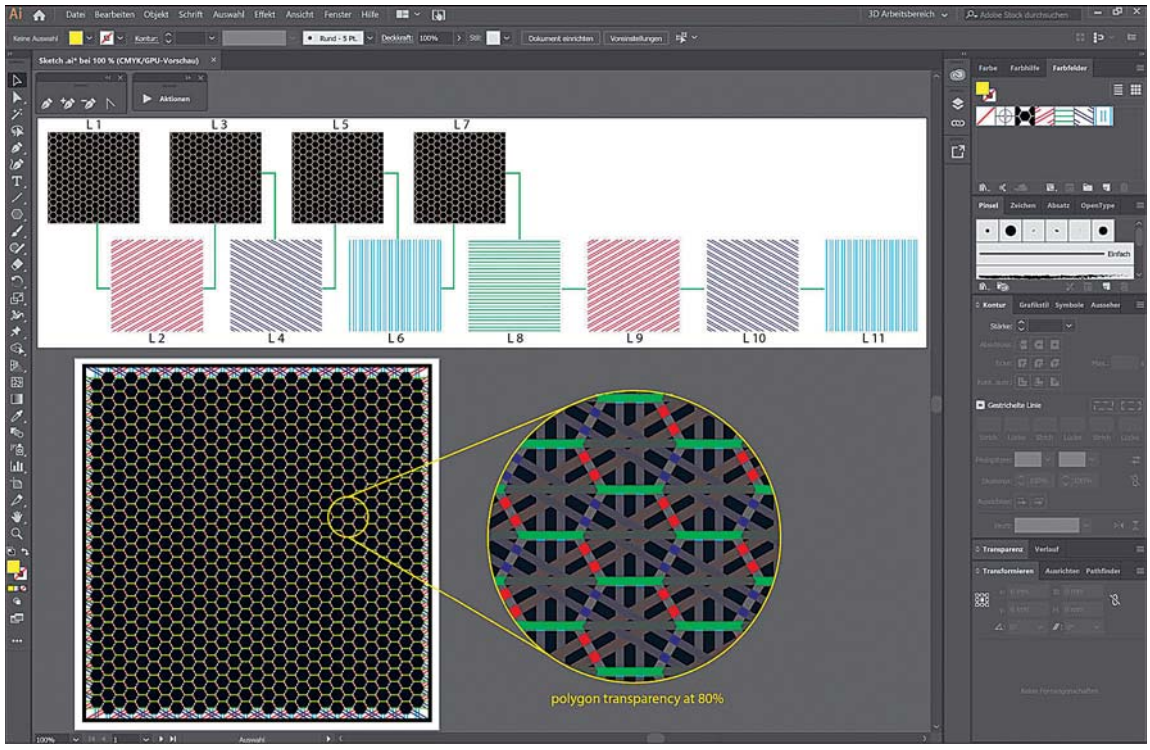

Figure 2: Sketch in Adobe Illustrator

2.2 Preparation of sketch

The sketches were created with the vector graphics editor Adobe Illustrator CC 2019. The creation of the sketch for this printing method is very detailed, each layer has its own sketch. In the end, the 10 cm × 10 cm model has over 2,000 individual elements. To simplify the drawing, Illustrator patterns were created [11]. This seamless repeating pattern can be applied to any graphic. By creating the patterns, certain dimensions must be adhered to. In this example, one pattern was created for the polygon surface and four patterns for the connecting strands with different orientations. The connecting strands were drawn with 1 point (pt) line thickness (0.35 mm), which corresponds to one extrusion of the 3D printer. The distance between the connecting strands was also 1 pt so that they do not fuse together. The repeating pattern of the polygon had the size 4 mm × 3.5 mm, the distance between the polygons was 1 pt. A frame was drawn around the textile-like surface for the individual strands to adhere to it during the printing process. The line thickness of the frame was 4 pt (cf. Figure 2). Patterns were converted into outlines, the so-called paths, before export. The operation was made easier by recording actions [12]. Several consecutive steps were performed by playing the action. The sketch was exported as an SVG-file for each layer and for each material individually. In this example, 11 SVG files were exported.

2.3 3D modelling

Blender version 2.78 was used in this study. Each SVG file was imported in Blender and extruded to a three-dimensional object. The extruded object is initially a curve object that must be converted to a mesh model. 3D models were exported individually as STL files. In this example, 11 STL files were exported.

2.4 Processing in Netfabb

The Autodesk Netfabb Premium Version 2018 was used to process the STL files. Since Blender does not work with real dimensions, the next step was to scale the exported STL models to their original size. The original size corresponds to the dimensions (X = width, Y = height) in Adobe Illustrator. Additionally, the Z-value was set in Netfabb to 0.15 mm. The Z-value should correspond to the Layer Height (LH) in the settings of the slicer program. Then, all layers were moved to their print position on the Z-axis. With an LH of 0.15 mm, the position of layer 1 (L1) is Z = 0 mm, L2 Z = 0.15 mm, L3 Z = 0.3 mm ... L11 Z = 1.5 mm. The layers were exported individually as STL. In this example, 11 STL files were exported.

2.5 Settings in slicer software

In this work, the software Simplify3D Version 4.0.0 was used for slicing the 3D models. Table 1 shows all relevant settings for the printing process. If certain settings are not listed, it can be assumed that the default values of Simplify3D were used.

2.6 3D printers and 3D printing filaments

For printing, the PLA and LAY-FOMM 40 materials were used. LAY-FOMM 40 is a micro-porous elastomer with a PVA filler, which will be dissolved in water after the printing and it only then gives the material its elastic properties. Since the material quickly absorbs moisture, the material must be dried before the printing according to the manufacturer's instructions [14]. Both filaments had the diameter of 1.75 mm.

The model was printed with the 3D printer X400. The printer was equipped with two extruders, each with a nozzle of 0.4 mm. PLA was fed to the left extruder, LAY-FOMM 40 to the right extruder. The distance between the print bed and nozzle was 0.15 mm. It was printed directly on the glass plate. The printing time of the 3D model was 2 h 29 min.

For the models made of more than two different materials (LAY-FOMM 40 plus two colours of PLA), a printer with more than two extruders was required; therefore, the 3D printer CR-10 (1 extruder, 0.4 mm nozzle) was used in combination with the Palette 2 Pro device. Palette 2 Pro is a device that combines up to four different materials into one filament, enabling multi-material printing with just one extruder [15].

2.7 Post-processing of printed models

The print model was removed from the print bed when cold, thus preventing the fine structures from being damaged with a scraper tool. The model was placed in water for 4 hours until the PVA was washed out, with the water being exchanged at least 3 times. In the next step, the model was dyed. To 1 litre of cold water, 6 tablespoons of RIT all-purpose dye (Nakoma Products LLC, Bridgeview, IL, USA) and 1 tablespoon of apple vinegar (Organic apple cider, Publix Supermarkets INC., Lakeland, FL,

Table 1: Settings for Simplify3D used in this study

Settings	Value	Comments
Extruder settings		
Extrusion width	auto	For both tools (extruders)
Retraction distance	1.0 mm	
Retraction vertical lift	1.0 mm	
Layer settings		
Layer height	0.15 mm	
First layer height	100%	
First layer width	100–120%	
First layer speed	40%	
Temperature settings		
Tool 0	200 °C	PLA
Tool 1	220 °C	LAY-FOMM 40
Heated Bed	60 °C	Glass plate
Scripts settings		
Tool change script [13]	G1 Y10 F4000 {IF NEWTOOL = 0}M104 S190 T1 {IF NEWTOOL = 0}M109 S200 T0 {IF NEWTOOL = 1}M104 S170 T0 {IF NEWTOOL = 1}M109 S220 T1	Go to Y 10 mm Set T1 to wait temperature Set T0 to print temperature Set T0 to wait temperature Set T1 to print temperature
Speed settings		
Default printing speed	2002 mm/min	
X/Y axis movement speed	3200 mm/min	
Other settings		
Tool change retraction distance	7 mm	
External thin wall type	Allow single extrusion walls	
Internal thin wall type	Allow gap fill	
Allowed perimeter overlap	20%	
Endpoint extension distance	0.9 mm	

USA) were added. The model was left in the dye bath for the next 6 hours and rinsed afterwards in running water. Next, the colour was fixed with RIT ColorStay Dye Fixative (Nakoma Products LLC, Bridgeview, IL, USA). The Color Fixative was sprayed pure onto the model and rinsed out after 1 hour under running water. The coloured model was carefully pressed dry with a paper towel. After the dyeing process, the porous LAY-FOMM 40 material was completely stained, on PLA, the dyeing process had no effect. Then, the model was placed in a water-glycerine solution (10% glycerine) (Vegetable Glycerin, Earth's Care Natural Products Inc., Long Beach, CA, USA) for one hour and then dried in the air. Glycerine is a naturally-occurring humectant that attracts and holds water molecules on a surface. It ensures that the LAY-FOMM 40 material does not dry out and retains its flexibility. In the end, the frame of the 3D model was cut off with scissors.

3 Results and discussion

By using the new printing method, various repeating patterns were created for the surface of textile-like structures. Furthermore, different effects on the

properties of textile-like surfaces were documented. Secondly, the surface of textile-like structures was modified with colours in order to meet the design-specific requirements of a textile. In the final step, the printing method was used to print a garment.

The following textile-like surfaces were created based on the new printing method. Different forms of repeating patterns such as polygons (cf. Figure 3A), rectangles (cf. Figure 3B) and floral shapes (cf. Figure 3C) were created and printed from PLA. It was shown that the choice of the pattern influences the properties of the textile-like surface. A patterned surface of polygons (4 mm × 3.5 mm each) is showing a different drape than a repeating pattern of rectangles (3.3 mm × 3.3 mm each) (cf. Figures 3D–E). Larger patterns (23.1 mm × 22.5 mm each) were also used; the larger the pattern, the more rigid the textile-like surface became (cf. Figure 3F). The size of the repeating pattern also has a large influence on the printing time of the model. The smaller the pattern, the longer the printing process takes. In this study, a repeating pattern of 4 mm × 4 mm was considered to be a good compromise between surface flexibility and printing time. In further experiments, the limit values should be investigated in order to answer the question which minimum size a repeating pattern could have in order to obtain the greatest possible flexibility of the textile-like surface. On the other hand, the maximum printing speed should be set for the printing method which ensures the same print quality.

The basic structure (connecting strands) was always adapted to different forms of the repeating pattern. Due to the different orientation of connecting strands, it was attempted to take into account the tensile directions acting on a textile surface. The flexibility of the surface could also be influenced by the number of layers and especially by the number of connecting strands. The more connecting strands the structure contains, the more rigid the surface became (cf. Figures 4 A–C) and at the same time, the tensile strength of the structure increased. In this study, a good compromise between flexibility, elasticity and tensile strength of the textile-like surface was perceived with a print model consisting of 11 layers (cf. Figure 4C). Future work will include the determination of mechanical properties such as tensile strength due to the differences in the number of connecting strands, the orientation of connecting strands, printing speed and the value of Extrusion

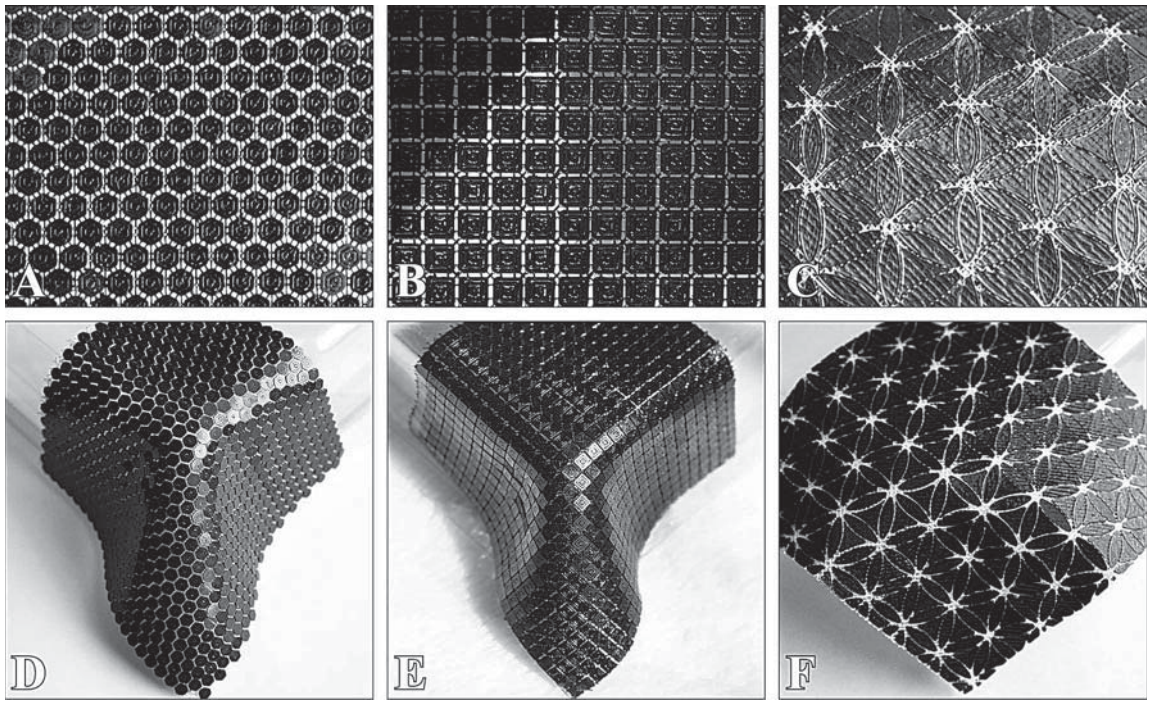

Figure 3: Illustration of different repeating patterns: A) polygon pattern, B) rectangles pattern, C) floral pattern, D) fabric-like drape with polygon pattern, E) fabric-like drape with rectangles pattern, F) drape with big patterns

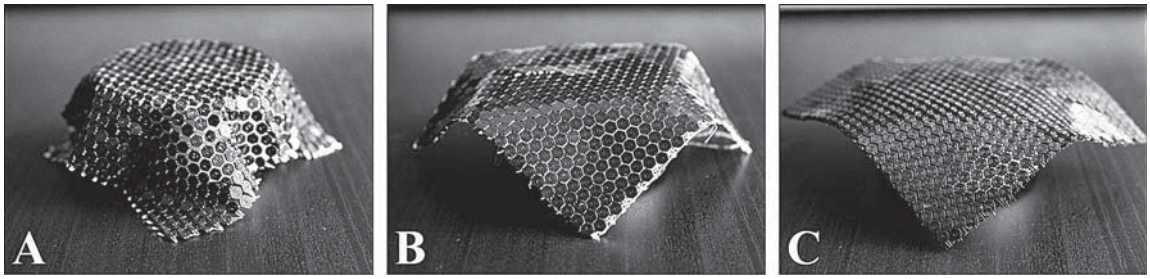

Figure 4: Different flexibilities due to number of layers: A) 5 layers (3 layers PLA, 2 layers LAY-FOMM 40), B) 7 layers (4 layers PLA, 3 layers LAY-FOMM 40), C) 11 layers (6 layers PLA, 5 layers LAY-FOMM 40)

Multiplier (EM). This experiment showed that it is possible to print multi-material textile-like structures by using the FDM technology.

An important aspect of this work was to ensure the wearing comfort of textile-like surfaces. These properties could be ensured by the flexible and elastic printing material LAY-FOMM 40. According to the manufacturer, LAY-FOMM 40 is harmless and food-safe [14]; therefore, four layers of LAY-FOMM 40 were printed on each model to serve as a skin contact surface (cf. Figure 5A). Basically, it is a printed layer of an inner lining, which is also incorporated in conventional clothing. With manual intervention during the printing process on the Z-height of a layer, special effects could be achieved. On the one hand, by reducing the actual Z-height of the last four layers, it was possible to achieve a fusion of these layers, which form a dense surface (cf. Figure 5B). On the other hand, by increasing the Z-height between 7 and 8 layers, it was possible to separate the inner lining and the textile-like surface, which were only held together through the common edge (cf. Figure 5C). In this experiment, it was shown that the garment processing steps, such as attaching an inner lining to a garment, can be implemented in a single printing process.

In the further part of the study, the colour of the textile-like surface was modified in order to meet the design-specific requirements. At first, the repeating pattern was modified with different colours. The different colours were exported as a separate STL file and assigned to different processes in Simplify3D [16]. Figure 6A shows a textile-like surface with a two-colour pattern similar to an all-over print of a textile. In Figure 6B, every single surface was assigned to a different colour, to the so-called houndstooth pattern. The smaller the repeating patterns, the better the resolution of the image. In the next step, a simple image (Logo of University of Central Florida) was transferred onto a textile-like surface (cf. Figure 6C). At the edge of the image, individual polygons were divided into two colour areas. Even though the print became less accurate overall, the result was a clear presentation of the image. For the textile industry, this printing method could mean the elimination of dyeing and printing processes in the textile supply chain.

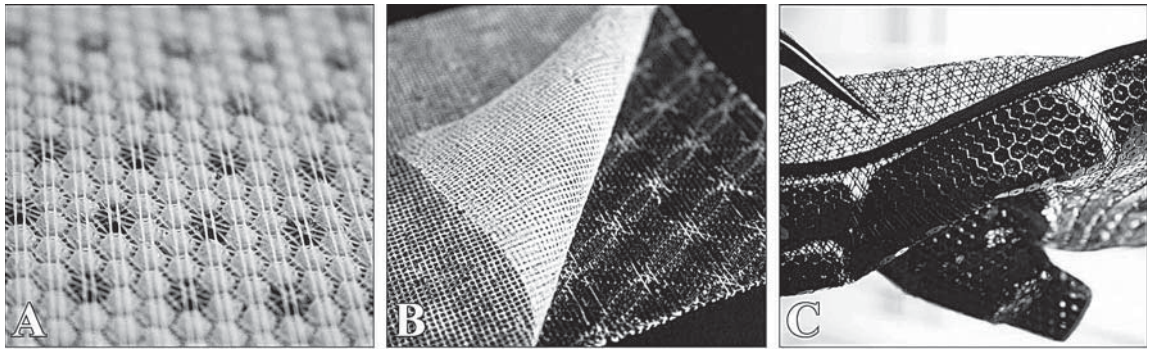

Figure 5: Printed inner lining: A) four layers LAY-FOMM 40 on top of textile-like surface, B) fusion of four layers of LAY-FOMM 40 by reducing Z-height, C) separation of inner lining and textile-like surface by increasing Z-height

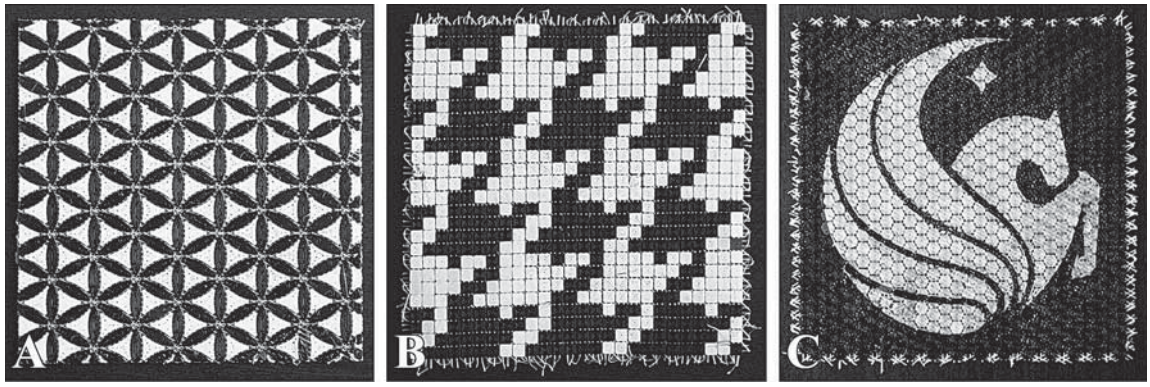

Figure 6: Colour modification of textile-like surfaces: A) two-colour pattern, B) coloured "pixels" to hound-stooth pattern, C) transferred UCF Logo on textile-like surface

In the last step of the study, the developed printing method was applied to one application case. In collaboration with a PhD project at the University of Central Florida in Orlando, a glove with incorporated sensors was printed on the basis of textile-like structures [17]. For the glove, sewing patterns were developed (cf. Figure 7A), which are also used in the textile industry to create garments. It was printed with the 3D printer X400, and the materials PLA and LAY-FOMM 40. Figures 7B–C show the surface design of the glove, the surface was printed partially with polygons, so that the connecting strands (natural colour of LAY-FOMM 40) can be seen in-between. The printed pattern pieces were post-treated as described above (without dyeing process) and sewn together to form a three-dimensional garment (cf. Figure 7D). In further experiments, it will be worked out how 3D printed textile-like surfaces can be sensibly connected with each other. On the one hand, special joining techniques such

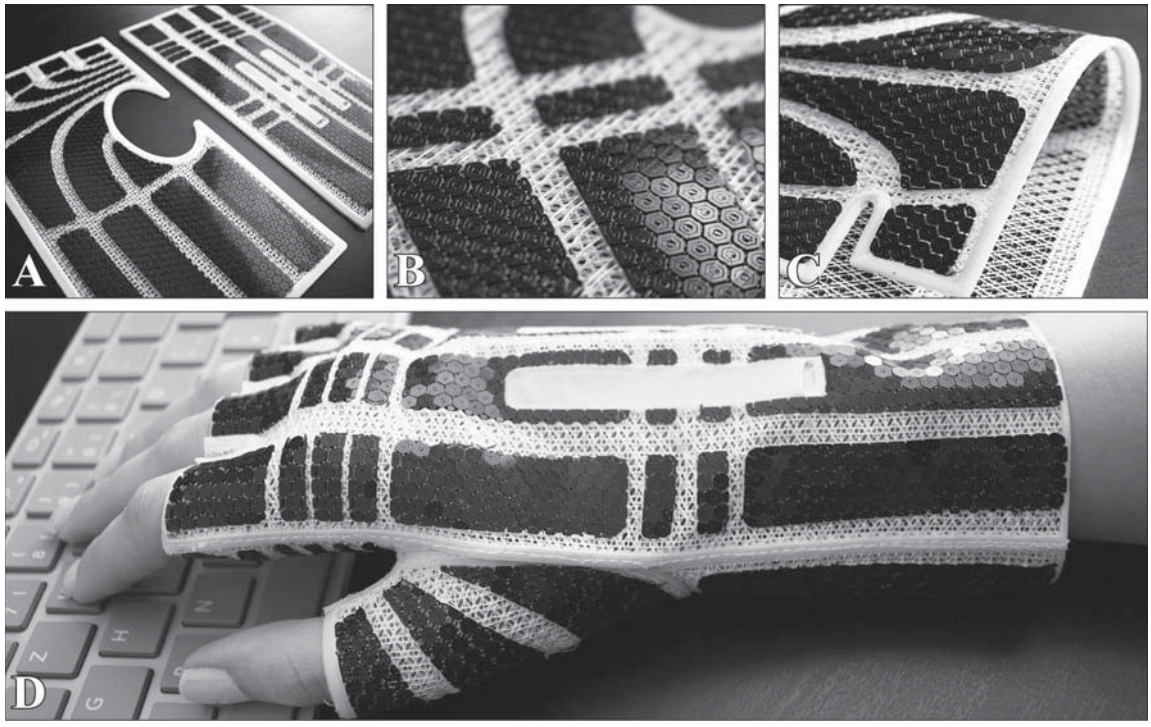

Figure 7: 3D printed glove: A) sewing pattern printed from two materials, B) surface design of glove, C) flexible sewing pattern with inner lining, D) pattern pieces sewn together to three-dimensional garment

as ultrasound could be used, whereas on the other hand, 3D printed connections could be developed, which connect textile-like surfaces without a further need for tools. In this experiment, it was shown that clothing patterns can be printed from several materials in one printing process. For the textile industry, this could mean the elimination of the cutting process in the textile supply chain.

4 Conclusion and outlook

A new method for printing textile-like surfaces was developed. Several materials were combined in the printing process (FDM) to a flexible coherent structure. On the basis of this printing method, sewing patterns were printed and assembled to a three-dimensional garment. It was shown that production steps of the textile supply chain such as fabric production, dyeing, colour printing, cutting and the application of other components such as inner linings can be implemented in a single printing process. Further developments will focus on improving the printing method and lead to further applications for the textile industry. The results of this study are showing the possibilities of 3D printed textiles, and serve as an inspiration for other researchers and designers to design garments by using the 3D printing technology.

Acknowledgement

The author offers her sincerest gratitude to the Prototype Development and 3D Print Lab (PD3D Lab) for giving the opportunity to print all samples as well as for providing the material and support for this research work.

References

1. ATTARAN, Mohsen. The rise of 3-D printing: The advantages of additive manufacturing over traditional manufacturing. *Business Horizons,* 2017, **60**(5), 677–688, doi: 10.1016/j.bushor.2017.05.011.
2. *Adidas* [online]. Adidas breaks the mould with 3D-printed performance footwear. [accessed 5. 7. 2019]. Available on World Wide Web: <https://www.adidas-group.com/en/media/news-archive/press-releases/2015/adidas-breaks-mould-3d-printed-performance-footwear/>.
3. *Jewelry* [online]. Shapeways [accessed 5. 8. 2019]. Available on World Wide Web: <https://www.shapeways.com/marketplace/jewelry>.
4. MELNIKOVA, Rimma, EHRMANN, Andrea, FINSTERBUSCH, Karin. 3D printing of textile-based structures by fused deposition modelling (FDM) with different polymer materials. *IOP Conference Series: Material Science and Engineering,* 2014, **62**, doi: 10.1088/1757-899X/62/1/012018.
5. SABANTINA, Lilia, KINZEL, Franziska, EHRMANN, Andrea, FINSTERBUSCH, Karin. Combining 3D printed forms with textile structures - mechanical and geometrical properties of multi-material systems**.** *IOP Conference Series: Material Science and Engineering,* 2015, **87**, doi: 10.1088/1757-899X/87/1/012005.
6. KORGER, Michael, BERGSCHNEIDER, Julia, LUTZ, Mirja, MAHLTIG, Boris, FINSTERBUSCH, Karin, RABE, Maike. Possible applications of 3D printing technology on textile substrates. *IOP Conference Series: Material Science and Engineering,* 2016, **141**(1), doi: 10.1088/1757-899X/141/1/012011.
7. GRIMMELSMANN, Nils, KREUZIGER, Mirja, KORGER, Michael, MEISSNER, Hubert, EHRMANN, Andrea. Adhesion of 3D printed material on textile substrates. *Rapid Prototyping Journal,* 2018, **24**(1), 166–170, doi: 10.1108/RPJ-05-2016–0086.
8. UNGER, Lena, SCHEIDELER, Marvin, MEYER, Pia, HARLAND, Julia, GÖRZEN, Andreas, WORTMANN, Martin, DREYER, Axel, EHRMANN, Andrea. Increasing adhesion of 3D printing on textile fabrics by polymer coating. *Tekstilec,* 2018, **61**(4), 265–271, doi: 10.14502/Tekstilec2018.61.265–271.
9. KOZIOR, Tomasz, DÖPKE, Christoph, GRIMMELSMANN, Nils, JUHÁSZ JUNGER, Irén, EHRMANN, Andrea. Influence of fabric pretreatment on adhesion of three-dimensional printed material on textile substrates. *Advances in Mechanical Engineering,* 2018, **10**(8), doi: 10.1177/1687814018792316.
10. RICHTER, Christoph, SCHMÜLLING Stefan, EHRMANN, Andrea, FINSTERBUSCH, Karin. FDM printing of 3D forms with embedded fibrous materials. *International Conference on Design, Manufacturing and Mechatronics*, 2015, 961–969, doi: 10.1142/9789814730518_0112.

11. *Adobe* [online]. Create and edit patterns [accessed 23. 7. 2019]. Available on World Wide Web: <https://helpx.adobe.com/illustrator/using/create-edit-patterns.html>.
12. *Adobe* [online]. Automation with actions. [accessed 23. 7. 2019]. Available on World Wide Web: <https://helpx.adobe.com/illustrator/using/automation-actions.html>.
13. *DocPlayer* [online]. X400 German RepRap Dual printing X400V3. Printing successfully with water soluble material [27. 9. 2019]. Available on World Wide Web: <https://docplayer.org/53517474-X400-german-reprap-dual-printing-x400v3-printing-successfully-with-water-soluble-material.html>.
14. *Matter Hackers* [online]. 3D printer filament – PORO-LAY LAY-FOMM 40 porous filament – 1.75 mm (0.25kg) [accessed 16. 6. 2019]. Available on World Wide Web: <https://www.matterhackers.com/store/3d-printer-filament/poro-lay-lay-fomm-filament-175mm>.
15. *Mosaic* [online]. Palette 2 Pro. Mosaic manufacturing [accessed 18. 7. 2019]. Available on World Wide Web: <https://www.mosaicmfg.com/products/palette-2?variant=12502310256734>.
16. *YouTube* [online]. Slicing with simplify3d for palette/ palette+ [accessed 5. 6. 2019]. Available on World Wide Web: <https://www.youtube.com/watch?v=EydvbCmaKmc&feature=youtu.be>.
17. KIRAN, Kattoju Ravi, UYSAL, Rimma, STUBBS, Jack, LAVIOLA, Joe. Correct me: Detection and correction of wrist extension using electrical muscle stimulation and design of 3D printed flexible glove. *CHI*, 2020, submitted.

Sujit Kumar Sinha,[1] Akshay Sharma,[1] Subhankar Maity[2]
[1] Dr. B. R. Ambedkar National Institute of Technology, Department of Textile Technology, Jalandhar, 144011, Punjab, India
[2] Uttar Pradesh Textile Technology Institute, Department of Textile Technology, Kanpur, 208001, India

Thermal Resistance and Moisture Management Behaviour of Nettle/Polyester Nonwoven Fabrics

Toplotni upor in prenos vlage skozi vlaknovine iz vlaken koprive in poliestra

Original Scientific Article/*Izvirni znanstveni članek*
Received/*Prispelo* 3-2019 • Accepted/*Sprejeto* 9-2019

Abstract

Thermal resistance and moisture management characteristics are important attributes of textile materials for the characterisation of their ability to provide thermal comfort. Nettle fibre consists of a hollow core that is expected to enable good thermal and moisture regulation properties. Nonwoven fabrics of three different mass per unit area values, made from nettle, polyester and blends thereof, were prepared on a needle-punching machine, maintaining the same punch density and depth of penetration. The thermal conductivity, water vapour permeability, water retention, wicking, moisture management, drying rate and air permeability of these fabrics were evaluated. Nonwoven fabric prepared with 100% nettle fibres exhibited good thermal conductivity, while polyester fabric demonstrated good thermal insulation. The nettle fibre fabric showed good water retention, drying rate and moisture management properties. On the other hand, polyester-enriched fabric exhibited good wicking behaviour.
Keywords: Himalayan nettle, needle-punching, thermal insulation, wicking, moisture management, Girardinia diversifolia

Izvleček

Toplotni upor in prenos vlage sta pomembni lastnosti tekstilij za zagotavljanje toplotnega udobja. Vlakno iz koprive ima votlo jedro (lumen), ki naj bi tekstilijam zagotovilo dobro toplotno izolacijo in uravnavanje vlage. Iz vlaken koprive, poliestrskih vlaken in njihove mešanice so bile izdelane iglane vlaknovine s tremi različnimi ploščinskimi masami in enako gostoto iglanja ter enako globino penetracije igel. Ocenjeni so bili toplotna prevodnost, prepustnost vodne pare, zadrževanje vode, kapilarni prenos vlage, celoten prenos vlage, hitrost sušenja in zračna prepustnost. Vlaknovina iz 100-odstotnih vlaken koprive se je odlikovala po dobri toplotni prevodnosti, vlaknovina iz poliestrskih vlaken pa po dobri toplotni izolativnosti. Vlaknovina iz vlaken koprive je dobro zadrževala vodo, se hitro sušila in imela dober celoten prenos vlage. Vlaknovina iz mešanice vlaken koprive in poliestrskih vlaken je dobro prenašala kapilarno vlago.
Ključne besede: himalajska kopriva, iglanje, toplotna izolacija, kapilarni prenos vlage, prenos vlage, Girardinia diversifolia

1 Introduction

Nettle fibre is a cellulose fibre with a long and fascinating history that can be traced back to the Bronze Age, when it was used to make cloth. Probably the best-known find is from the Danish Voldtofte grave, where nettle cloth was used to wrap human bones, and dates back to between 900 and 750 BC [1]. Several species

Corresponding author/*Korespondenčni avtor:*
Subhankar Maity
E-mail: maity.textile@gmail.com

of the nettle family (*Urticaceae*) are known today and are used to produce bast fibres similar to flax. Many of those species have been used to produce fibre for making textiles and clothing for thousands of years. There are two main species of the fibre: European nettle (or stinging nettle) and Himalayan nettle. European nettle is difficult to grow commercially. Himalayan nettle (*Girardinia diversifolia*) is a large nettle grown mainly in the Himalayan region, in areas such as tropical Africa (from Ethiopia to Madagascar), and in Yemen, Nepal, India, Sri Lanka, southern China, Taiwan and Indonesia [2–4]. In all of these species, the fibre comes from the stem and, incidentally, there is no sting left in the extracted fibre. The plant grows from 1 to 3 meters in height. The physical and tensile properties of the Himalayan nettle fibre is reported to be better than other high-strength bast fibre such as flax, hemp and ramie, as shown in Table 1 [4]. Nettle fibre is thus used for a wide range of applications, as shown in Table 2.

The fibres contain 48% cellulose, which is much lower than that of ramie and flax, in which the cellulose content is approximately 73% and 75%, respectively. Lignin and hemicellulose, which are considered to be useless and even harmful in textile processing, should be removed through degumming. After degumming, the fibre contains 11% moisture, 67% cellulose, 8% hemicellulose, 4% lignin and 3% ash [2]. The fibre is used to spin durable yarns from which nets, ropes and fishing nets are traditionally made [3]. The fibre is blended with other natural and synthetic fibres spin yarns to make dresses, jackets, scarves and shawls. Because nettle fibre is hollow, it is used to produce a composite that helps to improve vibration absorption capacity [5]. Thermal insulation is one of the desirable attributes of textiles. It is important for assessing apparel comfort for the user. In addition to thermal insulation, moisture management is also one of the key performance criteria in today's apparel industry and influences the comfort level of the wearer. Apparel manufacturers have shifted their attention to the high-performance end of the moisture management fabric market, while the performance of garments is of increasing importance to consumers.

In recent times, a wide range of textile materials has been used as thermal insulators in many industrial applications, such as the insulation of buildings, boilers, chimneys, furnaces, etc. [6–7]. The thermal insulating properties of textile fabrics depend on their thermal resistance, porosity and thickness. One major hazard that synthetic fibres pose to the environment is their non-biodegradability. On the other hand, most natural fibres are biodegradable and sustainable, provided that eco-friendly techniques are employed in every stage of their production and disposal. In the natural fibre

Table 1: Average physical and tensile properties and the associated standard deviation of single nettle fibre compared with other bast fibres [4]

Fibre	Length [mm]	Area of cross section [μm^2]	Breaking extension [%]	Young modulus [GPa]
Himalayan nettle fibre (*G. diversifolia*)	478 ± 21	479 ± 186	6.2 ± 1.3	73 ± 22
Flax	27 ± 3	183 ± 87	3.3 ± 0.4	54 ± 15
Hemp	20 ± 5	764 ± 260	0.8 ± 0.1	19 ± 4
Ramie	135 ± 15	270 ± 93	2.5	24.5

Table 2. Products produced from various parts of the nettle plant

Material	Uses
Long bast fibre of exceptional strength	Textile manufacturers
Wood fibres	Paper making
Leavulose	Sugar that can be used in food
Chlorophyll	Medicinal purposes
Powdered leaves	Cattle feed

sector, environmental concerns have prompted the search for substitute textiles to replace cotton. In recent years, a great deal of research has been conducted to develop environmentally friendly textiles that are economically viable. Hemp, flax and stinging nettle have all received considerable attention. Both hemp and flax produce coarser fibres than nettle, resulting in a strong but rather rough fabric [8]. Although these fibres are unable to replace cotton, nettle has emerged as a substitute for other natural fibres, such as jute and flax, due to its distinguishing attributes [9]. To provide a viable alternative to textile fibre, it is necessary to extract the fibres from nettle plant efficiently and profitably. Nettle fibre loft, i.e. the amount of air entrapped by the fibrous structure is, similar to that of cotton [10]. Nettle is stronger, finer and more flexible than linen [10–12]. This indicates that eco-friendly clothing made from nettle will be more durable and of better quality. Nettle fibre morphology is similar to that of cotton, with a lumen in the middle of a kidney-shaped cross section [11]. Its surface has grooves that increase the fibre's surface area [11, 13]. This hollow core may be useful in creating fabrics for both warm and cold conditions. Nettle fibre has been reported to show excellent moisture management properties [14–16]. There is little information available in literature about the thermal and physiological comfort of textile fabrics made of nettle fibre. This fibre must therefore be studied for its use in thermal insulation, and in terms of physiological comfort. In this study, needle-punched nonwoven fabrics were prepared from polyester and nettle fibres for the purpose of assessing their thermal insulation and moisture management properties for potential applications in both the apparel and industrial sectors.

2 Materials and methods

2.1 Materials

Nettle and polyester staple fibres were used for the preparation of nonwoven samples. Polyester fibres of 1.67 dtex and a cut length of 80 mm were procured from Reliance Industries, India. Himalayan nettle fibres of 1.38 dtex and a cut length of 100 mm were purchased from Uttrakhand Bamboo Research Corporation, Dehradun, India. A total of nine needle-punched nonwoven fabrics with three different mass per unit area values were prepared using these nettle and polyester fibres, as shown in Table 3.

Table 3. Data regarding prepared nonwoven samples

Fibre	Mass per unit area [g/m^2]		
Nettle	75	125	175
Nettle/polyester (N/P) blend (80:20)	75	125	175
Polyester	75	125	175

2.2 Preparation of needle-punched nonwoven fabrics

The samples were prepared on a DILO needle-punch nonwoven machine at IIT Delhi, India. The parallel laid nonwoven samples of the above-stated mass per unit area were prepared by varying the feed of the web. A punch density of 100 needles/cm^2 and a penetration depth of 10 mm were maintained while giving two passages in a needle loom.

2.3 Measurement of porosity and air permeability

The porosity of the prepared samples was determined by measuring the total volume of fabric and calculating the total volume of fibre in the sample. The difference between these two values is deemed air space and when it is calculated as a percentage of the total volume, it is referred to as the void fraction or porosity of the fabric. This can be calculated using equation 1 below:

$$\text{Porosity} = = 1 - \frac{\text{Density of fabric}}{\text{Average density of constituent fibres}} (\%) \quad (1).$$

Air permeability (cm^{3}cm^{2}s^{-1}) was measured using an FX 3300 Labortester III (Textest Instruments) air permeability tester according to BS 6636 standard.

2.4 Measurement of thermal conductivity

The thermal conductivity of the samples was measured using a thermal conductivity tester fabricated (Figure 1) by the Department of Textile Technology, NIT Jalandhar, India [17]. The instrument was fabricated according to the guidelines of the ASTM C518-10 standard for the measurement of the thermal conductivity of high-loft thick fibrous material, where the simulated measurement conditions were exactly the same as application conditions. The thermal conductivity tester consisted of a top hot plate (φ = 20 cm) and a bottom cold plate (φ = 20 cm)

between which the sample was mounted. The distance between top and bottom plate was adjustable according to sample thickness. The temperature of the top plate can be raised from room temperature to 100 °C, while the temperature of the bottom plate can be reduced from room temperature to 0 °C. The temperature of both plates was monitored by circulating water to the container of the plates. The temperature difference between top and bottom plates was measured using an attached chromel-alumel thermocouple, while heat flow across the sample was measured using a heat flux sensor (Captec, France). The temperature of the top plate was kept fixed at 37 °C (average temperature of the human body core), while the temperature of the bottom plate was varied from room temperature to 0 °C to achieve different temperature differences to simulate variations in environmental temperature. After mounting the sample in the tester, the heat flux sensor was positioned under the sample at the centre. After that, about 20 minutes was required to achieve a steady state heat flow. The output signals of the heat flux sensor (q/A) and thermocouple (ΔT) were recorded using a micro-voltmeter and converted to actual units using conversion charts. The thermal conductivities of the samples were calculated using Fourier's law, as given in equation 2:

$$k = \frac{q}{A} \times \frac{s}{\Delta T} \quad (2),$$

where, k is the thermal conductivity of the fabric ($Wm^{-1}K^{-1}$), q/A is the heat flux through the fabric (W/m^2), s is the thickness of the fabric (m) and ΔT is the temperature difference (°C).

Thermal resistance was calculated using equation 3:

$$\text{Thermal resistance} = \frac{\text{Thickness}}{\text{Thermal conductivity}} \ (m^2K/W) \quad (3).$$

The thickness of the sample was calculated using a digital thickness tester (TESTEX Instrument ltd., China).

2.5 Measurement of water retention

The water retention of a fabric was measured by cutting 10 cm × 10 samples. First, the oven dry weight of the samples was measured after drying them at 105 °C for 180 hours inside an oven dryer. The samples were then immersed in deionised water for 30 minutes and hung for 10 minutes in a laboratory room at 22 °C and 65% relative humidity for the removal of excess water. Next, the weight of the samples was measured and the water retention capacity was calculated using equation 4:

$$\text{Water retention} = \frac{\text{Wet weight (g)} - \text{Oven dry weight (g)}}{\text{Oven dry weight (g)}} \times 100\ (\%) \quad (4).$$

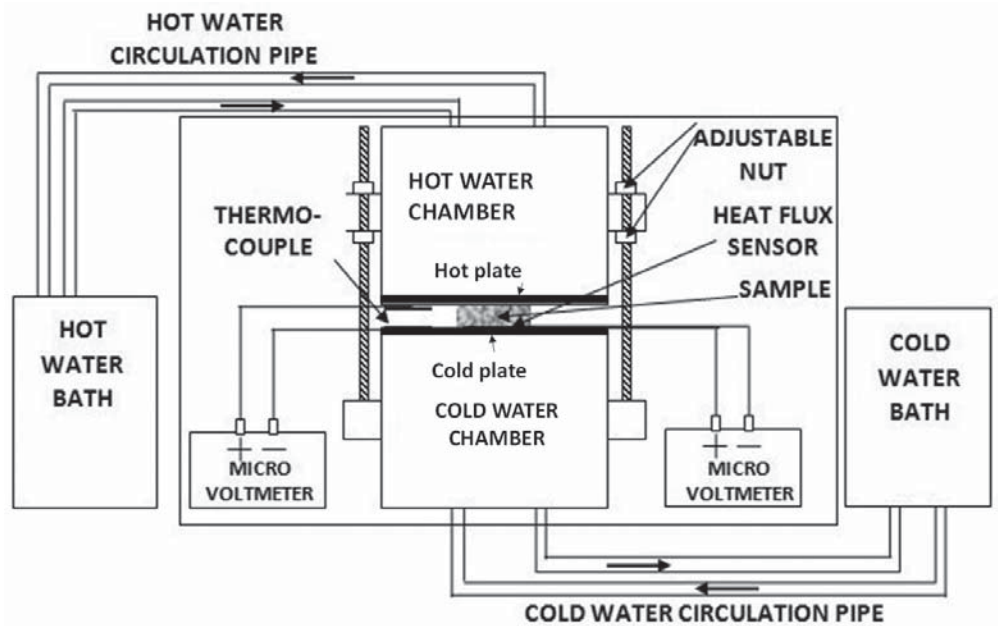

Figure 1: Schematic diagram of thermal conductivity tester

2.6 Measurement of wicking behaviour

An experimental set-up was prepared for the measurement of wicking behaviour, as shown in Figure 2. Specimens measuring 200 mm × 25 mm were cut. The bottom ends of the specimens were vertically immersed in water to a depth of 20 mm. A three-gram weight was affixed to the bottom end of each specimen. The wicking height versus time was observed for 15 minutes.

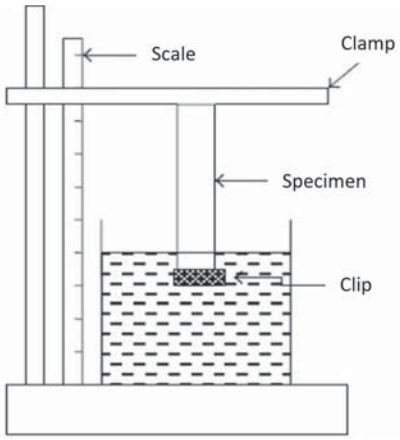

Figure 2: Wicking tester

2.7 Measurement of drying rate

The drying rate was defined using a drying rate tester (AL204). The standard applied for measurement purposes was AATCC 201. The sample size used was 15 cm × 15 cm. The test conditions used were a temperature of 22 °C ± 2 °C and a relative humidity of 66% ± 2%. The test sample was placed inside the weighing balance and 1 ml of deionised water was spread on top surface of the fabric. After measuring drying for 20 minutes, the instrument yielded the drying rate percentage of the sample.

2.8 Measurement of moisture vapour permeability

Moisture vapour permeability was measured using a water vapour permeability tester (SDL ATLAS M261) in accordance with the ASTM 1653-13 standard, as follows: an open cup containing water was sealed with a nonwoven fabric. The assembly was then placed in the test chamber at a controlled temperature of 20 °C ± 2 °C and a relative humidity of 65% ± 2%. The rate of water vapour loss was calculated by measuring the weight change of the cup containing the water after at least 1 hour. Moisture vapour permeability was calculated using equation 5:

$$\text{Moisture vapour permeability} = \frac{24\,M}{At}\ (\text{gm}^{-2}\text{day}^{-1}) \quad (5),$$

where, M is water vapour loss expressed in the time period (g), A is the area of the exposed specimen (m^2) and t is time of exposure (h).

2.9 Measurement of moisture management properties

Moisture management properties were measured using a moisture management tester according to the AATCC 195 test standard. A sample size of 8 cm × 8 cm was used. The testing conditions used were a temperature of 22 °C ± 2 °C and a relative humidity of 66% ± 2%. The moisture management tester was used to spray water on the fabric surface for 20 seconds and then measured moisture management properties for 120 seconds. The moisture management tester measured the dynamic liquid transport properties of textiles in three dimensions. They were (i) wetting time: the moisture absorption time of the fabric's inner and outer surfaces; (ii) one-way transportation capability: liquid moisture one-way transfer from the fabric's inner surface to its outer surface; and (iii) spreading rate: the speed at which liquid moisture spreads on the fabric's inner and outer surface.

3 Results and discussion

3.1 Porosity and air permeability of nonwoven fabrics

A porous structure is required for air permeability, which relates to the comfort of textiles. A porous textile structure creates stationary air pockets that are ideal for good thermal insulation. A nonwoven

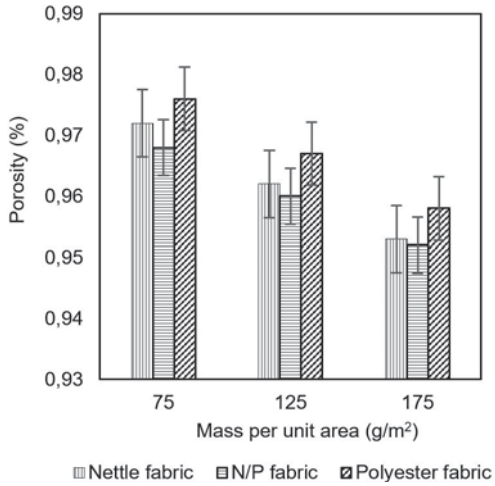

Figure 3: Porosity of nonwoven fabrics

structure is inherently porous, requiring the study of the porosity and air permeability of nonwoven fabric samples. The porosity and air permeability of all nonwoven fabrics were measured and the results are presented in Figure 3 and Table 4, respectively. It is evident from Figure 3 that polyester nonwoven fabrics have the highest porosity, followed by 100% nettle and N/P blended nonwoven fabrics, while the air permeability of polyester nonwoven fabric was the lowest. This may be due to the presence of small and uniform-sized pores in a larger numbers in polyester nonwoven fabrics, creating stationary air pockets that restricted heat flow.

Table 4: Air permeability of the nonwoven fabrics

Fabric composition	Air permeability [a] [$cm^3\ cm^{-2}s^{-1}$]		
	75 g/m²	125 g/m²	175 g/m²
Nettle	206.7 ± 6.2	158.8 ± 4.2	139.2 ± 4.1
N/P	211.6 ± 6.3	167.3 ± 3.9	142.6 ± 4.2
Polyester	174.8 ± 4.5	136.3 ± 3.2	88.6 ± 2.3

[a] Average value and the associated ± 95% confidence interval

3.2 Thermal conductivity of nonwoven fabrics

The thermal conductivity of all the samples was measured 20 times in repeated tests. The average thermal conductivity of the samples is shown in Table 5. For the same types of fabrics, an increase in mass per unit area results in a decrease in thermal conductivity and an increase in thermal resistance, as shown in Figures 4 and 5. However, the thermal conductivity of the fabrics decreases as the polyester content increases. This was found to be lowest in the case of 100% polyester nonwoven. For the same mass per unit area, polyester nonwoven fabrics comprise a higher number of fibres, producing a thicker fabric. As thickness increases, thermal resistance increases. The result is the better thermal resistance of polyester nonwoven fabric compared with nettle fibre nonwoven fabric. The thermal resistance of a nonwoven structure is influenced by its structural compactness with optimum porosity [17]. A good

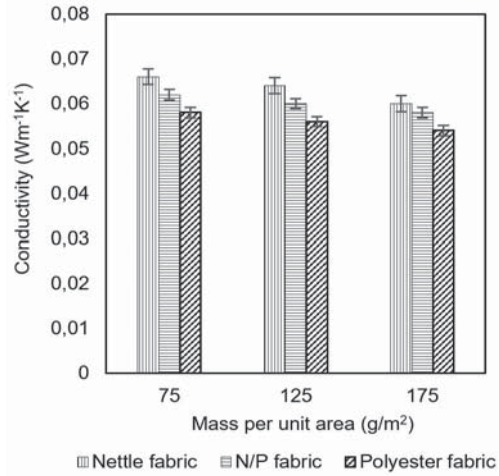

Figure 4: Thermal conductivity of nonwoven fabrics

Table 5: Thermal conductivity, thickness and thermal resistivity of nonwoven fabrics

Fabric composition	Mass per unit area [a] [g/m²]	Thermal conductivity [a] [$Wm^{-1}K^{-1}$]	Thickness [a] [mm]	Thermal resistance [m^2K/W]
Nettle	75 ± 3	0.066 ± 0.002	1.65 ± 0.11	0.025
	125 ± 5	0.064 ± 0.002	2.21 ± 0.12	0.035
	175 ± 6	0.060 ± 0.002	2.54 ± 0.12	0.042
Nettle/polyester (N/P) blend (80:20)	75 ± 3	0.062 ± 0.002	1.58 ± 0.11	0.025
	125 ± 6	0.060 ± 0.002	2.11 ± 0.11	0.035
	175 ± 6	0.058 ± 0.002	2.45 ± 0.13	0.042
Polyester	75 ± 2	0.058 ± 0.001	2.02 ± 0.13	0.035
	125 ± 3	0.056 ± 0.001	2.38 ± 0.15	0.043
	175 ± 4	0.054 ± 0.001	2.80 ± 0.14	0.052

[a] Average value and the associated ± 95% confidence interval

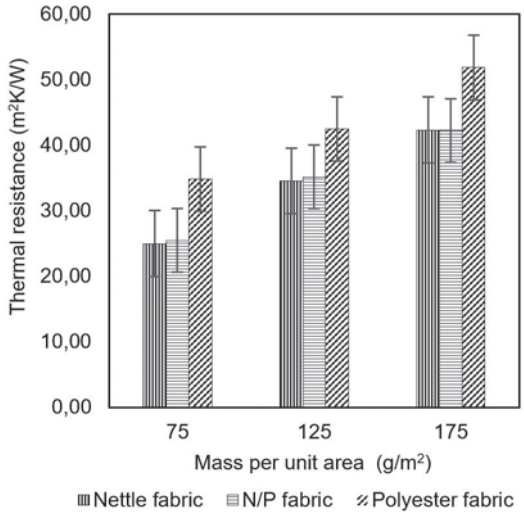

Figure 5: Thermal resistance of nonwoven fabrics

statistical correlation (r = 0.76) between thermal conductivity and porosity of nonwoven samples was identified.

3.3 Moisture vapour permeability

Moisture vapour permeability is defined as the ability of a textile material to allow water vapour to pass through it. How water in a gaseous form (vapour) passes through a material is influenced by pore size and the distribution of pores in the material. It was observed that moisture vapour permeability (Figure 6) decreased with an increase in mass per unit area. As mass per unit area increased, the fabrics became thicker and, as a result, the size of the pores

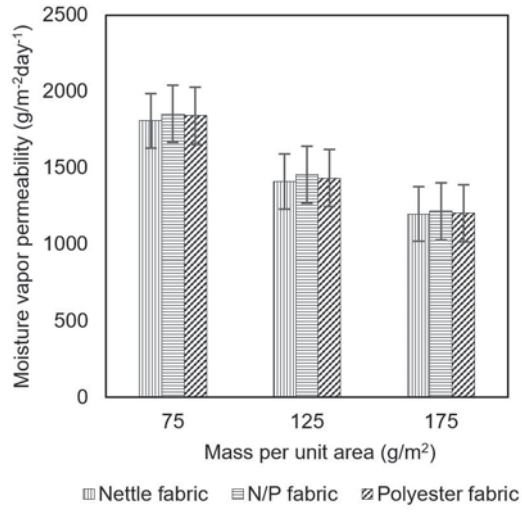

Figure 6: Moisture vapor permeability of nonwoven fabrics

decreased, which restricted the flow of moisture vapour across the thicker fabric structure. However, the moisture vapour permeability of all the three fabrics was similar and the differences were not statistically significant.

3.4 Water retention

The average water retention capacity of the nonwoven samples was measured and plotted, as shown in Figure 7. The water retention capacity of nettle fibre nonwoven fabric was found to be highest due to its hydrophilic nature. The water retention capacity increased with an increase in the mass per unit area of nettle and N/P blended nonwoven fabrics, while no significant difference was observed in the water retention capacity of various 100% polyester nonwoven fabrics. In the case of 75 g/m^2 nettle and N/P blended fabrics, no significant difference in water retention capacity was observed. This may have been due to the presence of hydrophobic polyester fibres and the thinner structure of the fabrics, allowing for the removal of moisture across the thickness in a similar way.

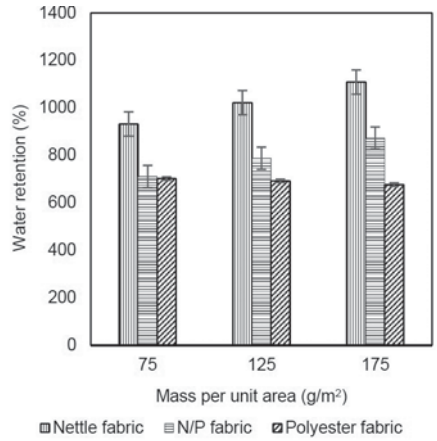

Figure 7: Water retention capacity of nonwoven fabrics

3.5 Wicking behaviour

Wicking behaviour is defined as the performance of fabric, which facilitates the movement of moisture away from the surface. It works by absorbing and spreading moisture out across the fabric to enhance the evaporative drying rate. The results of wicking height measured using the experimental set-up (as discussed in the experimental section) is shown in Figure 8. Figure 8 shows that the polyester nonwoven fabric demonstrated excellent wicking property compared with nettle. Wicking efficiency increased with

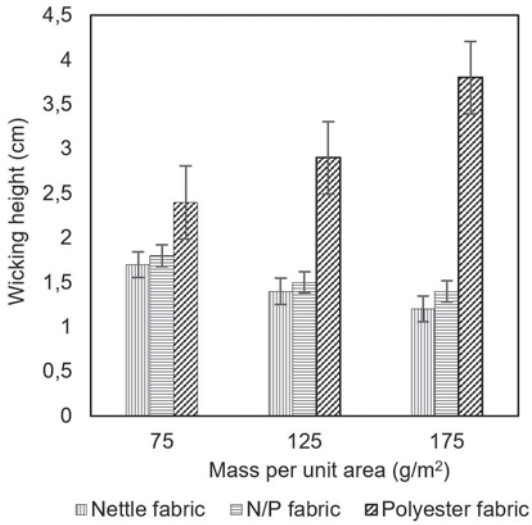

Figure 8: Wicking behaviour of nonwoven fabrics

an increase in the mass per unit area of the polyester nonwoven fabrics. In the case of nettle and nettle-polyester nonwoven fabrics, wicking efficiency decreased with an increase in mass per unit area. The hydrophobic nature of polyester did not result in any absorption and facilitated the transfer of moisture. In the case of nettle and nettle-polyester nonwoven fabrics, moisture was absorbed by the fibres instead of being transferred due to the hydrophilic nature of fibre. In the case of N/P blended nonwoven fabric (80/20), the polyester fibre content is only 20% that is solely responsible for wicking. As a result, nettle fibre was a significant factor for the poor performance demonstrated by blended nonwoven fabrics. Moreover, the difference in the mechanical properties of the two fibres does not facilitate a close association to form a uniform structure after needle-punching. This led to a variation in the inter-fibre spacing, leading to the inefficient transfer of liquid through wicking.

3.6 Moisture management properties

Moisture management behaviour describes the ability of fabric to regulate the transmission of moisture. The moisture management properties were evaluated through the assessment of (a) top and bottom wetting time, (b) top and bottom absorption rate, (c) top and bottom spreading (mm/s) and (d) overall moisture management capacity.

3.6.1 Top and bottom wetting time

Top and bottom wetting time is the time period in which the top and bottom surfaces of a fabric just begin to become wetted [18]. It evident from Figure 9a and Figure 9b that both the top and bottom wetting time of blended nonwoven fabrics was significantly higher than either the 100% nettle or the 100% polyester nonwovens fabrics.

The top and bottom wetting time of a fabric depends on its affinity to liquid and on the amount of available space in the structure for the movement of a liquid. Nettle fibre is hydrophilic in nature, so it quickly absorbs water and demonstrates a shorter wetting time (top and bottom). In the case of polyester nonwoven fabric, polyester fibre has the ability of the quick dispersion of water supported by wicking, even though the fabric is hydrophobic in nature. For this reason, its wetting time is the shortest. The nettle/polyester blend demonstrated the highest wetting time due to its two contradictory behaviours of water absorption and transfer.

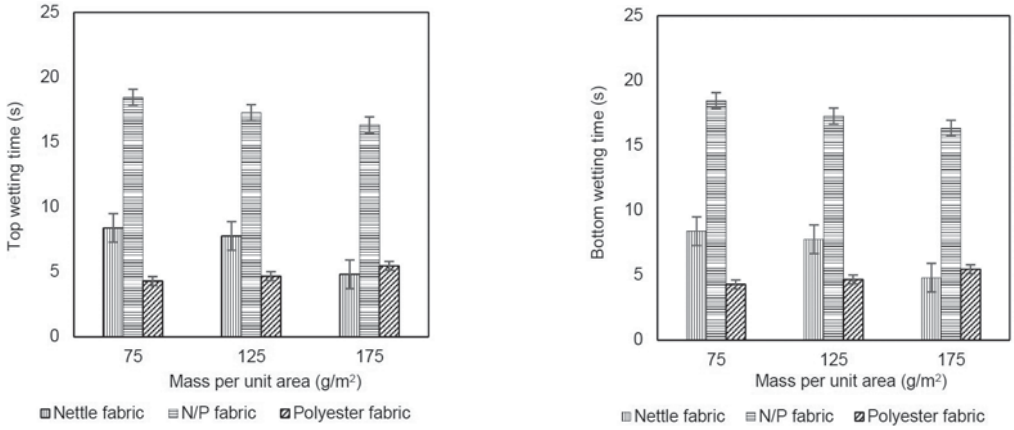

Figure 9: Wetting time of nonwoven fabrics: a) top and b) bottom

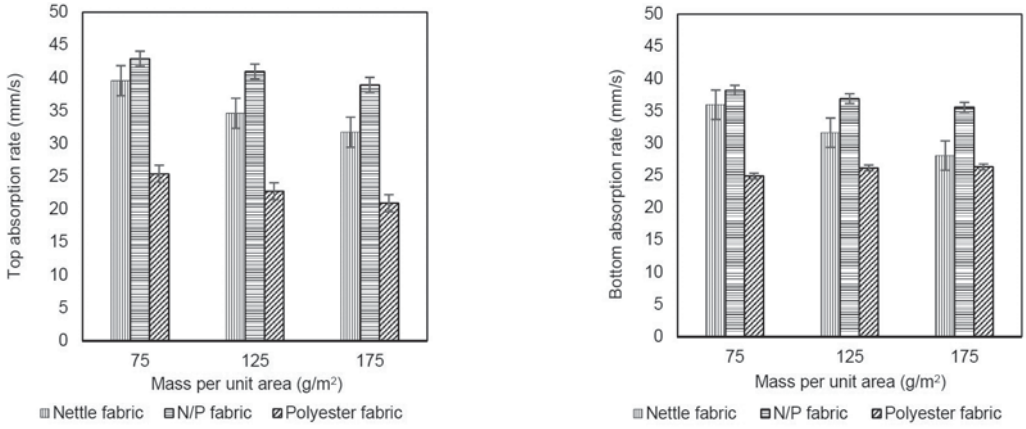

a) *b)*

Figure 10: Effect of mass per unit area: a) on top absorption rate and b) on bottom absorption rate

3.6.2 Top and bottom absorption rate

The top and bottom absorption of liquid by a textile substrate indicates the degree of transfer of liquid on its surface. The absorption of liquid by a fabric is influenced by the type of fibre, fabric structure and porosity of the structure [18]. It is evident that the top and bottom absorption rate (Figure 10) is highest in case of blended fabrics. The absorption rate depends on the porosity of the fabric. As the mass per unit area increases, the top and bottom absorption rate decreases due to a decrement in porosity with an increment in mass per unit area. Exceptional trans-planar behaviour was identified for nettle/polyester blended fabric. This might be the result of better wicking due to better micro-capillary action.

3.6.3 Top spreading and bottom spreading

Spreading speed refers to the ability of a fabric to allow liquid to move outward across its plane. A fibre with a lower liquid holding capacity will allow such trans-planar movement [18]. The top and bottom spreading behaviour of the nonwoven fabrics is shown in Figure 11. Both top and bottom spreading rates were the slowest in the case of 100% nettle nonwoven fabric. The presence of polyester fibre in the nonwoven fabrics significantly accelerated the spreading of water. This is due to hydrophobic nature of the polyester fibre attributable to the pronounced capillary effect, which facilitates the adsorption of water molecules on the surface of the fibres and the spreading of the same at a faster rate without absorption. Hydrophilic nettle fibre absorbs water quickly,

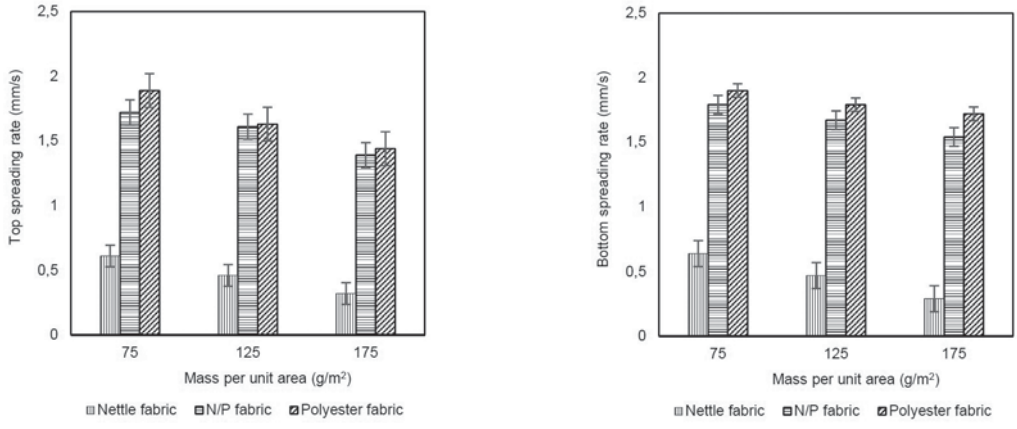

a) *b)*

Figure 11: Effect of mass per unit area: a) on top spreading and (b) on bottom spreading

which limits the spreading of water on the surface. The top and bottom spreading speed decreased with an increase in mass per unit area due to the presence of nettle fibres that can absorb moisture.

3.6.4 Overall moisture management capacity

Overall moisture management capacity is an index that indicates the overall ability of a fabric to manage the transport of liquid moisture. This includes three aspects of performance, i.e. spreading speed or drying speed, the moisture absorption rate of the bottom side and one-way liquid transport ability. A higher overall moisture management capacity indicates the better overall moisture transportability of a fabric [18]. The overall moisture management capacity of fabrics is shown in Figure 12.

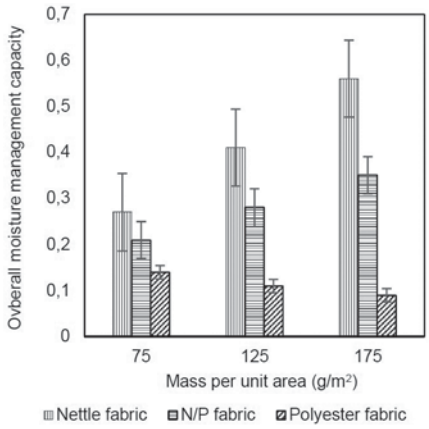

Figure 12: Overall moisture management capacity of nonwoven fabrics

It is evident from Figure 12 that overall moisture management capacity increases with an increase in nettle fibre content, as well as the mass per unit area of the nettle-enriched nonwoven fabrics, while overall moisture management capacity decreases with an increase in mass per unit area for 100% polyester fabric.

4 Conclusion

Needle-punched nonwoven fabrics with three different mass per unit area values (77 g/m^2, 125 g/m^2 and 175 g/m^2) of nettle, polyester and nettle polyester blend were prepared in a DILO needle-punched nonwoven machine, while maintaining the same levels of punch density and depth of penetration. It was determined that the preparation of a uniform nonwoven structure in terms of equal pore size from 100% nettle fibre is difficult, and that it would be easier if polyester fibres are blended with the nettle fibre. The polyester nonwoven fabric exhibited the best thermal resistance due to its structural uniformity, in terms of a large number of small and uniform pores, and its greater thickness. The polyester nonwoven fabrics also had the highest wicking rate, as their hydrophobic nature facilitated the capillary flow of the fibre. On the other hand, the nettle nonwoven fabrics demonstrated high water vapour and air permeability, and the best overall moisture management capacity and water retention properties. Thus, nettle fibre nonwoven fabrics, as biodegradable and sustainable material, could serve as an alternative for various industrial and household applications. In recent years, organisations such as the European Union and the Interactive European Network for Industrial Crops and their Applications (IENICA) have been encouraging scientists to develop environmentally friendly textiles from natural fibres, such as jute, hemp, flax, etc. that are economically viable. Nettle fibre is also garnering considerable attention due to the promising attributes discussed in this article. Although nettle is unable to replace cotton, it may emerge as a substitute for synthetic and other natural fibres due to its distinguishing attributes.

However, the behaviour of the nettle fibre may become softer, similar to cotton to a certain extent, after lignin is removed from its surface. Its hollow structure and antimicrobial property (with lignin) can be studied in more detail in the future in order to find suitable applications of this fibre in practical use.

References

1. HARWOOD, Jane, EDOM, Gillian. Nettle fibre: its prospects, uses and problems in historical perspective. *Textile History,* 2012, **43** (1). 107–119, doi: 10.1179/174329512X1328447132 1244.
2. SRIVASTAVA, Nupur, RASTOGI, Deepali. Nettle fiber: Himalayan wonder with extraordinary textile properties. *International Journal of Home Science*, 2018, **4**(1), 281–285.
3. AGUS SURYAWAN, I. G. P., SUARDANA, N. P. G., SUPRAPTA WINAYA, I. N. BUDIARSA SUYASA, I. W., TIRTA NINDHIA, T. G. Study

of stinging nettle (Urtica dioica L.) fibers reinforced green composite materials: a review. In *IOP Conference Series: Materials Science and Engineering*, 2017, **201**(1), 1–7, doi: 10.1088/1757-899x/201/1/012001.

4. LANZILAO, Gabriella, GOSWAMI Parikshit, and BLACKBURN Richard S. Study of the morphological characteristics and physical properties of Himalayan giant nettle (*Girardinia diversifolia* L.) fibre in comparison with European nettle (*Urtica dioica* L.) fibre. *Materials Letters,* 2016, **181**, 200–203, doi: 10.1016/j.matlet.2016.06.044.
5. SETT, Sunil Kumar, RAY, Sadhan Chandra, MUKHERJEE, Asis. Processing of Himalayan giant nettle (*Girardinia Diversifolia*) and its potential uses in textile applications. *International Conference. on Natural Fibres.* The Indian Natural Fibre Society, 2013.
6. ABDEL-REHIM, Zeinab S., SAAD, M. M., EL-SHAKANKERY, M., HANAFY, I. Textile fabrics as thermal insulators. *AUTEX Research Journal*, 2006, **6**(3), 148–161.
7. BRIGA-SÁ, Ana, NASCIMENTO, David, TEIXEIRA, Nuno, PINTO, Jorge, CALDEIRA, Fernando, VARUM, Humberto, PAIVA, Anabela. Textile waste as an alternative thermal insulation building material solution. *Construction and Building Materials*, 2013, **38**,155–160, doi: 10.1016/j.conbuildmat.2012.08.037.
8. CHEN, Yan, SUN, Liangfeng, NEGULESCU, Ioan, WU, Qinglin, HENDERSON, Gregg. Comparative study of hemp fiber for nonwoven composites. *Journal of Industrial Hemp*, 2007, **12**(1), 27–45, doi: 10.1300/J237v12n01_04.
9. BERGFJORD, Christian, MANNERING, Ulla, FREI, Karin Margarita, GLEBA, Margarita, SCHARFF, Annemette Bruselius, SKALS, Irene, HEINEMEIER, Jan, NOSCH, M.-L., HOLST, Bodil. Nettle as a distinct Bronze Age textile plant. *Scientific Reports*, 2012, **2**(1), 1–4, doi: 10.1038/srep00664.
10. HUANG, G. Nettle (*Urtica cannabina* L) fibre, properties and spinning practice. *Journal of the Textile Institute.* 2005, **96**(1), 11–15, doi: 10.1533/joti.2004.0023.
11. BERGFJORD, Christian, HOLST, Bodil. A procedure for identifying textile bast fibres using microscopy: Flax, nettle/ramie, hemp and jute. *Ultramicroscopy,* 2010, **110**(9), 1192–1197, doi: 10.1016/j.ultramic.2010.04.014.
12. BODROS, Edwin, BALEY, Christophe. Study of the tensile properties of stinging nettle fibres (*Urtica dioica*). *Materials Letters,* 2008, **62**(14), 2143–2145, doi: 0.1016/j.matlet.2007.11.034.
13. KUMAR, Navdeep, DAS, Dipayan. Nonwoven geotextiles from nettle and poly(lactic acid) fibers for slope stabilization using bioengineering approach. *Geotextiles and Geomembranes,* 2018, **46**(2), 206–213, doi: 10.1016/j.geotexmem.2017.11.007.
14. SHARMA, Akshay. Study on thermal and moisture management behaviour of nettle fibre blended nonwovens : M. Tech. Thesis, 2016. Jalandhar : Dr. B. R. Ambedkar, National Institute of Technology, Department of Textile Technology.
15. LANZILAO, Gabriella. *Properties and applications of Himalayan nettle fibre : PhD Thesis*. University of Leeds, 2015. Available on World Wide Web: <http://etheses.whiterose.ac.uk/id/eprint/11104>.
16. SUMMERSCALES, John, DISSANAYAKE, Nilmini, VIRK, Amandeep, HALL, Wayne. A review of bast fibres and their composites. Part 2–Composites. *Composites Part A: Applied Science and Manufacturing,* 2010, **41**(10), 1336–1344, doi: 10.1016/j.compositesa.2010.05.020.
17. GHOSH, Subrata, RIPAN Das, SUBHANKAR Maity. Optimization of material and process parameters of fibrous quilt for comfortable heat loss from human body. *The Journal of the Textile Institute*, 2018, 1–9, doi: 10.1080/00405000.2018.1531742.
18. KUMAR, Pawan, KUMAR SINHA, Sujit, GHOSH, Subrata. Moisture management behaviour of modified polyester wool fabrics. *Fashion and Textiles,* 2015, **2**(1), 1–5, doi: 10.1186/s40691-015-0027-8.

Zhong Lv, Jin-Ping Guan, Ren-Cheng Tang, Guo-Qiang Chen
Soochow University, College of Textile and Clothing Engineering, National Engineering Laboratory for Modern Silk, Suzhou 215123, China

Flame-retardant Treatment of Silk Fabric with Sodium phytate and Chitosan Using the Layer-by-layer Padding Technique

Oplemenitenje svilene tkanine z ognjeodpornim natrijevim fitatom in hitosanom s pomočjo tehnike impregniranja plast za plastjo

Original Scientific Article/*Izvirni znanstveni članek*
Received/*Prispelo* 3-2019 • Accepted/*Sprejeto* 9-2019

Abstract

Bio-based flame-retardant agents and layer-by-layer assembly have attracted a great deal of attention in the flame-retardant fields of textiles, composites and polymeric materials. In this study, the electrostatic layer-by-layer assembly of chitosan and sodium phytate on silk fabric was carried out using a padding technique. The effects of the concentration and assembled bilayer of chitosan and sodium phytate on the weight gain, flammability, surface morphology, whiteness, stiffness, lustre, tensile strength, and washing durability of silk fabric were studied, and the heat release, thermal stability and flame-retardant mechanism of the coated fabric were analysed. The results revealed that at 10 to 15 assembled bilayers, the coated fabrics exhibited high limiting oxygen indexes and passed the vertical burning test, and their good flame retardancy was maintained even after 15 washing cycles. Moreover, the coated fabrics exhibited a significant decrease in peak the heat release rate and a strong charring ability at high temperatures. The chitosan and sodium phytate system acted as flame retardants in the condensed phase. Given the high weight gain of silk fabric, the layer-by-layer assembly of chitosan and sodium phytate using a padding technique was more applicable to the flame-retardant treatment of furnishing fabrics.
Keywords: layer-by-layer, padding, chitosan, sodium phytate, silk, flame-retardancy

Izvleček

Zaviralci gorenja na biološki osnovi in tvorba premaza z nanašanjem plasti za plastjo so pritegnili veliko pozornost na področju ognjevarnih tekstilij, kompozitov in polimernih materialov. V tej raziskavi je bil z uporabo impregnirnega postopka po postopku plast za plastjo na svileno tkanino nanesen elektrostatični premaz hitozana in natrijevega fitata,. Proučevana sta bila vpliva koncentracije in število slojev hitozana in natrijevega fitata na povečanje mase, vnetljivost, morfologijo površine, belino, togost, lesk, natezno trdnost in obstojnost pri pranju svilene tkanine. Analizirani so bili sproščanje toplote, toplotna stabilnost in mehanizem zaviranja gorenja premazane tkanine. Rezultati so pokazali, da so tkanine, prevlečene z 10 do 15 dvoplastmi, imele visok mejni kisikov indeks in so prestale vertikalni test gorenja ter tudi po 15 ciklih pranja ohranile dobro sposobnost zaviranja gorenja. Poleg tega so premazane tkanine pokazale veliko znižanje hitrosti sproščanja toplote in močno sposobnost pooglenitve pri visokih temperaturah. Sistem hitozana in natrijevega fitata je ognjevarno deloval v kondenzirani fazi. Glede na veliko obtežitev svilene tkanine je bil impregnirni postopek nanosa premaza hitozana in natrijevega fitata po postopku plast za plastjo bolj uporaben za ognjevarno obdelavo dekorativnih tkanin.
Ključne besede: plast za plastjo, impregniranje, zaviranje gorenja

Corresponding author/*Korespondenčni avtor:*
Prof. Dr. Jin-Ping Guan
E-mail: guanjinping@suda.edu.cn

Tekstilec, 2019, ***62****(4), 269-277*
DOI: 10.14502/Tekstilec2019.62.269-277

1 Introduction

Silk, sometimes referred to as the 'Queen of fibres' , has a gentle lustre, high moisture and permeability, good comfort and feeling, health care applications and good dry elasticity. It is used widely in a variety of clothing and interior decoration materials. Silk is considered a flammable fibre and has a limit oxygen index (LOI) of around 23–24%, although it has high nitrogen content. Furnishing silk textiles require a flame-retardant (FR) property. Thus, the FR treatment of silk is required to meet the market requirement of FR silk textiles.

Compared with wool and cotton, there are fewer studies of silk in terms of FR treatment. Silk can be treated using FR agents that are originally used for wool and cotton. These FR agents include fluorotitanate and fluorozirconate, [1] and phosphorus- and nitrogen-containing agents [2]. Fluorotitanate and fluorozirconate are applied using a dipping technique, but their washing fastness is inadequate [1]. Most phosphorus- and nitrogen-containing FRs originally used for cotton are resin-type agents, and are applied using a pad-dry-cure process [2]. However, curing at high temperatures gives rise to the deterioration of silk. On the other hand, the effluent discharge of phosphorus compounds during laundering and use causes water eutrophication [3]. Another disadvantage of phosphorus-based and nitrogen-based FRs with methylol groups is formaldehyde release [4]. In addition to the aforementioned FR agents, other FR agents and techniques, such as nano-materials, sol-gel and graft polymerisation, have been studied to enhance the FR properties of silk [5–8].

With the awareness of the toxicity and environmental pollution of FR agents, eco-friendly FR agents and innovative techniques must be used to address existing issues [9]. In this regard, bio-based FR agents such as chitosan (CH), alginates, proteins, and phytic acid or sodium phytate (SP) have been studied to improve the FR properties of textiles [10, 11]. Among them, the use of phytic acid and sodium phytate as FRs has shown great potential because they contain six phosphate groups.

In terms of innovative FR techniques, electrostatic layer-by-layer (LbL) assembly has garnered a great deal of attention [12, 13]. Electrostatic LbL assembly is usually a self-assembled molecular technique where positively and negatively charged polyelectrolytes spontaneously interact and deposit themselves, primarily via electrostatic forces, to form a membrane. The first study of the application of an LbL assembly in the FR treatment of textiles involved the alternate dipping of silk in CH and polyphosphoric acid solutions [14]. To date, the LbL assembly that is usually carried out using a repeated dipping approach has been widely studied in the FR finishing of textiles, with the application of a number of oppositely charged substances with FR properties [12]. Among them, CH and phytic acid and its salts exhibit good FR effects and positive environment benefits because they are naturally-occurring compounds [15–19]. The CH and phytic acid dip coating at 30 bilayers conferred a self-extinguishing behaviour to cotton fabric with a 16% increase in fabric weight and a 60% reduction in the peak heat release rate [17]. However, washing durability was not reported. In addition, a similar dip coating was also applied to polyamide 66 fabric [16]. At 5 to 10 bilayer assemblies with weight increases of 10–15%, the coated fabrics stopped melt-dripping, suppressed the spread of flames and decreased the peak heat release rate. The subsequent crossing with sodium tetraborate could obviously improve the washing durability of coated fabrics.

In this study, the electrostatic LbL assembly of CH and SP on silk fabric was carried out using a padding technique. The effects of the concentration and assembled bilayer of CH and SP on the weight gain, flammability, surface morphology, whiteness, stiffness, and washing durability of silk fabric were studied. The heat release, thermal stability and FR mechanism of the coated fabric were analysed.

2 Materials and methods

2.1 Materials

Silk habotai (fabric code 11206) was obtained from China Jiangsu Huajia Holding Group. The specifications of this fabric are as follows: warp and weft count: 23.3 dtex/2; warp density: 50 threads/cm; weft density: 45 threads/cm; and weight per unit area: 35 g/m^2. Chitosan (purity of 99%) (CH) with a molecular weight of 50–100 kDa and a deacetylation degree of around 95% was purchased from Shandong Western Asia Chemical Industry Inc., China. Sodium phytate (purity of 98%) (SP) was bought from Shanghai Yuanye Bio-Technology Co. Ltd., China. Sodium hydroxide and acetic acid used for the adjustment of pH were analytically pure reagents. A commercial

detergent designed for the household cleaning of silk and wool textiles was purchased from Shanghai Zhengzhang Washing and Dyeing Co., China, and had a solid content of 15.3% and a pH of 6.5 (2 g/L detergent solution).

2.2 FR coating

CH solutions (0.5% wt and 1.0% wt) were prepared by dissolving CH in an acetic acid (0.8% wt) solution. SP solutions of 0.5% wt and 1.0% wt were also prepared in advance. The pH of CH and SP solutions was adjusted to 5 and 4 using acetic acid. Silk fabric was first dipped into a CH solution, and then squeezed through a roller using a laboratory padder. The fabric prepared as such was dipped into an SP solution, and then squeezed through a roller. During the squeezing, the silk fabric achieved a wet pick-up rate of 100%. After one cycle of padding with CH and SP solutions, the assembly of the first bilayer (BL) was completed. Later, the assembly process was repeated until the desired number of BLs was achieved. The same concentration (0.5% wt or 1.0% wt) of CH and SP was used in each LbL assembly. After the completion of assemblies, the coated fabric was dried at 90 °C in an oven for 2 min.

2.3 Measurements

The weight gain of silk fabric was calculated as the difference in the dry weight of the fabric before and after coating. The whiteness of silk fabric was measured according to GB/T 8424.2-2001 using an UltraScan PRO colorimeter (HunterLab, USA). The stiffness of silk fabric in the warp and weft directions was measured according to GB/T 18318-2009 using a YG(B) 022D automatic fabric stiffness tester (Wenzhou Darong Textile Instrument Co. Ltd., China), while the tensile strength of silk fabric in the warp and weft directions was measured using an Instron 5967 tester (Illinois Tool Works Inc., USA) according to GB/T 3923.2-2013. Before testing, samples were placed in an atmospheric environment of 65% relative humidity and 20 °C for 24 hours. The average result of five specimens was used for each sample. The lustre of silk fabric was characterised using the reflectivity of light measured by a Gonio Photometer GP-200 (Murakami Color Research Laboratory Co. Ltd., Japan) in the following conditions: incident angle: 60°; and light-reflection angle: –90° to 90°. The average result of five specimens was reported. The surface morphological structures of coated silk fabrics were observed using a TM-3030 type scanning electron microscope (SEM) (Hitachi, Japan) at an acceleration voltage 5 kV.

The flammability of silk fabric was evaluated using LOI and vertical burning tests. The LOI of silk fabric was measured using an FTT0080 oxygen index apparatus (Fire Testing Technology Ltd., UK) according to the ASTM D2863 Standard Test Method. The vertical burning of silk fabric was conducted using a YG815B automatic vertical flammability cabinet (Ningbo Textile Instrument Factory, China) according to the ASTM D6413 Standard Test Method. A pyrolysis combustion flow calorimetry (PCFC) analysis was performed using a FTT0001 microscale combustion calorimetry (Fire Testing Technology Ltd., UK) according to the ASTM D7309 Standard Test Method. The thermogravimetry (TG) analysis of silk fabric (about 5–6 mg) was conducted using a TG/DSC 5700 thermal analyser (Perkin-Elmer) at a heating rate of 10 °C/min in the temperature range of 30 to 600 °C under a nitrogen flow of 100 mL/min.

The washability of coated fabric was tested using an XW-ZDR-25X12 low-noise oscillating dyeing machine (Jingjiang Xinwang dyeing and finishing equipment factory, China) using 2 g/L commercial detergent and a bath ratio of 50:1. Each washing cycle was performed at 40 °C for 30 min.

3. Results and discussion

3.1 Weight gain and surface morphology of coated silk fabric

As shown in Figure 1, the weight gain of silk fabric increased with an increase in the number of assembly layers at two concentrations of CH/SP. Except for the experimental point at 1.0% CH/SP and 20 BLs, two sets of experimental points showed a good linear correlation between weight gain and assembly layers. Varying weight gain resulted in different FR parameter values, as discussed later. This indicates the possibility that assembly layers and CH/SP concentration can be selected according to requirements for the weight gain and FR properties of silk fabrics. At this point, several weight-gain points should be mentioned. As 0.5% CH/SP was used, the weight gain of silk fabric was 13.66% and 21.46% at 10 and 15 BL assemblies, respectively. At 1.0% CH/SP and 10 BL assemblies, the weight gain was 24.81%.

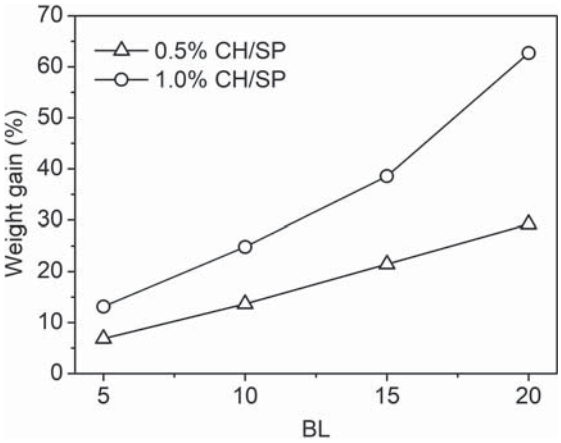

Figure 1: Weight gain of silk fabrics obtained using two concentrations of CH/SP at different BLs

After dip coating, the surface morphology of silk fabric showed different degrees of change, as shown in Figure 2. The untreated fabric had a smooth surface. As assembly layers and CH/SP concentration increased, more deposits were found on the fabric surface, and accumulated between fibres. At 0.5% CH/SP and 20 BLs, and at 1.0% CH/SP and 15 and 20 BLs, fibre bundles could not be observed (images not shown) due to excessive deposits of CH/SP on the fabric surface. The surface coatings can confer positive fire-protection properties to silk fabric, as discussed later.

3.2 Flammability of coated silk fabric

LOI and vertical burning tests were used to evaluate the flammability of silk fabrics. In the LOI test (Figure 3), as the assembled layers increased, the LOI of silk fabric increased (LOI was 23% for original silk). Several experimental points were given: LOI was 29.4% and 30.7% at 0.5% CH/SP at 10 and 15 BLs, respectively; at 1.0% CH/SP and 10 BLs, the weight gain was 32.2%. Increasing CH/SP concentration and BLs further increased LOI relative to the points described above.

In the vertical burning test, the original silk fabric burned quickly and was completely burned within the ignition time (12 s), producing a char length of 30 cm, and thus had no after-flame time and afterglow time. As shown Figure 3, the coated fabrics at two concentrations of CH/SP had a char length of less than 15 cm when the number of assembly layers was equal to or greater than 10 BLs, indicating that they meet the B1 level requirement of FR decorative fabrics for char length according to GB/T 17591-2006, where the char length must be less than 15 cm. However, the fabrics assembled at 5 BLs could not pass the vertical burning test because of their long char length. The photos presented in Figure 4 further illustrate the visual results of vertical burning. At the same BLs, the fabrics coated with a high concentration of CH/SP showed smaller burned areas and shorter char length.

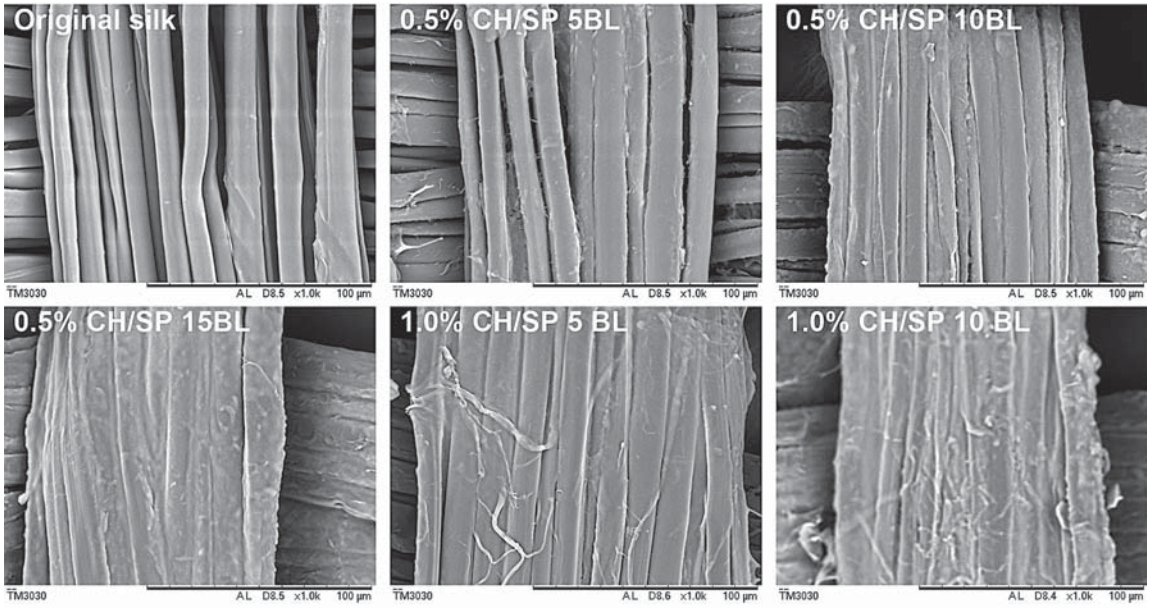

Figure 2: SEM images of silk fabrics obtained using two concentrations of CH/SP at different BLs

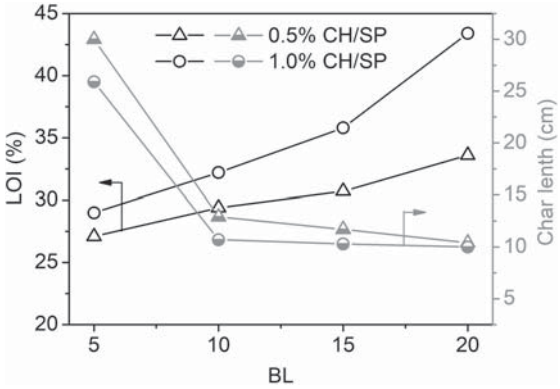

Figure 3: LOI and char length of silk fabrics obtained using two concentrations of CH/SP at different BLs

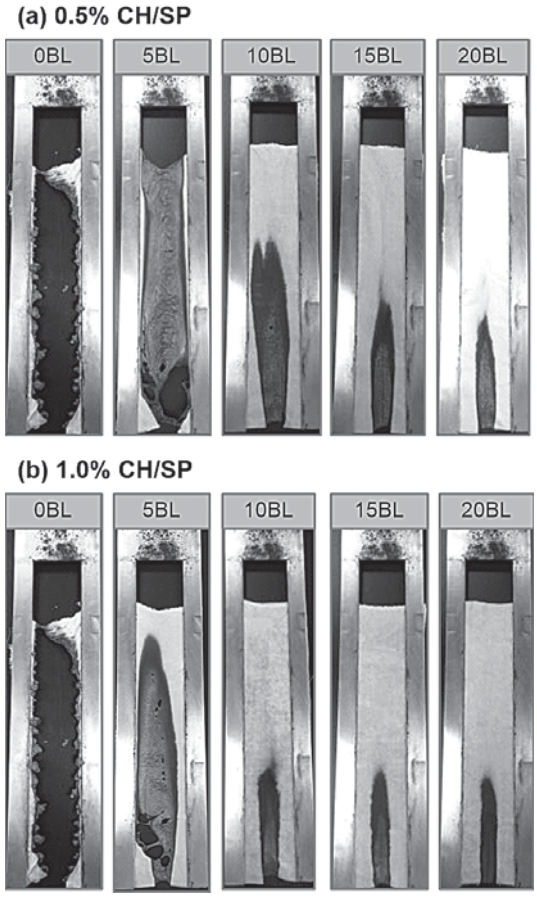

Figure 4: Vertical burning results of silk fabrics obtained using two concentrations of CH/SP at different BLs

3.3 Whiteness, stiffness, lustre and tensile strength of coated silk fabric

SP has a slightly yellow appearance, and the yellowing of SP occurs during heating due to oxidation [20]. These factors would affect the colour of the coated fabric. In addition, the advantages of silk include its soft touch and gentle lustre. The coating of CH polymer on the surface of silk thus has a negative effect on the softness and lustre of silk fabric. The whiteness, stiffness and lustre of coated silk fabric were therefore evaluated.

Figure 5 shows that there was an obvious decrease in whiteness with an increase in CH/SP concentration and assembled BLs. Taking this into account, an excessively high concentration of CH/SP and a high number of assembled BLs should be avoided.

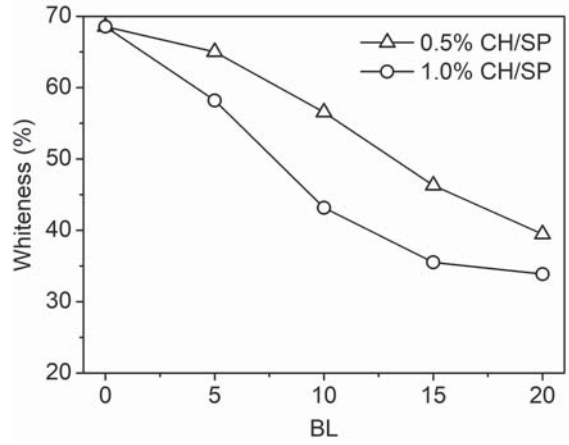

Figure 5: Whiteness of silk fabrics obtained using two concentrations of CH/SP at different BLs

Figure 6 shows that the stiffness of silk fabric increased greatly as the concentration of CH/SP and the number of assembled BLs were increased. In the case of 0.5% CH/SP, 5 and 10 BL assemblies had a

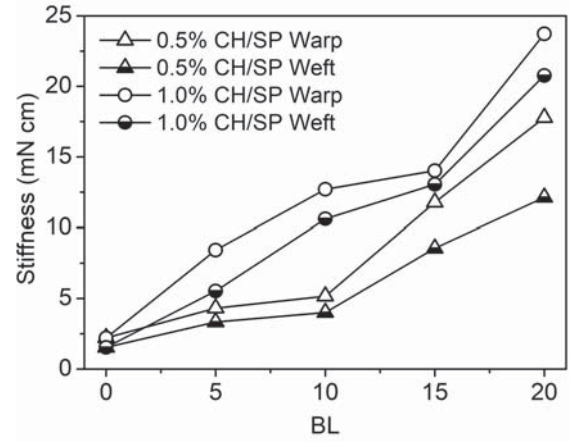

Figure 6: Stiffness of silk fabrics obtained using two concentrations of CH/SP at different BLs

relatively small effect on the stiffness of silk fabric. Taking into account both stiffness and FR properties (Figures 3 and 4), an excessively high concentration of CH/SP and a high number of assembled BL should also be avoided. Here it should be noted that the decreased softness of silk fabric caused by FR coating is sometimes a disadvantage and sometimes an advantage, depending on the applications of silk fabric. For example, the use of silk fabrics as tablecloths, sofa fabrics, wall furnishing fabrics, jackets, etc. usually requires decreased softness or increased stiffness. Thus, the coated fabrics obtained using the present approach can meet the requirement for increased stiffness. The proper weight gain and stiffness can be determined according to the results of Figures 1 and 6 and the end-uses of silk fabrics.

Figure 7 shows that the reflectivity of silk fabric, as an expression of its lustre, decreased considerably as the concentration of CH/SP and the number of assembled BLs increased, due to an increase in the roughness of fabric surface on account of deposits of CH polymer. The decrease in the lustre of silk fabric is a disadvantage of the present LbL assembly.

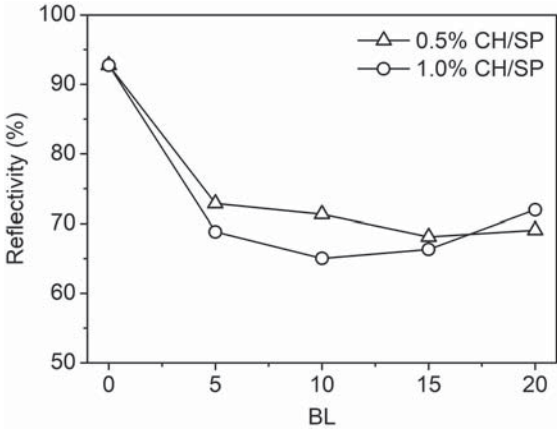

Figure 7: Light reflectivity of silk fabrics obtained using two concentrations of CH/SP at different BLs

The tensile strength of silk fabric was also measured. As shown in Figure 8, the tensile strength of silk fabric in the warp and weft directions increased significantly with an increase in the concentration of CH/SP and the number of assembled BLs. This is associated with the reinforcement effect of CH polymer. Increased tensile strength would be beneficial for the application of silk fabric in decorative materials.

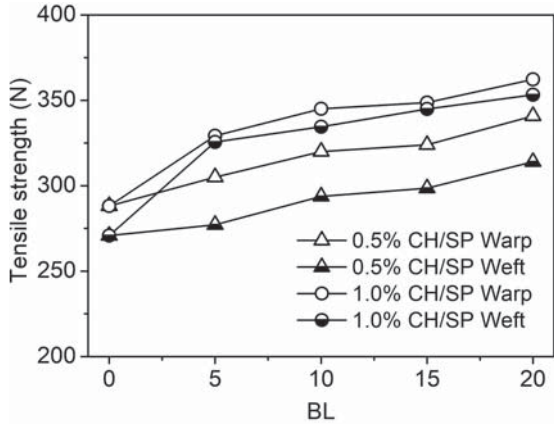

Figure 8: Tensile strength of silk fabrics obtained using two concentrations of CH/SP at different BLs

3.4 Washing durability of coated silk fabric

Silk fabrics for furnishings are subjected to different degrees of washing, depending on the end-uses of fabrics. The washing durability of the coated silk fabric was thus evaluated. Figure 9 shows that the LOI of the coated fabric gradually decreased with an increase in the number of washing cycles. The decrease in LOI was related to the LOI of the unwashed sample or CH/SP concentration and assembled BLs. After 15 washing cycles, all samples still had a char length of less than 15 cm, and passed the vertical burning test for the B1 level. It was worthy of noting that the samples obtained using 0.5% CH/SP and 15 BLs and 1.0% CH/SP and 10 BLs exhibited high LOI, even after 10 or 15 washing cycles, indicating their good washing durability. The good washing durability of coatings is associated with *in situ* formation and the insolubilisation of CH/SP polyelectrolytes on the surface of silk [17, 21].

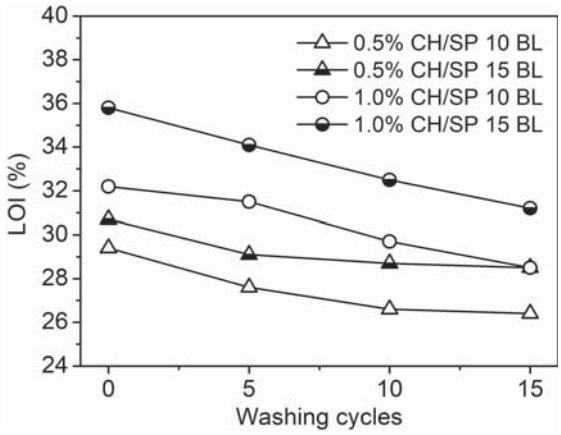

Figure 9: Washing durability of silk fabrics obtained using two concentrations of CH/SP at 10 and 15 BLs

3.5 PCFC analysis of coated silk fabric

A microcalorimeter was further used to evaluate the flammability of silk fabric. A sample of several milligrams was required for the PCFC analysis. The sample was first pyrolyzed in nitrogen. The volatile products were then mixed with oxygen and burned in a combustion zone in order to measure the combustion heat of pyrolysis products [22]. Several flammability parameters were obtained, including the heat release rate (HRR), total heat release (THR), heat release capacity (HRC), the peak heat release rate (pHRR), temperature at maximum heat release rate (T_{max}) and char residue yield. Figure 10 shows the measured HRR values of silk fabrics as a function of temperature, while Table 1 lists the associated PCFC parameters.

Figure 10 shows that the HRR of the coated fabrics decreased in the temperature range of 300 °C to 500 °C and that the T_{max} shifted to a lower temperature (also see Table 1) compared to that of the original sample. The decreased T_{max} of the coated fabrics is due to the lower initial thermal stability of CH and SP [20, 23]. It is evident from Table 1 that the coated fabrics exhibited significant decreases in HRR, THR and HRC, indicating their low heat release during combustion. Such fabrics would represent a low fire hazard [24]. Moreover, the coated fabrics yielded higher char amounts in the heat pyrolysis than the original sample. This implies the reduced volatility of products and the formation of thermal protection layers. The latter can inhibit the further burning of polymeric substrates and thus lead to the enhanced FR properties of the fabrics.

3.6 Thermal stability of coated silk fabric

The TG curves of silk fabrics are shown in Figure 11. The weight loss process of uncoated silk was divided into three stages: the first stage where the loss of adsorbed water occurred before 250 °C; the second stage where that loss occurred between 250 °C and 350 °C, which represents a major thermal decomposition of silk causing the splitting of protein chains; and the third stage where that loss occurred above 350 °C, which represents the further pyrolysis of degraded products. The residual weight was around 27% at 600 °C.

After coating, silk displayed significant changes in weight loss. Decreased weight loss occurred below 310 °C. One important reason for this is that CH has a higher degradation below 300 °C than the original

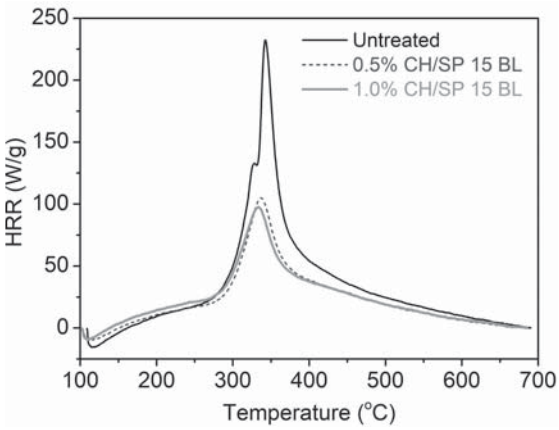

Figure 10: Heat release rate curves of silk fabrics obtained using two concentrations of CH/SP at 15 BL

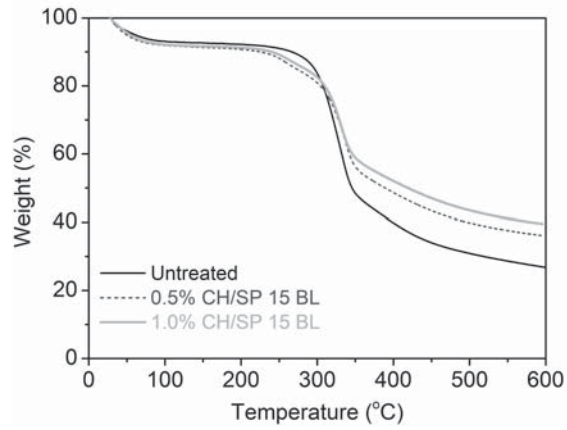

Figure 11: TG curves in nitrogen of silk fabrics obtained using two concentrations of CH/SP at 15 BL

Table 1: PCFC parameters of silk fabrics obtained using two concentrations of CH/SP at 15 BL

CH/SP conc. (% wt)	BL	pHRR (W/g)	HRC ($Jg^{-1} K^{-1}$)	THR (KJ/g)	T_{max} (°C)	Char yield (%)
0	0	232.4	251	17.9	342.7	26.58
0.5	15	105.1	112	12.3	336.5	37.89
1.0	15	97.5	105	12.8	333.4	39.30

silk [23, 25]. Above 310 °C, the coated fabrics exhibited lower weight loss than the original silk. There were two reasons for this. One reason is the good thermal stability of the degraded products of CH and SP on silk at high temperatures [23, 26]. The other reason is that SP containing six phosphate groups is a charring agent that promotes the dehydration and char forming of silk. At 600 °C, the residual weight of the fabrics coated with 0.5% and 1.0% CH/SP was 36% and 40%, respectively. This correlates well with those in the PCFC analysis (Table 1).

Taking into account the results of the PCFC and TG analyses, it can be concluded that the CH/SP FR system acts in the solid phase by catalysing the charring of silk and thus providing thermal protection layers during combustion.

4 Conclusion

The FR modification of silk fabric with CH and SP was performed using a LbL padding assembly. With regard to the weight gain, FR properties, whiteness, stiffness and washing durability of coated fabrics, the assemblies using 0.5% CH/SP at 10 and 15 BLs and 1.0% CH/SP at 10 BLs were good selections. The resulting fabrics exhibited good FR properties, as indicated by LOI and vertical combustion tests, and could be subjected to more than 15 cycles of washing. The PCFC and TG analyses revealed that the condensed phase FR mechanism was suitable for coated fabrics. Because of the high weight increase of coated fabrics, the present LbL approach seemed to be more suitable for the FR finishing of decorative silk textiles.

Acknowledgements

This study was funded by the Jiangsu Provincial Key Research and Development Program of China (BE2015066) and the Priority Academic Program Development (PAPD) of Jiangsu Higher Education Institutions (No. 2014-37).

References

1. ZHANG, Xibiao, ZHOU, Xian-You, CHENG, Xian-Wei, TANG, Ren-Cheng. Phytic acid as an eco-friendly flame retardant for silk/wool blend: A comparative study with fluorotitanate and fluorozirconate. *Journal of Cleaner Production*, 2018, 198, 1044–1052, doi: 10.1016/j.jclepro.2018.07.103.
2. GUAN, Jinping, YANG, Charles Q, CHEN, Guoqiang. Formaldehyde-free flame retardant finishing of silk using a hydroxyl-functional organophosphorus oligomer. *Polymer Degradation and Stability*, 2009, **94**(3), 450–455, doi: 10.1016/j.polymdegradstab.2008.10.024.
3. LEE, G. Fred. Role of phosphorus in eutrophication and diffuse source control. *Water Research*, 1973, **7**, 111–128, doi: 10.1016/0043-1354(73)90156-5.
4. ŠEHIĆ, Alisa, TAVČER, Petra Forte, SIMONČIČ, Barbara. Flame retardants and environmental issues. *Tekstilec*, 2016, **59**(3), 196–205, doi: 10.14502/Tekstilec2016.59.196-205.
5. CHAIWONG, C., TUNMA, S., SANGPRASERT, W., NIMMANPIPUG, P., BOONYAWANAB, D. Graft polymerization of flame-retardant compound onto silk via plasma jet. *Surface and Coatings Technology*, 2010, **204**(18–19), 2991–2995, doi: 10.1016/j.surfcoat.2010.02.044.
6. CHENG, Xian-Wei, GUAN, Jin-Ping, YANG, Xu-Hong, TANG, Ren-Cheng. Improvement of flame retardancy of silk fabric by bio-based phytic acid, nano-TiO_2, and polycarboxylic acid. *Progress in Organic Coatings*, 2017, **112**, 18–26, doi: 10.1016/j.porgcoat.2017.06.025.
7. GUAN, Jinping, CHEN, Guoqiang. Flame resistant modification of silk fabric with vinyl phosphate. Fibers and Polymers, 2008, **9**(4), 438–443, doi: 10.1007/s12221-008-0070-9.
8. LIU, Chun, XING, Tieling, WEI, Bingju, CHEN, Guoqiang. Synergistic effects and mechanism of modified silica sol flame retardant systems on silk fabric. *Materials*, 2018, **11**(10), 1842, doi: 10.3390/ma11101842.
9. ALONGI, Jenny, CAROSIO, Federico, MALUCELLI, Giulio. Current emerging techniques to impart flame retardancy to fabrics: an overview. *Polymer Degradation and Stability*, 2014, **106**, 138–149, doi: 10.1016/j.polymdegradstab.2013.07.012.
10. COSTES, Lucie, LAOUTID, Fouad, BROHEZ, Sylvain, DUBOIS, Philippe. Bio-based flame retardants: When nature meets fire protection. *Materials Science and Engineering R*, 2017, **117**, 1–25, doi: 10.1016/j.mser.2017.04.001.
11. MALUCELLI, Giulio, BOSCO, Francesca, ALONGI, Jenny, CAROSIO, Federico, Di BLASIO,

Alessandro, MOLLEA, Chiara, CUTTICA, Fabio, CASALE, Annalisa. Biomacromolecules as novel green flame retardant systems for textiles: an overview. *RSC Advances*, 2014, **4**(86), 46024–46039, doi: 10.1039/c4ra06771a.

12. HOLDER, Kevin M., SMITH, Ryan J., GRUNLAN, Jaime C. A review of flame retardant nanocoatings prepared using layer-by-layer assembly of polyelectrolytes. *Journal of Materials Science*, 2017, **52**(22), 12923–12959, doi: 10.1007/s10853-017-1390-1.
13. MALUCELLI, Giulio. Surface-engineered fire protective coatings for fabrics through sol-gel and layer-by-layer methods: an overview. *Coatings*, 2016, **6**(3), 33, doi: 10.3390/coatings6030033.
14. SRIKULKIT, Kawee, IAMSAMAI, Chularat, DUBAS, Stephan T. Development of flame retardant polyphosphoric acid coating based on the polyelectrolyte multilayers technique. *Journal of Metals, Materials and Minerals*, 2006, **16**(2), 41–45.
15. CAROSIO, Federico, Di BLASIO, Alessandro, ALONGI, Jenny, MALUCELLI, Giulio. Green DNA-based flame retardant coatings assembled through layer by layer. *Polymer*, 2013, **54**(19), 5148–5153, doi: 10.1016/j.polymer.2013.07.029.
16. KUNDU, Chanchal K., WANG, Xin, SONG, Lei, HU, Yuan. Borate cross-linked layer-by-layer assembly of green polyelectrolytes on polyamide 66 fabrics for flame-retardant treatment. *Progress in Organic Coatings*, 2018, **121**, 173–181, doi: 10.1016/j.porgcoat.2018.04.031.
17. LAUFER, Galina, KIRKLAND, Christopher, MORGAN, Alexander B, GRUNLAN, Jaime C. Intumescent multilayer nanocoating, made with renewable polyelectrolytes, for flame-retardant cotton. *Biomacromolecules*, 2012, **13**(9), 2843–2848, doi: 10.1021/bm300873b.
18. LI, Zhong-Fang, ZHANG, Chuan-Jie, CUI, Li, ZHU, Ping, YAN, Chao, LIU, Yun. Fire retardant and thermal degradation properties of cotton fabricsbased on APTES and sodium phytate through layer-by-layer assembly. *Journal of Analytical and Applied Pyrolysis*, 2017, **123**, 216–223, doi: 10.1016/j.jaap.2016.11.026.
19. LIU, Juan, XIAO, Congming. Fire-retardant multilayer assembled on polyester fabric from water-soluble chitosan, sodium alginate and divalent metal ion. International *Journal of Biological Macromolecules*, 2018, **119**, 1083–1089, doi: 10.1016/j.ijbiomac.2018.08.043.
20. DANELUTI, André Luis Máximo, MATOS do ROSÁRIO, Jivaldo. Study of thermal behavior of phytic acid. *Brazilian Journal of Pharmaceutical Sciences*, 2013, **49**(2), 275–283, doi: 10.1590/S1984-82502013000200009.
21. ZHANG, Tao, YAN, Hongqiang, SHEN, Lie, FANG, Zhengping, ZHANG, Xianming, WANG, Jiajun, ZHANG, Baoyue. Chitosan/phytic acid polyelectrolyte complex: a green and renewable intumescent flame retardant system for ethylene-vinyl acetate copolymer. *Industrial and Engineering Chemistry Research*, 2014, **53**(49), 19199–19207, doi: 10.1021/ie503421f.
22. ALONGI, Jenny, CUTTICA, Fabio, CAROSIO, Federico, BOURBIGOT, Serge. How much the fabric grammage may affect cotton combustion? *Cellulose*, 2015, **22**(5), 3477–3489, doi: 10.1007/s10570-015-0717-9.
23. ZHANG, Sheng, LIU, Xiaodong, JIN, Xiaodong, LI, Hongfei, SUN, Jun, GU, Xiaoyu. The novel application of chitosan: effects of cross-linked chitosan on the fire performance of thermoplastic polyurethane. *Carbohydrate Polymers*, 2018, **189**, 313–321, doi: 10.1016/j.carbpol.2018.02.034.
24. LYON, Richard E., WALTERS, R. N., STOLIAROV, S. I. Screening flame retardants for plastics using microscale combustion calorimetry. *Polymer Engineering and Science*, 2007, **47**(10), 1501–1510, doi: 10.1002/pen.20871.
25. LV, Zhong, HU, Yi-Ting, GUAN, Jin-Ping, TANG, Ren-Cheng, CHEN, Guo-Qiang. Preparation of a flame retardant, antibacterial, and colored silk fabric with chitosan and vitamin B2 sodium phosphate by electrostatic layer by layer assembly. *Materials Letters*, 2019, **241**, 136–139, doi: 10.1016/j.matlet.2019.01.005.
26. PAN, Ying, ZHAN, Jing, PAN, Haifeng, WANG, Wei, TANG, Gang, SONG, Lei, HU, Yuan. Effect of fully biobased coatings constructed via layer-by-layer assembly of chitosan and lignosulfonate on the thermal, flame retardant, and mechanical properties of flexible polyurethane foam. *ACS Sustainable Chemistry and Engineering*, 2016, **4**(3), 1431–1438, doi: 10.1021/acssuschemeng.5b01423.

J N Chakraborty, Yashdeep Sharma
Dr. B R Ambedkar National Institute of Technology, Department of Textile Technology, Jalandhar 144011, Punjab, India

Comparative Performance of Synthesised Silica Nanoparticles for Enhanced Hydrophilic Properties on Cotton

Primerjalna zmogljivost sintetiziranih nanodelcev silicijevega dioksida za izboljšanje hidrofilnosti bombaža

Original Scientific Article/*Izvirni znanstveni članek*
Received/*Prispelo* 4-2019 • Accepted/*Sprejeto* 10-2019

Abstract

Chemicals in nano-form are free from aggregates and low concentration effective. The nanoparticles of certain chemicals have been found to be of substantial importance for application in textiles as well as allied fields. Nano-silica is one of such nanoparticles possessing enormous potential for multi-functional application on cotton. However, the cost of nanoparticles is remarkably high, thus limiting their commercial applications. This study discusses the manufacture of silica nanoparticles in a laboratory, their characterisation, succeeded by their application on cotton. The performance was compared with those obtained with tailor-made silica nanoparticles from manufacturers. It was found that laboratory-made silica nanoparticles are relatively capable of developing a parallel finishing effect on cotton compared to those obtained with tailor-made silica nanoparticles.

Keywords: tetraethyl orthosilicate, nano-silica, absorbency, tensile strength

Izvleček

Snovi v nanoobliki ne vsebujejo agregatov in so učinkovite pri nizki koncentraciji. Ugotovljeno je bilo, da so nanodelci nekaterih snovi pomembni za uporabo v tekstilstvu in na sorodnih področjih. To velja za nanodelce silicijevega dioksida, ki imajo velike možnosti za oblikovanje večfunkcionalnih lastnosti na bombažu. Vendar pa izjemno visoka cena nanodelcev omejuje njihovo tržno uporabo. Ta študija obravnava laboratorijsko izdelavo nanodelcev silicijevega dioksida in njihovo karakterizacijo, ki ji je sledila uspešna uporaba na bombažu. Njihova učinkovitost je bila primerjana s tržnimi produkti nanodelcev silicijevega dioksida. Ugotovljeno je bilo, da so bili laboratorijsko izdelani nanodelci silicijevega dioksida sposobni na bombažu oblikovati primerljive plemenitilne učinke kot tržno dostopni silicijevi nanodelci.

Ključne besede: tetraetil ortosilikat, nanosilica, vpojnost, natezna trdnost

1 Introduction

Applied technology has witnessed remarkable progress due to the inclusion of nanotechnology. By minimizing the cluster size of particles, gigantic changes have been observed in the properties exhibited by the particles due to the quantum effect shown by nanoparticles [1]. These enhanced properties may be inherited on a fabric substrate by applying nano chemicals to a fabric. Different functional properties are induced in the fabric using nanoparticles such as water/oil repellence, self-cleaning properties, UV blocking and antimicrobial properties [2–6]. In some cases, nanoparticles are also observed to enhance colour fastness [7].

Corresponding author/*Korespondenčni avtor:*
J N Chakraborty
E-mail: chakrabortyjn@gmail.com

Out of several types of nanoparticles possessing technological importance, i.e. TiO_2, ZnO and SiO_2, the latter , i.e. SiO_2 has been found to be rather interesting. Acrylic-based polyurethane nano-particulate clearcoats are reinforced with fumed and precipitated nano-silica reinforcements to induce scratch proofing as well as improved abrasion resistance [8].

Mini-emulsified butylacrylate/acrylonitrile (BA/AN) copolymer-silica nanoparticles nanocomposites containing three different concentrations of silica nanoparticles, i.e. 1, 3 and 5 (wt%), were applied as a functional binder via silk screen printing on 100% cotton and 100% polyester. The prepared copolymer, silica nanoparticles and their nanocomposites were characterised. The evaluation of surface morphology, colourfastness, hydrophobic behaviour and UV protection of printed fabrics showed an improvement in colour fastness, UV protection and self-cleaning properties against only 1% silica nanoparticles. Moreover, almost all silica nanoparticles remained strongly adhered to the binder that provides long activity for printed fabrics with no harmful effects for users [9].

Imparting a water repellent treatment on a cotton fabric by sequentially coating the cotton fabric with a polymer nanocomposite comprising a C-6 perfluorinated acrylic copolymer and silica nanoparticles and polydimethylsiloxane (PDMS) resin resulted in repelling water droplets at the roll-off angles well below 20°, even impinging small droplets (8 mL) could be repelled with the droplet roll-off angle of 17°. The treated fabrics were able to hold a hydrostatic head pressure of 2.56 kPa before leak. The finished cotton fabric resisted wear abrasion under 17.5 kPa up to 30 abrasion cycles. Furthermore, the open porous structured was preserved allowing breathability. The application of low-cost polymers and non-toxic ingredients in this finish opens scope for commercial application [10].

Silver nanoparticles with the average size of 14 nm were immobilised on silica nanoparticles surfaces with the average particle size of 150 nm derived from rice husk, dispersed in binder and coated on a textile surface. The mass ratio of silica nanoparticles was varied. The UV protection factor (UPF) of treated textiles was substantially enhanced by more than 6 and 7 folds compared to the textile binder treated and control textile, respectively. The antibacterial properties faced a drastic increase as well. The textile coated with silver nanoparticles immobilised over silica nanoparticles achieved an increase in the clear inhibition zone compared to the textile containing only silver nanoparticles, where only a 30 mm clear zone was recorded [11]. In addition, an excellent hydrophobic surface was obtained at the water contact angle of 145°.

In fields other than textile, silica nanoparticles are extensively used in the manufacturing of durable superamphiphobic nano-silica and epoxy composites [12], surface treatments [13], coating and film formation [14–17], cement technology [18, 19], drilling fluid in natural gas extraction [20], multifunctional effects on wooden materials [21], in the field of medicines [22], immobilisation of protein [23], separation of components from emulsion [24], constructing pig houses [25] and many others. However, very high costs of silica nanoparticles restrict their use in commercial application.

Although the application of silica nanoparticles was studied on textile fabrics to develop numerous functional properties, e.g. improvement in colour fastness, UV protection, self-cleaning, water repellent breathable fabrics, anti-bacterial and hydrophobic fabrics etc, no such study has yet been carried out to enhance the water absorption of treated cotton fabrics.

In this work, a pre-treated cotton fabric was finished with three types of SiO_2, i.e. normal bulk, laboratory synthesised and tailor-made, to see their comparative performance in the hydrophilic silica finish on cotton. Organometallic hydrolysis followed by condensation reaction was used for the sol gel synthesis of nanoparticles. Synthesised nanoparticles were characterised for particle size, chemical and physical characteristics, and colour. The finished cotton fabric was evaluated for absorbency, cyclic wash fastness, tensile strength, pore size and stiffness.

2 Materials and methods

2.1 Materials

A plain, woven, pre-treated cotton fabric, possessing 55.0 ends/cm, 28.3 picks/cm, with 14.76 tex of the linear density of warp yarn, 14.76 tex of the linear density of weft yarn and 126 g/m^2 of mass per unit area was used in this study.

The precursor tetraethyl orthosilicate (TEOS, $SiC_8H_{20}O_4$, AR) was procured from M/s Sigma Aldrich. Propan-2-ol (Isopropyl alcohol, C_3H_8O, AR), ammonium hydroxide (NH_4OH, 25% v/v), ammonium fluoride (NH_4F, AR) and acrylic acid

binder ($C_3H_4O_2$, AR) were procured from M/s SDFCL, Mumbai and distilled water was used for synthesis. Glass apparatus was boiled in a nitric acid solution prior to use.

2.2 Methods

SiO_2 nanoparticles were synthesised in a laboratory after the optimisation in the experimental setup as shown in Figure 1.

Different combinations of the recipe for the SiO_2 nanoparticle synthesis were tested for the smallest nanoparticle obtained. A further optimised recipe was used for the synthesis and application on the fabric. The complete process was conducted at room temperature.

For the synthesis of SiO_2 nanoparticles, 0.01 mole (2.08 g) of TEOS was dissolved in 60 mL of propanol and this solution was labelled as solution A. 0.02 mole (0.36 g) of water and 0.04 mole (1.40 g) of ammonia solution was dissolved in 60 mL propanol and was labelled as solution B. Solution C was prepared by dissolving 1.852 g of ammonium fluoride in 20.50 g of ammonium hydroxide (30%), and then dissolving this solution in 100 mL of distilled water.

Solution A was transferred to a flat bottom flask and vigorously stirred using a magnetic stirrer. Solution B was transferred to a burette and was added to solution A over 80 min of uniformly drop by drop pouring with constant stirring. The drop of water had to be from the height closest to the fabric, yet not touching it, otherwise the fabric might absorb more water. After solution B was emptied completely into solution A, the flat bottom flask was covered and the stirring continued for another 60 min to get a colourless clear solution. This solution was nano sol.

At the end of stirring, 5–6 drops of solution C were added to nano sol and this solution was then shifted to a beaker. Within a few seconds, the final solution transformed into a slightly bluish white gel. This gel was heated up to evaporate the solvent and obtain bulky, flower shaped and very light powdery SiO_2 nanoparticles.

2.3 Characterisation

The nanoparticles were characterised for their size, chemical and physical characteristics using the ultraviolet visible (UV-VIS) spectroscopy (Lambda 365, Perkin Elmer), particle size analysis (Beckman Coulter, US), and primary salt analysis techniques, e.g. colours of both, nano sol formed and nanoparticles obtained, colour change upon heating, visual appearance and texture of nanoparticles.

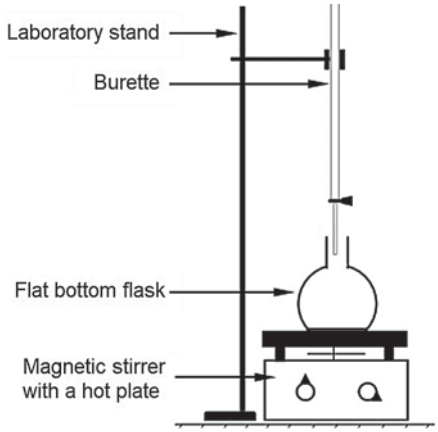

Figure 1: Schematic of experimental setup for synthesis of SiO_2

2.4 Process optimisation

To synthesise smallest nanoparticles, the Box and Behnken design of experiment was used. The variable parameters were the amount of solvent (propanol), molar ratio of water and ammonia solution with respect to TEOS for catalyst solution, and time of adding catalyst solution to precursor solution. Different combinations of recipes were used to obtain nanoparticles. The nanoparticles obtained from design combinations were analysed with UV-VIS spectroscopy at constant weight by volume solution of nanoparticles and water.

For different particle sizes and identical concentration of the nanoparticle solution, the absorption value of a characteristic peak of the chemical under observation varied according to its size. The larger the size of particles, the lower is the absorption value. This is due to the fact that as the surface area of particles decreases, the number of active sites decreases, which consequently decreases the absorption value. Thus, the nanoparticle solution with the highest absorption value has the smallest particle size. For the analysis of the Box and Behnken design, making surface plots and obtained results, the Statease Design-Expert® 6 software was used.

2.5 Coating of nanoparticles on fabric

The pad-dry-cure method was followed for the application of nanoparticles to the fabric. SiO_2 nanoparticles at varying concentrations, i.e. 0.5%, 1% and 1.5%, were used to prepare pad liquor with

0.5% acrylic acid as binder. The fabric was padded with liquor in a padding mangle with 1 kg/cm^2 to achieve around 80% expression. The padded samples were dried at 80 °C in a hot air oven and were cured at 150 °C for 5 min.

2.6 Functional and wash fastness testing

Absorbency time was taken as a parameter to evaluate the functional properties of silica nanoparticles applied to the fabric. A drop of water was allowed to fall onto a dry fabric surface and the time taken for the drop to completely disappear into the fabric was noted with the help of a stop watch.

The wash fastness of the finish was conducted in line with the International Standard Organisation Method 3 (ISO-3) specifications. The washing was done with a soap solution (5 g/L), sodium carbonate (Na_2CO_3, 2 g/L), liquor ratio (1 : 50), temperature (60 ± 2) °C for 30 min. The fabric underwent 5 wash cycles and the functional testing was carried out after each wash.

2.7 Physical testing of fabric

The tensile behaviour of the finished fabric was tested using the ASTM D5035 test method on a Universal testing machine (Zwick, Switzerland). The particle size analyser (Beckman Coulter, US) was used to measure the size of silica nanoparticles and the pore size measurement (ASTM 316) was done to evaluate the change in pore size of the fabric after applying the finish (Capillary Flow Porometer, CFP 1100AN, PMI, India). In this test, a wetting liquid is allowed to spontaneously fill the pores of the specimen (2 cm) and non-reacting pressurised gas is allowed to displace the liquid from the pores. The gas pressure and flow rates through the wet and dry samples are accurately measured. The gas pressure required to remove the liquid from the pores and cause gas to flow is given by the Washburn equation: $D = 4\gamma\cos\theta/p$, where D is pore diameter, γ is surface tension of liquid, θ is contact angle of liquid, and p is differential gas pressure. From the measured gas pressure and flow rate, the pore throat diameter, pore size distribution and gas permeability are calculated.

The ASTM D 1388 cantilever test method was used to determine fabric stiffness. In this test, the fabric specimen is allowed to bend under its own weight. The free length, which bends under its own weight sufficiently to make its leading edge intersect the line of 41.5° inclinations, is called the bending length of the fabric. The dimension of the specimen used for the testing is 20 cm × 5 cm.

The ASTM D 1388 cantilever test method and stiffness tester (Unilab, India) were used to evaluate fabric stiffness. The sample size of 20 cm × 5 cm was allowed to bend under its own weight to just intersect the 45° line.

3 Results and discussion

3.1 Characterisation of nanoparticles

The characterisation of nanoparticles was performed using UV-VIS spectroscopy to confirm the SiO_2 synthesis. A further particle size analysis (PSA) was done to confirm the formation of nanoparticles and analyse the size of synthesised particles. The characteristic peak of SiO_2 was observed in the range 190–195 nm. The absorption peak wavelength coincides with the SiO_2 nanoparticles procured from M/s Sigma Aldrich.

The particle size analysis was conducted on a Beckman Coulter Delsa™ Nano. The particle diameter was 345.3 nm. The intensity distribution curve is shown in Figure 2.

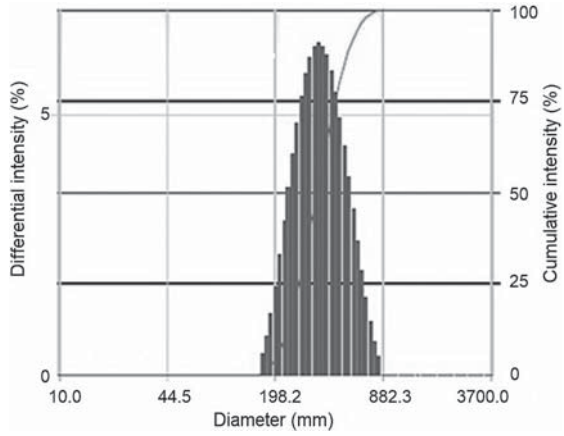

Figure 2: Intensity distribution of SiO_2 nanoparticles

3.2 Process optimisation of synthesis

For the optimisation of synthesis, the Box and Behnken design of experiment was used. The amount of water and ammonia used in terms of parts per unit part of TEOS was 2 to 6, propanol 60 mL to 80 mL and the time of introducing solution B into solution A (pouring time) was 30 min to 90 min, these data being used as process parameters and end points for the design of the experiment. Different

Table 1: Combinations of reaction parameters for synthesis of SiO_2 nanoparticles

S. no.	Water (parts for 1 part TEOS)[a)]	Ammonia (parts for 1 part TEOS) [a)]	Propanol (mL)	Pouring time (min)	Absorbance
1	2	4	60	30	0.25
2	4	4	80	30	0.16
3	6	2	60	60	0.13
4	4	2	40	60	2.66
5	4	4	60	60	2.59
6	4	6	60	90	1.31
7	4	2	80	60	0.06
8	4	2	60	30	0.5
9	4	6	40	60	2.51
10	4	6	60	30	0.17
11	6	4	80	60	1.74
12	4	6	80	60	0.24
13	4	4	60	60	2.59
14	6	4	60	90	0.07
15	6	6	60	60	2.78
16	2	4	60	90	1.5
17	2	6	60	60	1.79
18	4	4	60	60	2.59
19	6	4	40	60	1.33
20	4	4	80	90	0.13
21	4	4	60	60	2.59
22	2	4	40	60	1.86
23	4	2	60	90	1.35
24	4	4	40	90	2.72
25	4	4	40	30	2.98
26	2	4	80	60	3.34
27	2	2	60	60	2.53
28	6	4	60	30	0.43
29	4	4	60	60	2.59

[a)] Part for 1 part in terms of weight

combinations of reaction parameters were used and their respective absorbance values are shown in Table 1.

The R^2 value was found to be 0.6639 and the computed equation for absorption is:

Absorption (AU) = –4.69 + 0.62 × (*water/parts for 1 part of TEOS*) + 0.31 × (*ammonia/parts for 1 part of TEOS*) + 0.03 (*propanol/mL*) + 0.18 (*time/min*) – 0.10 (*water/parts for 1 part of TEOS*)^2 – 0.16 × (*ammonia/parts for 1 part of TEOS*)^2 – 4.61 × (*propanol/ml*)^2 – 1.33 × (*time/min*)^2 + 0.21 × *[(water/parts for 1 part of TEOS) × (ammonia/parts for 1 part of TEOS)]* – 6.68 × [(*water/parts for 1 part of TEOS) × (propanol/ml*)] – 6.70 × *[(water/parts for 1 part of TEOS) × (time/min)]* + 2.06 × *[(ammonia/parts for 1 part of TEOS)× (propanol/mL)* + 1.20 × *[(ammonia/parts for 1 part of TEOS) × (time/min)]* + 9.58 × [(*propanol/mL) × (time/min*)]

The 0.6639 value of R^2 is relatively good, possessing 66% accuracy on the above equation. In general, R^2

should approach 1 for best performance; however, in the case of the synthesis of a chemical, the value R^2 remains substantially below 1 and more than 60% is considered satisfactory arising from the presence of impurities in chemicals.

Surface plots describing the effect of the combination of different parameters on absorbance for the experiment are shown in Figure 3. The optimised recipe used for the synthesis of SiO_2 was the combination no. 16, i.e. water 2 parts, ammonia 4 parts,

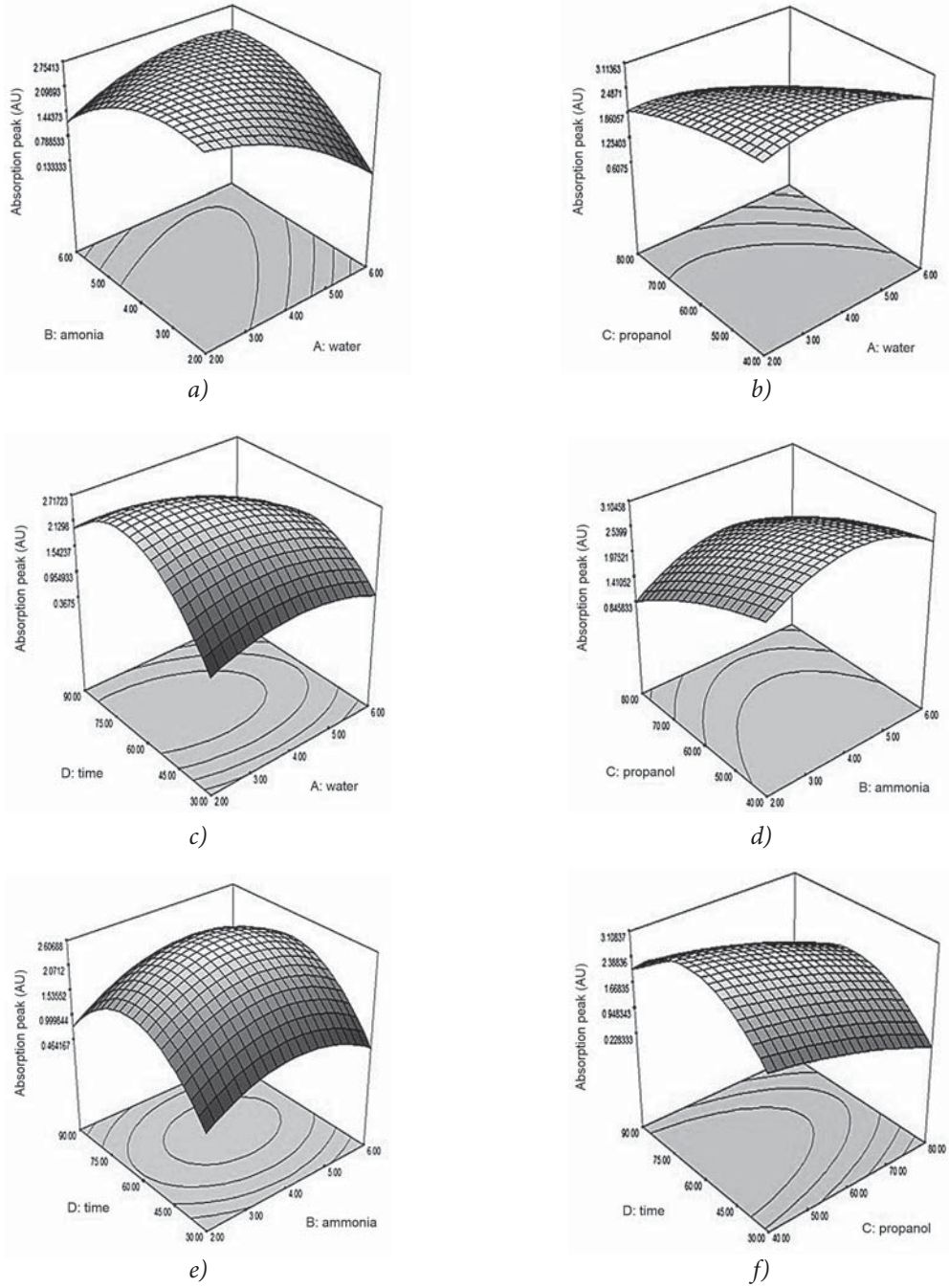

Figure 3: Surface plots for change in absorbance against different combinations of: a) ammonia and water, b) propanol and water, c) pouring time and water, d) propanol and ammonia, e) pouring time and ammonia, f) pouring time and propanol

propanol 60 mL, pouring time 90 min and absorption 1.5.

The interaction of water and ammonia has been depicted in the surface plot (Figure 3a), according to which, a higher amount of ammonia (in parts) as compared to water leads to a higher absorption peak, i.e. an increase in the share of ammonia in the reaction mixture helps increase the absorption.

While the interaction of propanol and water (cf. Figure 3b) suggests that the lower the concentration of water in propanol, the higher the absorption peak, achieving higher absorption values, the water concentration shall be lower in propanol. In Figures 3c and 3f, it can be observed that prolonged pouring times of water in the reaction mixture give higher peak absorption values, and that the same trend is valid for propanol. Therefore, to achieve higher peak values, in general, the pouring time should be increased to an optimised limit. On the other hand, the too much increased time also increases the chances of possible coagulation of particles and decreased peak intensity. Whereas Figure 3e implies a decrease in the absorption peak when the pouring time and the amount of ammonia is below or above the optimised limit of 60 min of pouring and 4 parts of used ammonia, the pouring time and ammonia in the mixture has a specific ratio in which the highest absorption can be achieved. As observed in Figure 3d, lower amounts of propanol with respect to higher ammonia yields give a higher absorption peak value, but increased/decreased amount of ammonia than the optimised limit also leads to a decrease in the absorption peak.

A further relation of the absorption peak value and particle size can be interpreted as described in section 2.4. The higher the absorption peak values, the smaller the particle size.

3.3 Scanning electron microscopy (SEM)

SEM was conducted to study the surface morphology of the fabric surface after finishing and is shown in Figure 4.

It can be observed that the fibres retained a uniform layer of nanoparticles on them. A closer view (cf. Figure 4c) is indicative of a white ball shaped nanoparticle stuck on the fibre surface without any damage in the fibre structure. Finer cracks on the fibre (cf. Figure 4c) is a consequence of padding pressure during the application, developing a minor fibre damage, which is also too small to be noticeable at smaller resolutions.

3.4 Functional testing

The tests for absorbency were performed on an unfinished control, a sample finished with bulk SiO_2, synthesised nano SiO_2 and tailor-made nano SiO_2 (procured from M/s Sigma Aldrich, particle size less than 99 nm). The results of tests are shown in Table 2. The synthesised as well as tailor-made SiO_2 nanoparticles increased the hydrophilicity and absorbency up to the identical extent after each wash while the absorbency values slightly decreased yet remained better in performance against the unfinished control. Despite bulk SiO_2 showing some positive effects on absorbency, this went on decreasing remarkably and after 5 cycles, it became identical to the unfinished sample. This confirms that 0.50% of nanoparticles were adequate to improve absorbency, whereas an additional increase in the amount of nanoparticles could not further improve absorbency.

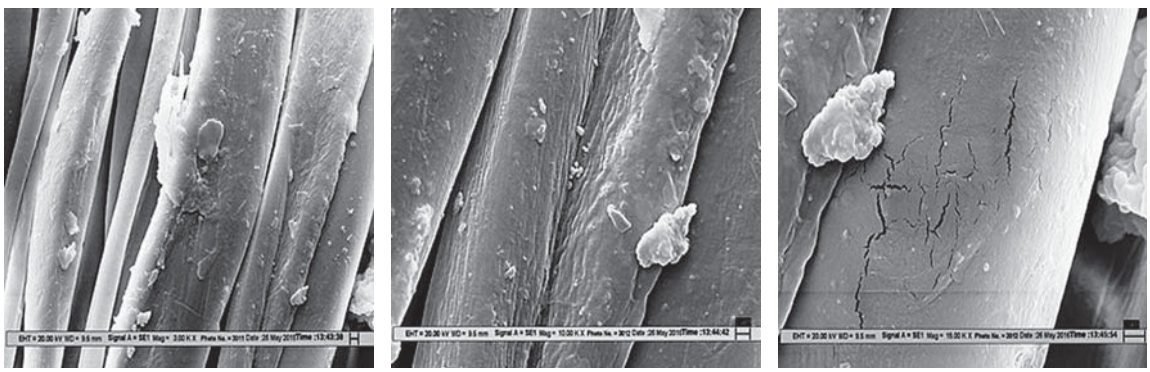

a) *b)* *c)*

Figure 4: SEM images of fabric sample surface after application of SiO_2 nano finish: a) 3,000× magnification, b) 10,000× magnification and c) 15,000× magnification

Table 2: Comparative performance of finished fabrics against cyclic wash fastness testing

Sample no.	Sample description		Wash 0 [s]	Wash 1 [s]	Wash 2 [s]	Wash 3 [s]	Wash 4 [s]	Wash 5 [s]
	Type of silica	[a] [%]						
1	Control sample	0. 00	2.5					
2	Bulk silica	0.50	< 1	1	1.5	2	2.5	2.5
3	Bulk silica	1.00	< 1	1	1.5	2	2.5	2.5
4	Bulk silica	1.50	< 1	1	1.5	2	2.5	2.5
5	Tailor-made	0.50	[b]	< 0.5	< 1	1	[c]	[d]
6	Tailor-made	1.00	[b]	< 0.5	< 1	1	[c]	[d]
7	Tailor-made	1.50	[b]	< 0.5	< 1	1	[c]	[d]
8	Synthesised	0.50	[b]	< 0.5	< 1	1	[c]	[d]
9	Synthesised	1.00	[b]	< 0.5	< 1	1	[c]	[d]
10	Synthesised	1.50	[b]	< 0.5	< 1	1	[c]	[d]

[a] SiO_2 nanoparticles concentrations, [b] Instant, [c] Little more than 1, [d] Around 2

3.5 Physical properties

3.5.1 Tensile strength

The obtained tensile strength of different samples is shown in Figure 5.

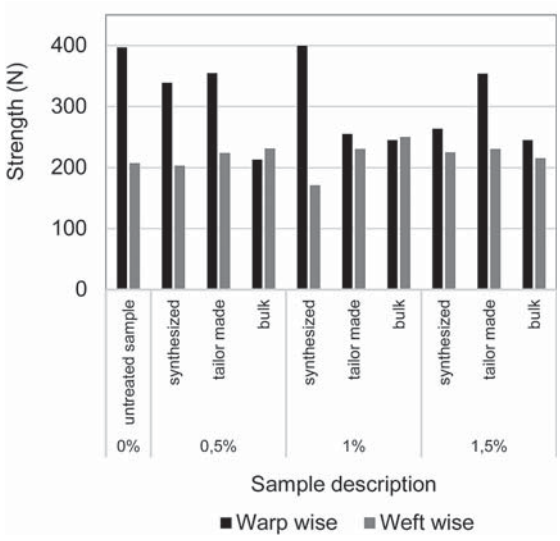

Figure 5: Tensile strength of finished samples

The tensile strength data in Figure 5 ensures that there was a strength loss in the specimen after the finish was applied, while the minimum strength loss was recorded in the case of synthesised nanoparticles with the respective concentration of 1%.

3.5.2 Stiffness

The bending length of the nano finished cotton fabric is shown in Figure 6.

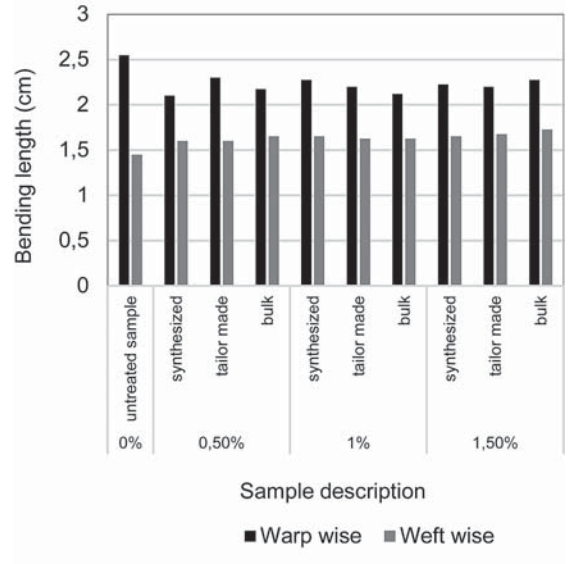

Figure 6: Bending length of finished specimen

It can be concluded that there was no substantial change in the stiffness of finished samples; however, there was a slight change in the stiffness of finished samples as compared to control. The samples were found to become marginally stiffer after the application of the finish.

3.5.3 Pore size

The finished fabric pore size data is given in Figure 7.

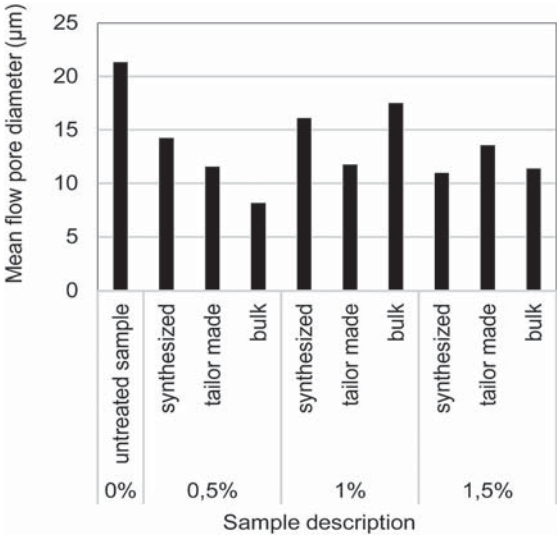

Figure 7: Pore size of different fabric specimen

From the data above, it can be inferred that the application of the nanoparticle finish resulted in a decreased pore size in the fabric substrate. Furthermore, it was observed that the pore size of finished samples was the largest in the case of the tailor-made nanoparticle finished fabric.

4 Conclusion

Synthesised SiO_2 nanoparticles showed enhanced hydrophilic properties and when applied to a fabric, the water absorbency of the fabric increased dramatically. The hydrophilicity was found similar to the tailor-made particle from tailor-made nanoparticles and much better than at bulk silica. Moreover, the synthesis of nanoparticles done at low temperatures facilitated the ease of the nanoparticle synthesis. The application of synthesised SiO_2 nanoparticles also improved physical properties such as tensile strength, while bending length (warp and weft wise) did not exhibit any substantial change even after the application of nanoparticles. These properties were found similar (better in some cases) in the case of synthesised nanoparticles with respect to the tailor-made nanoparticles. The performance of bulk particles was lower than at both types of nanoparticles used. These characteristics strongly suggest that the use of silica nanoparticles improves the hydrophilic property of the fabric substrate. These techniques can be easily scaled up to commercial level as well. The enhanced hydrophilic properties may aid the development of better and stronger absorbents for various uses.

References

1. SAWHNEY, A. P. S., CONDON, Brian Douglas, SINGH, Vikram Kumar, PANG, Su-Seng, LI, Guoqiang, HUI, David. Modern application of nanotechnology in textiles. *Textile Research Journal,* 2008, **78**(8), 731–739, doi: 10.1177/0040517508091066.
2. VOLKOV, V. A., SHCHUKINA, E. L., AMARLUI, A., AGEEV, A. A., KUKLEVA, K. K., ELEEV, A. F. Molecular stratification nanotechnology in antiadhesive modification of fabric fibres. *Fibre chemistry*, 2008, **40**(2), 127–135, doi: 10.1007/s10692-008-9024-7.
3. MAZROUEI-SEBDANI, Zahra, KHODDAMI, Akbar. Alkaline hydrolysis: A facile method to manufacture superhydrophobic polyester fabric by fluorocarbon coating. *Progress in Organic Coatings,* 2011, **72**(4), 638–646, doi: 10.1016/j.porgcoat.2011.07.006.
4. SIVAKUMAR, A., MURUGAN, Ramachandran, SUNDARESAN, Krishnakumar, PERIYASAMY, Soodamani. UV protection and self-cleaning finish for cotton fabrics using metal oxide nanoparticles. *Indian Journal of Fibre Textile Research,* 2013, **38**(3), 285–292.
5. KATHIRVELU, S., D'SOUZA, Louis, DHURAI, Bhaarathi. UV protection finishing of textiles using ZnO nanoparticles. *Indian Journal of Fibre Textile Research,* 2009, **34**(3), 267–273.
6. GUPTA, Deepti, BHAUMIK Somes. Antimicrobial treatments for textiles. *Indian Journal of Fibre Textile Research,* 2007, **32**(2), 254–263.
7. EL-MOLLA, M. M., EL-KHATIB, Eman Mohamed, EL-GAMMAL, Mahmoud, ABDEL-FATTAH, S. H. Nanotechnology to improve coloration and antimicrobial properties on silk fabrics. *Indian Journal of Fibre Textile Research,* 2011, **36**(3), 266–271.
8. MALAKI, Massoud, HASHEMZADEH, Yasser, TEHRANI, Alireza Fadaei. Abrasion resistance of acrylic polyurethane coatings reinforced by nanosilica. *Progress in Organic Coatings*, 2018, **125,** 507–515, doi: 10.1016/j.porgcoat.2018.07.034.
9. AHMED, Hend Mohamed, ABDELLATIF, Mohamed Mehawed, IBRAHIM, Saber, ABDELLA-

TIF, Faten Hassan. Mini-emulsified Copolymer/ Silica nanocomposite as effective binder and self-cleaning for textiles coating. *Progress in Organic Coatings*, 2019, **129,** 52–58, doi: 10.1016/j.porgcoat.2019.01.002.

10. ZAHID, Muhammad, HEREDIA-GUERRERO, Jose A., ATHANASSIOU, Athanassia, BAYER, Ilker, S. Robust water repellent treatment for woven cotton fabrics with ecofriendly polymers. *Chemical Engineering Journal*, 2017, **319**, 321–332, doi: 10.1016/j.cej.2017.03.006.
11. ATTIA, Nour, F., MOUSSA, Mona, SHETA, Aida, M. F., TAHA, Rehab, GAMAL, Heba. Synthesis of effective multifunctional textile based on silica nanoparticles. *Progress in Organic Coating*s, 2017, **106**, 41–49, doi: 10.1016/j.porgcoat.2017.02.006.
12. LI, Xiaoyan, LI, Hui, HUANG, Kai, ZOU, Hua, YU, Dengguang, LI, Ying, QIU, Biwei, WANG, Xia. Durable superamphiphobic nano-silica/ epoxy composite coating via coaxial electrospraying method. *Applied Surface Science*, 2018, **436**, 283–292, doi: 10.1016/j.apsusc.2017.11.241.
13. CAI, Ying, LI, Jing, YI, Lingmin, YAN, Xiaojie, LI, Jiawei. Fabricating superhydrophobic and oleophobic surface with silica nanoparticles modified by silanes and environment-friendly fluorinated chemicals. *Applied Surface Science*, 2018, **450**, 102–111, doi: 10.1016/j.apsusc.2018.04.186.
14. FALLAH, Fatemeh, KHORASANI, Manouchehr, EBRAHIMI, Morteza. Improving the mechanical properties of waterborne nitrocellulose coating using nano-silica particles. *Progress in Organic Coatings*, 2017, **109**, 110–116, doi: 10.1016/j.porgcoat.2017.04.016.
15. ZHOU, Chenglong, XU, Shouping, PI, Pihui, CHENG, Jiang, WANG, Li, YANG, Jinxin, WEN, Xiufang. Polyacrylate/silica nanoparticles hybrid emulsion coating with high silica content for high hardness and dry wear-resistant. *Progress in Organic Coatings*, 2018, **121**, 30–37, doi: 10.1016/j.porgcoat.2018.04.001.
16. SUTHABANDITPONG, W., TAKAI, Chika, FUJI, M., BUNTEM, Radchada, SHIRAI, Takashi. Studies of optical properties of UV-cured acrylate films modified with spherical silica nanoparticles. *Advanced Powder Technology*, 2016, **27**(2), 411–416, doi: 10.1016/j.apt.2016.01.022.
17. ESHAGHI, Akbar. Transparent hard self-cleaning nano-hybrid coating on polymeric substrate. *Progress in Organic Coatings*, 2019, **128**, 120–126, doi: 10.1016/j.porgcoat.2018.12.021.
18. LAVERGNE, Francis, BELHADI, R., CARRIAT, J., FRAJ, Amor Ben. Effect of nano-silica particles on the hydration, the rheology and the strength development of a blended cement paste. *Cement Concrete Composites*, 2019, **95**, 42–55, doi: 10.1016/j.cemconcomp.2018.10.007.
19. LIU, Huiting, YU, Yongjin, LIU, Huimin, JIN, Jianzhou, LIU, Shuoqiong. Hybrid effects of nano-silica and graphene oxide on mechanical properties and hydration products of oil well cement. *Construction and Building Materials*, 2018, **191**, 311–319, doi: 10.1016/j.conbuildmat.2018.10.029.
20. WANG, Ren, LIU, Tianle, NING, Fulong, OU, Wenjia, ZHANG, Ling, WANG, Zhen, LI, Peng, SUN, Jiaxin, LIU, Zhichao, LI, Tianshu, SUN, Huicui, JIANG, Guosheng. Effect of hydrophilic silica nanoparticles on hydrate formation: Insight from the experimental study. *Journal of Energy Chemistry*, 2019, **30,** 90–100, doi: 10.1016/j.jechem.2018.02.021.
21. HSIEH, Chien-Te, CHANG, Bi-Sheng, LIN, Jia-Yi. Improvement of water and oil repellency on wood substrates by using fluorinated silica nanocoating *Applied Surface Science*, 2011, **257**(18)**,** 7997–8002, doi: 10.1016/j.apsusc.2011.04.071.
22. CHEN, Fang, HABLEEL, Ghanim, ZHAO, Eric Ruike, JOKERST, Jesse V. Multifunctional nanomedicine with silica: role of silica in nanoparticles for theranostic, imaging, and drug monitoring. *Journal of Colloid Interface Science*, 2018, **521**, 261–279, doi: 10.1016/j.jcis.2018.02.053.
23. LEIDNER, Arnold, BAUER, Jens, KHONACHAH, Mojtaba Ebrahimi, TAKAMIYA, Masanari, STRÄHLE, Uwe, DICKMEIS, Thomas, RABE, Kersten S., NIEMEYER, Christof M. Oriented immobilization of a delicate glucose-sensing protein on silica nanoparticles. *Biomaterials*, 2019, **190–191**, 76–85, doi: 10.1016/j.biomaterials. 018. 10.035.
24. WANG, Jintao, WANG, Hongfei. Ultra-hydrophobic and mesoporous silica aerogel membranes for efficient separation of surfactant-stabilized water-in-oil emulsion separation. *Separation and Purification Technology*, 2019, **212**, 597–604, doi: 10.1016/j.seppur.2018.11.078.
25. JACOB, Jefferson De Santana, MASCELANI, Amadeu Grezzana, STEINMETZ, Ricardo L. R., DALLA COSTA, Filipe Antonio, DALLA COSTA, Osmar Antonio . Use of silica fume and nano-silica in mortars attacked by acids present in pig manure. *Procedia Structural Integrity,* 2018, **11**, 44–51, doi: 10.1016/j.prostr.2018.11.007.

Alenka Ojstršek[1, 2], Darinka Fakin[1]
[1] University of Maribor, Faculty of Mechanical Engineering, Institute for Engineering Materials and Design, Smetanova 17, 2000 Maribor, Slovenia
[2] University of Maribor, Faculty of Electrical Engineering and Computer Science, Institute of Automation, Koroška cesta 46, 2000 Maribor, Slovenia

Natural Dyeing of Wool Using *Junglans regia* (Common Walnut) Leaf Extract

Naravno barvanje volne z ekstraktom iz listov Junglans regia (navadni oreh)

Original Scientific Article/*Izvirni znanstveni članek*
Received/*Prispelo* 9-2019 • Accepted/*Sprejeto* 10-2019

Abstract

The main objective of the presented research was to study the possibility of using natural colourants obtained through the aqueous extraction of fresh leaves from the *Junglans regia* (*J. regia*), or common walnut tree, for the dyeing of wool yarn. A unique principle was explored by combining the phases of extraction and mordanting into one with the aim of shortening the dyeing procedure, while at the same time extracting more colouring components. Spectrophotometric studies revealed the significant impact of both mordant addition and dye-bath pH on the absorbance curve and thus on the colour and K/S values of the dyed samples. A meta-mordanting technique using ferrous sulphate produced a greater depth of shade at a wavelength of 400 nm, with respect to the concentration of mordant and the liquid ratio of the extraction. Finally, wool yarn dyed with pure leaf extracts exhibited a potent inhibiting activity against *Candida albicans* (*C. albicans*) with a moderate reduction rate of 59%, and an inhibited response against *Staphylococcus aureus* (*S. aureus*) with a low reduction rate of 38.6%.
Keywords: natural colourants, wool dyeing, walnut leaf extract, ferrous sulphate, colourimetry, antimicrobial activity

Izvleček

Namen predstavljene raziskave je bil proučiti možnost uporabe naravnih barvil, pridobljenih z vodno ekstrakcijo svežih listov iz drevesa Junglans regia (J. regia), navadnega oreha, za barvanje volnene preje. Raziskali smo edinstven pristop z združevanjem obeh faz, ekstrakcije in dodajanja anorganskih soli, v eno fazo, da bi skrajšali postopek barvanja in hkrati ekstrahiranja večje količine barvila za barvanje. Spektrofotometrična študija je pokazala pomemben vpliv uporabljene anorganske soli – čimže in pH barvalne kopeli na absorpcijsko krivuljo ter posledično na barvo in K/S vrednosti obarvanih vzorcev. Tehnika dodajanja železovega sulfata med barvanjem daje večjo globino obarvanja pri valovni dolžini 400 nm, to je odvisno od koncentracije oksida in kopelnega razmerja ekstrakcije. Prav tako smo dosegli zmerno protimikrobno delovanje obarvane volne proti glivičnemu sevu Candida albicans (C. albicans), z 59-odstotno stopnjo zmanjšanja in nizko stopnjo delovanja proti bakteriji Staphylococcus aureus (S. aureus) z 38,6-odstotno stopnjo zmanjšanja.
Ključne besede: naravna barvila, barvanje volne, ekstrakt orehovih listov, železov sulfat, barvna metrika, protimikrobno delovanje

Corresponding author/*Korespondenčna avtorica:*
Assist. Prof. dr. Alenka Ojstršek
Tel.: +386 2 220 7935
E-mail: alenka.ojstrsek@um.si

Tekstilec, 2019, ***62****(4), 288-298*
DOI: 10.14502/Tekstilec2019.62.288-298

1 Introduction

Eco-friendly dyeing could be achieved through various approaches, i.e. using biodegradable auxiliaries, optimising the amount of chemicals, replacing toxic chemicals with eco-friendlier chemicals, employing natural colouring compounds, etc. [1–3]. This paper focuses on dyeing with natural colouring compounds that are derived from different parts of plants, such as flowers, leaves, bark, roots and fruits, using various extraction technique, and that are believed to be ecologically-friendly with fewer negative effects on the organism on account of their low toxicity and non-carcinogenic nature. Moreover, natural colourants are biodegradable and thus do not cause pollution and wastewater problems. On the other hand, they provide a lesser amount of colouring component and inferior fastness properties, resulting in higher production costs compared with synthetic dyes [1]. Textiles dyed with natural dyes could therefore be suitable as niche products of high-added value for special markets.

Although known for a long time for dyeing and medical purposes, the structure and protective properties of natural colourants were not identified until recent decades [4]. Different papers have reported the selection of a variety of plants/parts of plants, i.e. henna leaves [5], lady's bedstraw root and big nettle leaves [6], turmeric rhizomes, harda fruits, safflower petals and barberry roots [1], madder roots and onion peel [2], purple sweet potato [7], weld [8], etc. for the natural dyeing of various natural fibres, and the optimisation of different exhaustion and dyeing procedures using chemically-different mordants in order to achieve an extensive palette of colour shades, and good to excellent colour-fastness. In this study, common walnut leaves were chosen as the source for a plant-based reddish-brown natural dye. The leaves are a promising dye source because of their easy availability and abundant nature [9]. Moreover, the removal of leaves is less harmful to trees compared with the stripping of bark. *J. regia* (common walnut) is a deciduous tree of the *Junglandaceae* family native to south-eastern Europe [10]. It reaches a height of up to 25–35 m and a diameter of up to 2 m. The water extracted from walnut leaves is reported to exhibit powerful antioxidative [10] and antimicrobial properties [1, 2] owing to the presence of large amounts of phenolic compounds, such as naphtoquinones and flavonoids, depending on the agricultural, geographical, and climatic conditions. From among the naphtoquinones, the juglone (5-hydroxyl-1,4-naphthoquinone; Figure 1) is of great interest due to its chemical reactivity. Because of its tendency to create dark orange-brown stains, juglone has been used traditionally as a natural dye for clothes and inks, and as a colouring agent for foods and cosmetics. It is also a well-known and widely used substance in folk medicine for the treatment of skin inflammations, hyperhydrosis, ulcers, venous insufficiency, and haemorrhoidal symptomatology, and for its proven antiseptic, anti-diuretic, antistringent and sedative properties [10].

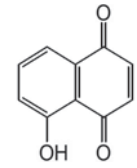

Figure 1: Chemical structure of 5-hydroxyl-1,4-naphthoquinone

Only a few natural dyes are substantive to fibres; all others require inorganic oxides or metallic salts, such as ferric sulphate, aluminium sulphate, potassium dichromate, stannous chloride and copper sulphate, known as mordants, which form a complex with a dye *in situ* within the wool fibre, resulting in a dramatic improvement in both the fastnesses of the dyeing to light and washing [11]. Three methods for mordant application are commonly used: pre-mordanting, meta-mordanting and post-mordanting. The method used depends on whether the mordant is applied before, during or after dyeing.

A unique principle was explored during the presented work by combining the phases of extraction and mordanting into one with the aim of shortening the dyeing procedure, while at the same time extracting more colouring compounds. Thus, ferrous sulphate, an eco-friendlier mordant (compared with the metal salts listed above) was added at the beginning of the extraction procedure to form a complex between the colourant and a metallic ion, as in the case of synthetic (pre-metallised) metal-complex dyes. For comparison purposes, standard dyeing and meta-mordanting using various amounts of metallic salts were also carried out. Thus, different factors affecting exhaustion ability and fastness properties were investigated to demonstrate commercial viability and to meet demands for eco-friendliness. The

colorimetric parameters (e.g. CIE colour values, colour differences and colour strength or K/S value) of the dyed samples were identified, as we were potential antimicrobial properties against common human pathogens, such as *C. albicans* and *S. aureus*, in accordance with the ASTM specification.

2 Experimental

2.1 Materials

Experiments were conducted on a rough, yellowish-coloured wool yarn (L^* = 75.10, C^* = 16.48, h = 90.11, and whiteness according to CIE –42.5), made from Slovenian sheep's wool by the company Soven (Selnica ob Dravi, Slovenia) for hand knitting, with a tow length of 73.6 mm, fineness of 82 × 2 tex and a fat content of 1%. The source yarn was pre-washed at 40 °C for 20 minutes using a neutral non-ionic washing agent in order to remove natural grease and potential additives. It was then rinsed in warm and cold water, and dried at a temperature of 60–70 °C. Ferrous sulphate ($FeSO_4 \times 7H_2O$) and other chemicals, such as sodium carbonate (Na_2CO_3) and acetic acid (CH_3COOH), were analytically graded reagents obtained from Sigma Aldrich.

2.2 Extraction of dye

J. regia leaves were collected during the summer (June 2016) in central Slovenia at an elevation of 240 m above sea level and a high thermal amplitude. The adult walnut trees selected for this research were not sprayed with pesticides, dunged or otherwise agronomically cultivated. The trees were also without traces of disease or pests.

Fresh leaves were separated from the stalks and chopped into small pieces. The extraction was carried out in deionised water using three liquor ratios, i.e. 1:10, 1:30 and 1:50 (1 g of plant material to 10, 30 or 50 mL of deionised water), with the aim of obtaining different concentrations of extracted colourants. The extraction was accomplished without mordanting (classical extraction) and with the addition of 2 g/L $FeSO_4 \times 7H_2O$ at the beginning of the extraction procedure.

The extraction procedure was carried out in a covered glass beaker at boiling temperature for 60 minutes. Afterwards, the extraction mixture (e.g. the extract and plant material) was kept at room temperature for approximately 18 hours and then filtered for further use.

After the extraction was completed, the pH value of individual extracts was measured (pH_E) using a MA 235 pH meter (Mettler Toledo) in accordance with the ISO 10523 standard, and then adjusted to a value of 3, 5 or 8 by adding CH_3COOH or Na_2CO_3 for spectrophotometric analysis. The extracts were characterised by measuring absorbance through the entire UV/Vis spectrum, from a wavelength of 250 nm up to 700 nm, using a 10 mm quartz cuvette on a Cary 50 spectrophotometer (Varian).

2.3 Dyeing procedures

A total of 10 g of wool yarn was dyed according to two dyeing procedures, i.e. standard dyeing and meta-mordanting, at a temperature of 98 °C and a liquor ratio of 1:20, using a Turby laboratory device (W. Mathis) with a medium bath circulation.

Standard dyeing was carried out using two extraction baths, i.e. pure walnut leaf extract and an extract with 2 g/L of ferrous mordant that was applied at the beginning of the extraction procedure. Three different initial concentrations of the extracted colourants were used, as the liquor ratios of extraction (LR_E) were 1:10, 1:30, or 1:50. The dyeing process was started at 24 °C when the wool yarn was added to the extracted bath, and the pH adjusted to 3 or 5. The temperature of the dye-bath was raised to 98 °C at a heating rate of 2 °C/minute. That temperature was maintained for 60 minutes and then reduced to 70 °C (at a rate of 2 °C/min). The dyed yarn was rinsed in warm and then cold water, and dried at room temperature.

In the case of meta-mordanting, dyeing was started at 24 °C by placing the wool yarn in a pure extracted bath that was obtained from the same quantity of fresh leaves (30 g) against a different volume of deionised water; LR_E was 1:10, 1:30 and 1:50. The temperature of the dye-bath was then gradually raised to 98 °C at a heating-rate of 2 °C/minute. Dyeing continued for 15 minutes. The dye-bath was then cooled to 70 °C (at a rate of 2 °C/min), when $FeSO_4 \times 7H_2O$ (0.5, 1 or 2 g/L) was added. The temperature of the dye-bath was again raised to 98 °C at a heating rate of 2 °C/minute. That temperature was maintained for 45 minutes and then reduced to 70 °C (at a rate of 2 °C/min). The dyed yarn was rinsed in warm and then cold water, and dried at room temperature, similar to the standard dyeing procedure.

Absorbance was measured on-line throughout the entire dyeing process using a Cary 50 spectrophotometer (Varian) with a measuring probe of 0.2 mm

optical length at a wavelength of 400 nm. In addition, the dye exhaustion rate was calculated using the following equation:

$$ER = \frac{A_0 - A_t}{A_0} \times 100\ (\%) \quad (1),$$

where ER is the dye exhaustion rate expressed as a percentage, A_0 is the initial absorbance and A_t is the absorbance over a fixed period.

2.4 Colour measurement

The dyed samples were colourimetrically evaluated according to the CIE colour system using a two-ray SF 600+ spectrophotometer (Datacolor) with an Ulbricht sphere and a measuring geometry of d/8°, within the spectral range of 400–700 nm wavelengths. The source of light was a halogen lamp with xenon lightning.

CIE differences in lightness (dL^*) and total colour differences (dE^*) between various dyed samples (original samples were dyed using the standard dyeing procedure) were calculated (equation 2) from the coordinate differences in all three directions of the colour space, i.e. lightness L^*, red/green axis a^* and yellow/blue axis b^*. C^* is the abbreviation for chroma and h for hue.

$$dE^*_{ab} = \sqrt{(dL^*)^2 + (da^*)^2 + (db^*)^2} \quad (2)$$

The colour strength of individual samples (K/S) was calculated from the reflectance values at 400 nm for each dyeing using the Kubelka-Munk equation:

$$K/S = \frac{(1 - R)^2}{2R} \Big) \quad (3),$$

where K is the absorption coefficient, S is the light-scattering coefficient and R is the decimal fraction of the dyed sample's reflectance.

2.5 Fastness testing

The colour fastnesses of the samples to washing was tested according to the EN ISO 20105-C01 Standard; Test 1: washing at 40 °C. Colour-fading and colour-leaching from dyed samples on two control strips made from cellulose and wool were visually evaluated using a normalised grey scale (on a scale of 1–5, where 1 = poor and 5 = excellent). The colour fastnesses of samples to light was tested using artificial illumination from a xenon arc light according to the EN ISO 105-B02 Standard and visually estimated using a standardised blue scale (on a scale of 1–8, where 1 = poor and 8 = excellent).

2.6 Antimicrobial screening test

ASTM Designation: The E 2149-01 Standard test method was used to assess the non-leachable antimicrobial activity (both bacterial and fungal) of the dyed wool yarns under dynamic contact conditions (24-hour contact time at ambient temperature). The analysis was performed by a certified laboratory. A gram-positive bacterium *S. aureus* and fungus *C. albicans* were selected. The reduction of the microorganisms by dyed yarn was calculated using equation 4:

$$R = \frac{(B - A)}{B} \times 100\ (\%) \quad (4),$$

where R is the reduction of the microbial population expressed as a percentage, A is the number of bacteria colonies (CFU/mL) for the flask containing the treated sample after 1 hour contact time and B is the number of bacteria colonies (CFU/mL) for the flask to determine A before the addition of the treated sample (time 0).

3 Results and discussion

With the aim of developing textiles of high added-value for special applications, the presented research work focused on the search for a mordant concentration, a mordant application technique and the quantity of fresh leaves per volume of water for extraction, as well as the optimal application conditions for obtaining natural dyes in a wide colour palette, with high colour-strength and outstanding fastness properties. The antibacterial and antifungal properties of dyed samples were also investigated. The obtained results and the relevant discussion are presented below.

3.1 UV/Vis analysis of the aqueous walnut leaf extract

Two extracted baths at LR_E 1:50, i.e. one bath without and one bath with 2 g/L of $FeSO_4 \cdot 7H_2O$, which was employed at the beginning of the extraction procedure, and at three pH values (3, 5, and 8), were characterised using spectroscopic measurement in order to study the effect of mordant application and the acidic or alkaline pH on colour hue. A turbid solution was formed during the extraction procedure. Part of the absorbance was thus probably due

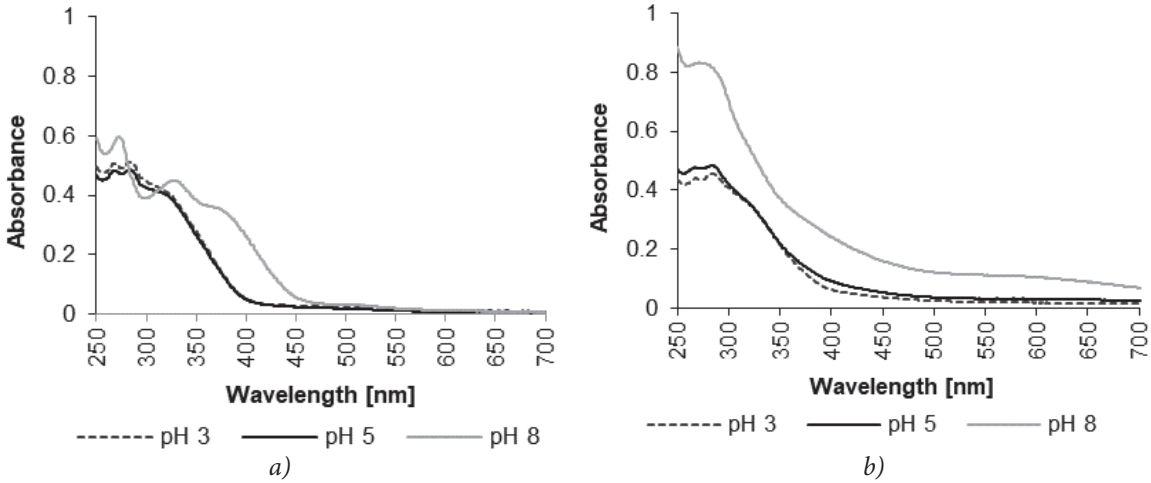

Figure 2: Influence of pH and mordant on the absorbance of walnut leaf extract, diluted 25x: a) pure extract mordant excluded; b) extract with $FeSO_4 \cdot 7H_2O$

to the presence of insoluble substances, which caused a problem in the spectrophotometric analysis, irrespective of the preceding filtration.

It is evident from Figure 2a that aqueous extraction at a boiling temperature removed various colouring compounds from the walnut leaves, thus influencing the appearances of two absorption maximums in the UV region at wavelengths of 268 nm and 283 nm. Pure walnut leaf extract (mordant excluded) had a pH value of 5 by itself, probably on account of various hydroxycinnamic and chlorogenic acids present in fresh leaves, which have been seasonally deviated and identified by different authors, using various skills [12, 13]. When pH is changed from acidic (pH values of 3 and 5) to alkaline (pH value of 8), the absorbance curves are shifted towards higher wavelengths; colour thus changes. This could be due to (i) the higher solubility of the extracted colourants at higher pH values, (ii) the deacidification of water-colour pigment and/or (ii) the fact that the structure of juglone may be represented in more potentially resonant forms, thus allowing for greater electronic distribution. Furthermore, the application of the selected mordant (Figure 2b) results in a different colour. The addition of Fe-salt to the extract yielded the corresponding Fe-complex of the extracted hydroxynaphthoquinone components, resulting in increased absorbance [14]. According to the analogy of 1-hydroxyantraquinone derivatives, juglone contains, as a basic unit, a six-membered chelate ring in which the metal ion is coordinated with the oxygen atom of the 1-hydroxy group and the quinone oxygen atom (Figure 3). Mordanting causes the colour of a dye to undergo an appreciable bathochromic shift because the donor properties of the hydroxyl group and the acceptor properties of the carbonyl group are both enhanced. Also, the ionisation of a hydroxynaphthoquinone dye by varying pH results in an irreversible bathochromic shift, as the oxide group is a more powerful electron donor than the hydroxyl group.

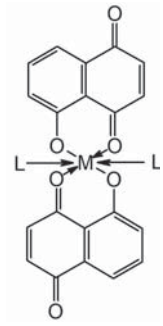

Figure 3: Scheme of coordination complex between juglone and metal ion; M = metal, L = ligand

3.2 Dye sorption

In order to observe the sorption degree of the extracted colourants onto wool fibres and the influence of metallic salt on exhaustion, a standard dyeing procedure was carried out using two extracted baths at LR_E 1:50, follows: one dye-bath mordant excluded and one mordant included at two pH values (3 or 5), as wool fibres are commonly dyed at acidic pH values. Therefore, dye-bath absorbance

was followed by on-line UV/Vis spectrophotometry throughout the entire dyeing process at a wavelength of 400 nm (extracted colourants have badly defined maximums within a visible region of the spectrum), while the exhaustion rate was calculated according to equation 1. Also, the pH of the dye-baths was measured on-line by means of a temperature-resistant electrode. The selected results of dye exhaustion rate *versus* dyeing time/temperature are graphically presented in Figure 4. Exhaustion curves define the distribution of the dye between the dye-bath and wool fibres during the dyeing process, and indicate that both the dye adsorption on the wool fibres' surfaces and the dye-diffusion into the fibres depend on the time and temperature, and on the pH of the dye-baths and mordant application method.

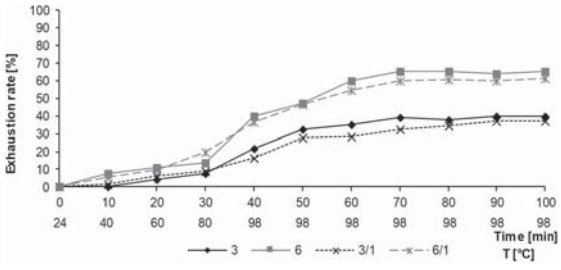

Figure 4: Selected exhaustion curves of representative dyeing using LR_E 1:50; 3 dyed at pH 5 mordant excluded, 6 dyed at pH 5 using $FeSO_4$, 3/1 dyed at pH 3 mordant excluded, and 6/1 dyed at pH 3 using $FeSO_4$

Absorbance was also measured during the meta-mordanting procedure, but the exhaustion rate could not be calculated. When metallic salt was applied during dyeing at 70 °C, enormous decreases in pH were observed, as well as major increases in absorbance at 400 nm. Thus, the initial absorbance (A_0) required for the exhaustion calculation (Equation 1) could not be the same for the whole process and is thus irregular.

The obtained results in Figure 4 demonstrate that the presence of mordant in the dye-bath could influence the dyeing behaviour of wool yarn, depending on the time and dyeing temperature, and on the pH of the dye-bath. The exhaustion rate increased very slowly for the representative trials during the first division of the dyeing process (first 28 minutes) when the dye-baths were heated, implying that the temperature required to start the exhaustion of natural colourants extracted from walnut leaves must be between 80 °C and 98 °C. From amongst the on-line absorbance measurements, the best sorption at the end of the individual dyeing process was achieved using a dye-bath containing ferrous sulphate pH 5, which is comparable with reported results [15, 16]. The exhaustion rate of the colourants from the dye-bath's mordant included after 100 minutes of dyeing at pH 5 was 65.3%, followed by an exhaustion rate under pH 3 dyeing of 61.4%. The obtained results were exceedingly low compared with the exhaustion of synthetic metal-complex dyestuffs that can attain values in excess of 90% [17]. According to literature, the situation in mordant dyeing with natural colourants is more complex than when synthetic metal-complex dyes are used [18]. Besides the change in the ionisation of the wool, the pH-dependent sorption of the Fe-ions on wool and the complex stability between the extracted colourants and the mordant must be considered.

Moreover, the exhaustion curves show gentler slopes at both pH values during dyeing using pure leaf-extract (mordant excluded) on account of the lower affinity of the colouring components to the substrate compared with the metal-colourant-complex formation. Nevertheless, all results illustrated in Figure 4 still exhibit some increases in exhaustion rate at the end of the dyeing period, and thus indicate the possibility of exhausting higher amounts of dyestuff-forming substances by prolonged dyeing time at boiling.

It can be concluded from the dye-uptake results of the representative experiments that dyeing conducted at a lower pH value (pH 3) leads to a lower exhaustion rate, and consequently to lighter dyeing. For this reason, all other dyeing experiments (standard dyeing and meta-mordanting) were carried out at pH 5.

3.3 Colour evaluation

CIE colour values and colour differences

With the aim of illustrating the wide-range of colours achieved, the CIE colour coordinates of samples dyed with walnut leaf extract using three different liquid ratios of extraction (1:10, 1:30 or 1:50), according to two dyeing procedures (standard dyeing and meta-mordanting), are given in Table 1. In total, 15 samples were dyed and colourimetrically evaluated. Moreover, the differences in lightness (dL^*) and the total colour differences (dE^*) were calculated between samples 1, 2 and 3 (standard samples), and all other samples at the same LR_E, using equation 3, in order to evaluate the effects of the

Table 1: CIE colour values and colour differences for dyed wool yarn using different dye-baths and dyeing procedures

Procedure	Sample number	LR_E	Mordant $FeSO_4$ c (g/L)	L^*	a^*	b^*	C^*	h	dL^*	dE^*
Standard dyeing (dye-bath mordant excluded) Standard dyeing (dye-bath mordant included)	**1**	1:10		43.37	11.96	22.38	25.37	61.88		
	2	1:30		47.42	10.88	20.96	23.62	62.57		
	3	1:50	2	55.95	9.98	20.31	22.63	63.83		
	4	1:10	2	35.36	0.38	12.50	12.51	88.25	–8.00	17.20
	5	1:30	2	40.27	0.73	12.06	12.06	86.54	–7.15	15.28
	6	1:50		45.72	0.79	13.15	13.18	86.55	–10.23	15.50
Meta-mordanting	**7**	1:10	0.5	24.10	4.47	11.96	12.77	69.53	–19.27	23.16
	8	1:10	1	22.61	3.83	10.49	11.17	69.93	–20.76	25.27
	9	1:10	2	20.22	3.11	8.85	9.38	70.62	–23.15	28.24
	10	1:30	0.5	27.83	3.59	11.70	12.23	72.96	–19.59	22.86
	11	1:30	1	24.25	2.85	10.08	10.48	74.23	–23.17	26.82
	12	1:30	2	22.89	2.43	9.55	9.85	75.70	–24.53	28.34
	13	1:50	0.5	32.92	2.78	11.70	12.03	76.63	–23.03	25.97
	14	1:50	1	28.63	2.35	10.27	10.53	77.10	–27.32	30.44
	15	1:50	2	27.70	2.24	9.88	10.13	77.21	–28.25	31.44

mordant, as well as the dyeing procedure, on the colour change. Because the preliminary sorption experiments showed better dye-bath exhaustion under slightly acidic conditions (Figure 4), all dyeing trials were carried out at pH 5.

It can be concluded from Table 1 that yarn dyed with walnut leaf extract showed some decrease in L^* and C^* values when metallic salt was added. That decrease became more apparent as the liquor ratio of extraction (LR_E) decreased and when the concentration of mordant increased (samples 7–15). Also, the application of mordant caused changes in the shades of samples. Generally, $FeSO_4$ mordant gives bluer and less red hues, when compared to the original non-mordanted samples dyed using the standard dyeing procedure (samples 1–3). The meta-mordanting technique using iron sulphate has a major influence on CIE colour values (samples 7–15) compared with the standard dyeing procedure's mordant excluded (samples 1–3). Total colour differences were between 22.86 and 31.44, while differences in lightness were between –19.27 and –28.25, as could already be expected on the basis of reported colouration results from different authors dealing with various natural colourants [9, 16, 18, 19]. Notable differences were also observed between samples dyed in dye-baths, where iron salt was added at the beginning of the extraction procedure (samples 4–6), and samples dyed using the meta-mordanting technique (samples 7–15); dE^* ranging from 12 to 22.26 and dL^* from 11.26 to 22.03.

Colour strength and fastness properties

An important aspect when selecting plant material for dyeing is the maximum colour depth that can be achieved. The extent and nature of this colour strength is illustrated by the K/S value versus wavelength plot, as shown in Figures 5 and 6.

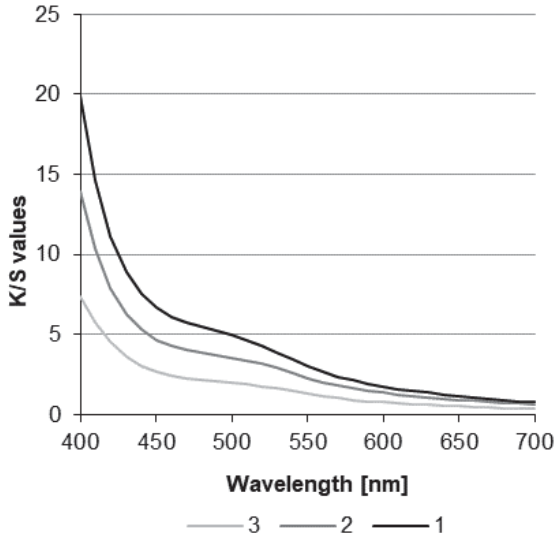

Figure 5: Influence of extraction liquor ratio on the K/S values of samples dyed using pure leaf extract; 1 – LR_E 1:10, 2 – LR_E 1:30, 3 – LR_E 1:50

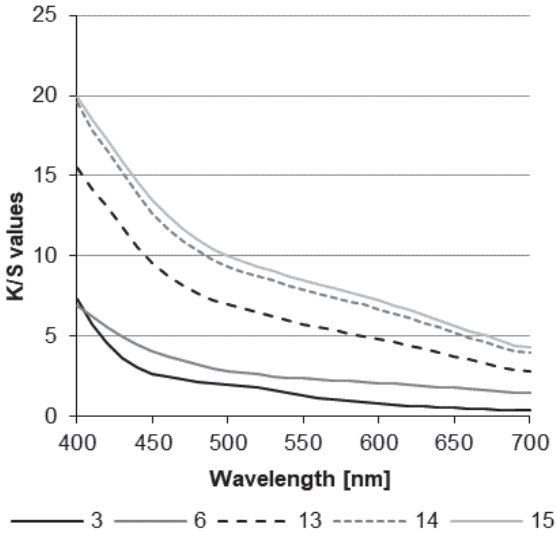

Figure 6: Influence of mordant and dyeing procedure on the K/S values of samples dyed using representative dyeing methods; LR_E 1:50; standard dyeing: 3 – without mordant, 6 – 2 g/L of $FeSO_4$; meta-mordanting: 13 – 0.5 g/L $FeSO_4$, 14 – 1 g/L $FeSO_4$, 15 – 2 g/L $FeSO_4$

The *K/S* values illustrated in Figure 5 indicate a decrease in the colour strength of dyed samples when the liquor ratio of walnut leaf extract increased, as could be expected from the absorbance measurement. However, the *K/S* value versus wavelength curves do not reflect the finding characteristic for synthetic dyes, where *K/S* measured at maximum wavelength increases equally with an increases in the dye concentration, resulting in a direct correlation between the colour strength and the dye absorbance/concentration. The addition of iron salt during dyeing leads to a major increase in the *K/S* values throughout the entire visible spectrum, compared with the original (non-mordanted) representative sample 3 (Figure 6). On the other hand, standard dyeing, using dye-baths' mordant included, caused a minor improvement in the colour strength.

Table 2 shows the influence of extraction liquor ratios, dyeing procedures, and the type and concentration of the mordant on the *K/S* values measured at a wavelength of 400 nm, and on the wash and light fastness properties of the resulting natural dyes.

It is clear from Table 2 that meta-mordanting under a given set of experimental conditions leads to the significant enhancement of colour strength, producing dyeing with better fastness properties than those dyed according to the standard procedure. Metal ion is well-known for its ability to form a coordinated complex, as the coordination number of iron is 6. Some coordination sites remained unoccupied when it interacted with the fibre. Thus, the amino groups on wool fibre occupied these sites (coordination bonding). Such a strong coordination tendency enhanced the interaction between the fibre and the dye, resulting in higher dye exhaustion compared with mordant-excluded standard dyeing (hydrogen bonding between -OH groups of dyes and carboxyl groups of wool fibre).

3.4 Determination of antimicrobial activities

Generally, textiles are carriers of microorganisms, such as pathogenic bacteria, odour-generating bacteria and moulds, as they provide larger surface areas and adsorb the moisture required for microbial growth and multiplication, leading to dermal infections, allergic responses, product deterioration, etc. [1, 2]. Because of the presence of large amounts of phenolic compounds in walnut leaf extract [10, 12], which are classified as active antimicrobial compounds, we presumed that textile materials dyed using such an extract could enhance the antimicrobial abilities of textiles. The presented research was therefore undertaken to determine the antimicrobial effectiveness of selected non-mordanted original dyed yarn (sample 3), as well as mordanted samples dyed

Table 2: K/S values at 400 nm and colour fastness to washing and light for dyed wool yarn using different dye-baths and dyeing procedures

Procedure	Sample number	LR_E	Mordant $FeSO_4$ c (g/L)	K/S	Wash fastness W/S/C[a)]	Light fastness
Standard dyeing (pure dye-bath; original shade) Standard dyeing (dye-bath mordant included)	1	1:10		19.90	3/1–2/3–4	3
	2	1:30		13.91	3/1–2/3–4	3–4
	3	1:50		7.35	3–4/2/4	3–4
	4	1:10	2	18.29	3–4/3/4	2–3
	5	1:30	2	14.45	3–4/3/4	2–3
	6	1:50	2	6.91	4/3–4/4	3–4
Meta-mordanting	7	1:10	0.5	30.65	3–4/3/3–4	3
	8	1:10	1	31.69	3–4/3/3–4	3
	9	1:30	2	32.61	3–4/3–4/4	2
	10	1:30	0.5	23.58	3–4/3–4/3–4	3–4
	11	1:30	1	26.35	3–4/3–4/4	3–4
	12	1:50	2	27.81	3–4/4/4	2–3
	13	1:50	0.5	15.49	3–4/3/3–4	3
	14	1:50	1	19.56	3–4/3–4/3–4	3
	15	1:10	2	19.93	3–4/4/4	3–4

[a)] W/S/C – staining on wool/change in colour of sample/staining on cotton

using two dyeing procedures, i.e. standard dyeing with a dye-bath mordant included (samples 4 and 6) and meta-mordanting (samples 7–15), with the aim of studying the influence of concentration of metallic salt and dyeing procedures on the growth and metabolism of two pathogens, *S. aureus* and *C. albicans*. The results are expressed as the relative reduction of inoculated microbes and are shown in Figure 7.

It is evident from Figure 7 that the yarn dyed with pure walnut leaf extract used as a model sample (sample 3) exhibited a potent inhibiting activity against C. albicans with a moderate reduction rate of 59%, and a low inhibited response against S. aureus, with a reduction rate of 38.6%. The major drawbacks of both antimicrobial strains' functions were seen when iron salt was applied, regardless of the dyeing procedure, the nature of the used microorganism and salt concentration during meta-mordanting: the higher the salt concentration, the lower the antibacterial activities of the textiles. In the case of mordant dyeing, a strong complex is formed between the colourant and the wool fibre, resulting in lower activity against the selected pathogens, although the exhaustion rate is higher compared to dyeing without a mordant.

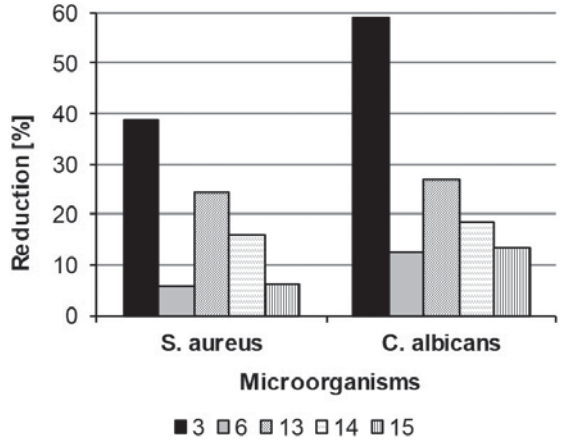

Figure 7: Percentage reduction of growth of two pathogenic strains (S. aureus and C. albicans) on the representative dyed yarns; LR_E 1:50; standard dyeing: 3 – without mordant, 6 – 2 g/L of $FeSO_4$; meta-mordanting: 13 – 0.5 g/L $FeSO_4$, 14 – 1 g/L $FeSO_4$, 15 – 2 g/L $FeSO_4$

4 Conclusion

Fresh leaves from the *J. regia* tree (common walnut) represent an inexpensive, ecologically-friendly raw

material that can be used for the extraction of reddish-brown natural colouring compounds. In this paper, a pure aqueous extract and an extract with $FeSO_4$ mordant included were used to dye wool yarn with the aim of achieving a wide palette of colour shades and good to excellent colour fastness, depending on the pH of the extract, the liquor ratio of the extraction, the type and amount of the applied mordant, and the type of dyeing procedure. Spectrophotometric studies revealed the significant impact of both the addition of a mordant and the pH of the dye-bath on the absorbance curve and thus on the hue and K/S values of the dyed samples. It can be concluded from a calorimetrical evaluation of the dyed samples that the application of $FeSO_4$ mordant gives bluer and less red hues compared to the original non-mordanted samples, regardless of the dyeing procedure. Generally, the meta-mordanting technique using iron salt gave a greater depth of shade than standard dyeing at a wavelength of 400 nm, regardless of the concentration of the mordant and the liquid ratio of the extraction. Finally, antimicrobial tests demonstrated a moderate antifungal activity of dyed wool samples against *C. albicans,* and a low antibacterial activity against *S. aureus*, as $FeSO_4$ reduced the inhibitory response against both pathogens.

Acknowledgement
The research that lead to these results received funding from the Slovenian Research Agency (ARRS) under a programme group for Textile Chemistry P2-0118.

References

1. ARORA, Jyoti, AGARWAL, Prerna, GUPTA, Gunjan. Rainbow of Natural Dyes on textiles using plants extracts: Sustainable and eco-friendly processes. *Green and Sustainable Chemistry*, 2017, **7**, 35–47, doi: 10.4236/gsc.2017.71003.
2. SELVAM, R. Mari, ATHINARAYANAN, G., NANTHINI, A. Usha Raja, SINGH, A.J.A. Ranjit, KALIRAJAN, K., SELVAKUMAR, P. Mosae. Extraction of natural dyes from *Curcuma longa*, *Trigonella foenum graecum* and Nerium oleander, plants and their application in antimicrobial fabric. *Industrial Crops and Products*, 2015, **70**, 84–90, doi: 10.1016/j.indcrop.2015.03.008.
3. HAFEEZULLAH, Memon, KHATRI, Awais, NAZAKAT, Ali, SAMIULLAH, Memon. Dyeing recipe optimization for eco-friendly dyeing and mechanical property analysis of eco-friendly dyed cotton fabric: Better fixation, strength, and color yield by biodegradable salts. *Journal of Natural Fibers*, 2016, **13**(6), 749–758.
4. SINGH, Rajni, JAIN, Astha, PANWAR, Shikha, GUPTA, Deepti, KHARE, S. K. Antimicrobial activity of some natural dyes. *Dyes and Pigments*, 2005, **66**, 99–102, doi: 10.1016/j.dyepig.2004.09.005.
5. YUSUF, Mohd, AHMAD, Aijaz, SHAHID, Mohammad, KHAN, Mohd Ibrahim, KHAN, Shafat Ahmad, MANZOOR, Nikhat, MOHAMMAD, Faqeer. Assessment of colorimetric, antibacterial, and antifungal properties of woollen yarn dyed with the extract of the leaves of henna (*Lawsonia inermis*). *Journal of Cleaner Production*, 2012, **27**, 42–50, doi: 10.1016/j.jclepro.2012.01.005.
6. FAKIN, Darinka, TEPEŠ, Darinka, MAJCEN Le MARECHAL, Alenka, OJSTRŠEK, Alenka, BOŽIČ, Mojca. Dyeing of wool with plant dyes and sample evaluation with CIE colour system. *Tekstilec* 2010, **53**, 179–193.
7. VELMURUGAN, Palanivel, KIM, Jae-In, KIM, Kangmin, PARK, Jung-Hee, LEE, Kui-Jae, CHANG, Woo-Suk, PARK, Yool-Jin, CHO, Min, OH, Byung-Taek. Extraction of natural colorant from purple sweet potato and dyeing of fabrics with silver nanoparticles for augmented antibacterial activity against skin pathogens. *Journal of Photochemistry and Photobiology B: Biology*, 2017, **173**, 571–579, doi: 10.1016/j.jphotobiol.2017.07.001.
8. MIRJALILI, Mohammad, NAZARPOOR, Khosro, KARIMI, Loghman. Eco-friendly dyeing of wool using natural dye from weld as co-partner with synthetic dye. *Journal of Cleaner Production*, 2011, **19**, 1045–1051, doi: 10.1016/j.jclepro.2011.02.001.
9. RAJA, A. S. M., THILAGAVATHI, G. Dyes from the leaves of deciduous plants with high tannin content for wool. *Coloration Technology*, 2008, **124**, 285–289, doi: 10.1111/j.1478-4408.2008.00153.x.
10. ALEMIDA, Isabel F., FERNANDES, Eduarda, LIMA, José L. F. C., COSTA, Paulo C., BAHIA, Maria Fernanda. Walnut (*Junglas regia*) leaf extracts are strong scavengers of pro-oxidant re-

active species. *Food Chemistry*, 2008, **106**, 1014–1020, doi: 10.1016/j.foodchem.2007.07.017.

11. BURKINSHAW, S.M., KUMAR, N. The mordant dyeing of wool using tannic acid and FeSO_4, Part 1: Initial findings. *Dyes and Pigments*, 2009, **80**(1), 53–60, doi: 10.1016/j.dyepig.2008.05.008.
12. AMARAL, Joana S., SEABRA, Rosa M., ANDRADE, Paula B., VALENTÃO, Patrícia, PEREIRA, José A., FERRERES, Federico. Phenolic profile in the quality control of walnut (*Junglas regia* L.) leaves. *Food Chemistry*, 2004, **88**(3), 373–379, doi: 10.1016/j.foodchem.2004.01.055.
13. NOUR, Violeta, TRANDAFIR, Ion, COSMULESCU, Sina. Optimization of ultrasound-assisted hydroalcoholic extraction of phenolic compounds from walnut leaves using response surface methodology, *Pharmaceutical Biology*, 2016, **54**(10), 2176–2187, doi: 10.3109/13880209.2016.1150303.
14. GORDON, Paul Francis, GREGORY, Peter. *Organic Chemistry in Colour*. Berlin : Springer-Verlag, 1987.
15. ALI, Shaukat, HUSSAIN, Tanveer, NAWAZ, Rakhshanda. Optimization of alkaline extraction of natural dye from Henna leaves and its dyeing on cotton by exhaust method. *Journal of Cleaner Production*, 2009, **17**(1), 61–66, doi: 10.1016/j.jclepro.2008.03.002.
16. PRUSTY, A. K., DAS, Trupti, NAYAK, A., DAS, N. B. Colourimetric analysis and antimicrobial study of natural dyes and dyed silk. *Journal of Cleaner Production*, 2010, **18**(16–17), 1750–1756, doi: 10.1016/j.jclepro.2010.06.020.
17. FAKIN, Darinka, OJSTRŠEK, Alenka, ČELAN BENKOVIČ, Sonja. The impact of corona modified fibres' chemical changes on wool dyeing. *Journal of Materials Processing Technology*, 2009, **209**(1), 584–589, doi: 10.1016/j.jmatprotec.2008.02.034.
18. BECHTOLD, Thomas, MAHMUD-ALI, Amalid, MUSSAK, Rita A. M. Reuse of ash-tree (*Fraxinus excelsior* L.) bark as natural dyes for textile dyeing: process conditions and process stability. *Coloration Technology*, 2007, **123**(4), 271–279, doi: 10.1111/j.1478-4408.2007.00095.x.
19. ESER, Ferda, SANAL, Semra, TEMIZ, Cengiz, YILMAZ, Fikret, ONAL, Adem. Effect of Acid Pretreatment on the Dyeing performance of walnut (*Juglans regia*) leaves on wool fibers. *Fibers and Polymers*, 2015, **16**(8), 1657–1662, doi: 10.1007/s12221-015-5137-9.

SHORT INSTRUCTIONS FOR AUTHORS OF SCIENTIFIC ARTICLES

Scientific articles categories:

- **Original scientific article** is the first publication of original research results in such a form that the research can be repeated and conclusions verified. Scientific information must be demonstrated in such a way that the results are obtained with the same accuracy or within the limits of experimental errors as stated by the author, and that the accuracy of analyses the results are based on can be verified. An original scientific article is designed according to the IMRAD scheme (Introduction, Methods, Results and Discussion) for experimental research or in a descriptive way for descriptive scientific fields, where observations are given in a simple chronological order.
- **Review article** presents an overview of most recent works in a specific field with the purpose of summarizing, analysing, evaluating or synthesizing information that has already been published. This type of article brings new syntheses, new ideas and theories, and even new scientific examples. No scheme is prescribed for review article.
- **Short scientific article** is original scientific article where some elements of the IMRAD scheme have been omitted. It is a short report about finished original scientific work or work which is still in progress. Letters to the editor of scientific journals and short scientific notes are included in this category as well.

Language: The manuscript of submitted articles should be written in UK English and it is the authors responsibility to ensure the quality of the language.

Manuscript length: The manuscript should not exceed 30,000 characters without spacing.

Article submission: The texts should be submitted only in their electronic form in the format *.doc (or *docx) and in the format *.pdf (made in the computer program Adobe Acrobat) to the address: tekstilec@a.ntf.uni-lj.si. The name of the document should contain the date (year-month-day) and the surname of the corresponding author, e.g. 20140125Novak.docx. The articles proposed for a review need to have their figures and tables included in the text. The article can also be submitted through a cloud-based file transfer service, e.g. "WeTransfer" (www.wetransfer.com).

Publication requirements: All submitted articles are professionally, terminologically and editorially reviewed in accordance with the general professional and journalistic standards of the journal Tekstilec. Articles are reviewed by one or more reviewers and are accepted for publication on the basis of a positive review. If reviewers are not unanimous, the editorial board decides on further proceedings. The authors can propose to the editorial board the names of reviewers, whereas the editorial board then accepts or rejects the proposal. The reviewers' comments are sent to authors for them to complete and correct their manuscripts. The author is held fully responsible for the content of their work. Before the author sends their work for publication, they need to settle the issue on the content publication in line with the rules of the business or institution, respectively, they work at. When submitting the article, the authors have to fill in and sign the Copyright Statement (www.tekstilec.si), and send a copy to the editors by e-mail. They should keep the original for their own personal reference. The author commits themselves in the Copyright Statement that the manuscript they are submitting for publication in Tekstilec was not sent to any other journal for publication. When the work is going to be published depends on whether the manuscript meets the publication requirements and on the time reference the author is going to return the required changes or corrections to the editors.

Copyright corrections: The editors are going to send computer printouts for proofreading and correcting. It is the author's responsibility to proofread the article and send corrections as soon as possible. However, no greater changes or amendments to the text are allowed at this point.

Colour print: Colour print is performed only when this is necessary from the viewpoint of information comprehension, and upon agreement with the author and the editorial board.

More information on: www.tekstilec.si